MOUNTAIN-FRONT RECHARGE FROM THE SANTA RITA MOUNTAINS TO THE TUCSON BASIN

by

August Merz III

A Thesis Submitted to the Faculty of the

DEPARTMENT OF HYDROLOGY AND WATER RESOURCES

In Partial Fulfillment of the Requirements
For the Degree of

MASTER OF SCIENCE
WITH A MAJOR IN HYDROLOGY

In the Graduate College

THE UNIVERSITY OF ARIZONA

1 9 8 5

STATEMENT BY AUTHOR

This thesis has been submitted in partial fulfillment of requirements for an advanced degree at The University of Arizona and is deposited in the University Library to be made available to borrowers under rules of the Library.

Brief quotations from this thesis are allowable without special permission, provided that accurate acknowledgment of source is made. Requests for permission for extended quotation from or reproduction of this manuscript in whole or in part may be granted by the head of the major department of the Dean of the Graduate College when in his or her judgement the proposed use of the material is in the interests of scholarship. In all other instances, however, permission must be obtained from the author.

SIGNED: August Wiley III

APPROVAL BY THESIS DIRECTOR

This thesis has been approved on the date shown below:

S. N. DAVIS
Professor of Hydrology
and Water Resources

Sept. 10, 1985
Date

This thesis is dedicated

to my father.

ACKNOWLEDGMENTS

Several people contributed to making this thesis a reality. I would like to thank Dr. Stanley N. Davis for suggesting the project, providing funding through the Spanish Grant, and giving valuable advice throughout the study. Dr. L. G. Wilson and Dr. Eugene S. Simpson reviewed the thesis and sat on my committee, and for this I thank them. Also, I thank Carl Mohrbacher and Mark Olsen for posing several challenging questions which greatly increased my understanding of mountain-front recharge. Finally, I thank the ranchers along the Santa Rita mountain-front for allowing access to their land.

The Department of Geosciences analyzed the water samples for isotopic content; the Arizona Department of Water Resources and the Water Resources Research Center provided well data; and the Santa Rita Experimental Range and the Smithsonian Institution provided precipitation data. I am indebted to each.

To conclude, I would like to acknowledge Ann Cottgageorge for drafting the figures and Sally Adams for typing the thesis.

TABLE OF CONTENTS

TABLE OF CONTENTS--Continued

LIST OF ILLUSTRATIONS

LIST OF ILLUSTRATIONS--Continued

LIST OF ILLUSTRATIONS--Continued

LIST OF TABLES

ABSTRACT

This study analyzes mountain-front recharge from the Santa Rita mountains. Trilinear diagrams, finger-print diagrams, and scattergrams suggest that two types of water recharge the regional aquifer by effluent seepage as Madera Canyon Stream flows onto Madera Canyon fan. One type of water is dominated by calcium and bicarbonate ions, and the other type is dominated by calcium and sulfate ions. Deuterium and oxygen-18 data support these interpretations and indicate that recharge occurs over a broad range of elevations. Furthermore, the isotopic data indicate that the deuterium and oxygen-18 gradients are -3.5 $^{o}/_{oo}$ and -0.4 $^{o}/_{oo}$, respectively, per 1000 foot increase. Evidence is lacking for the presence of deeply circulating waters.

Calculations based on a flow-net analysis and a water balance approximate annual mountain-front recharge to be between 200 and 400 ac-ft/yr/mi of mountain-front recharge.

Recharge studies from the nearby Santa Catalina mountains estimate recharge to be between 25 and 50 ac-ft/yr/mi of mountain front and present evidence for minor amounts of deep circulation through the mountain block into the basin. The Santa Rita Mountains, significantly, have a more permeable alluvial fan which favors recharge.

CHAPTER 1

INTRODUCTION

Mountain-front recharge has traditionally been considered either non-existent or inconsequential in regional ground-water studies. However, investigations in the past twenty years have revealed mountain-front recharge to be an important component in determining recharge to a ground-water basin.

A discussion of mountain-front recharge requires the use of some basic terms. The following terms are from Wilson, DeCook, and Neuman (1980):

Mountain-front recharge - recharge that occurs along the boundary of a regional aquifer system that parallels a mountain system.

Ground-water basin - an area within which ground-water flow paths are toward the regional aquifer. The basin boundary usually coincides with the watershed boundary (Fig. 1.1).

Regional aquifer- the largest body of continuous saturation in a ground-water basin (Fig. 1.1).

Local flow system - a small, isolated ground-water flow system that is siolated from the regional aquifer (Fig. 1.2).

Regional flow system - a saturated system that is connected to the regional aquifer (Fig. 1.2).

Mountain-front recharge occurs by two dominant mechanisms. First, precipitation circulates through local flow systems which discharge into streams and later recharges the regional aquifer by

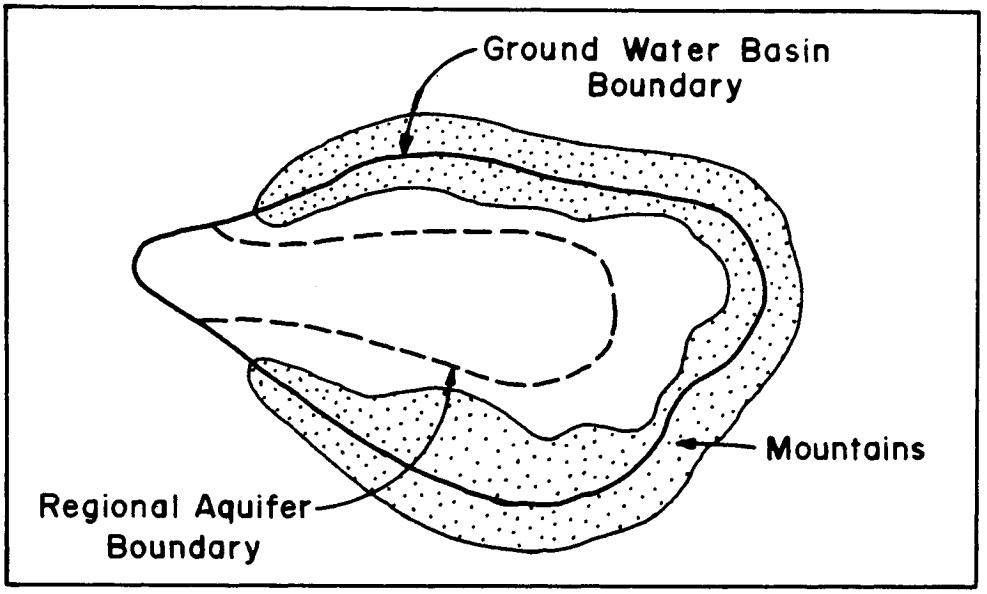

Figure 1.1a. Ground water basin and regional aquifer boundaries in plan. (After Wilson and others, 1980)

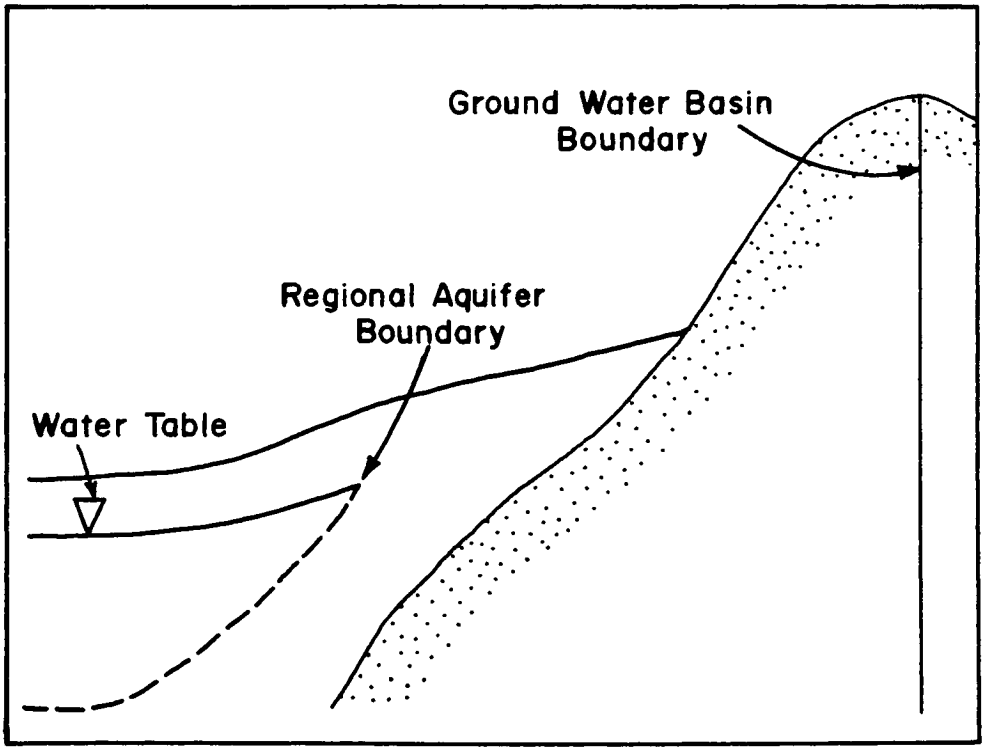

Figure 1.1b. Ground water basin and regional aquifer boundaries in cross-section. (After Wilson and others, 1980)

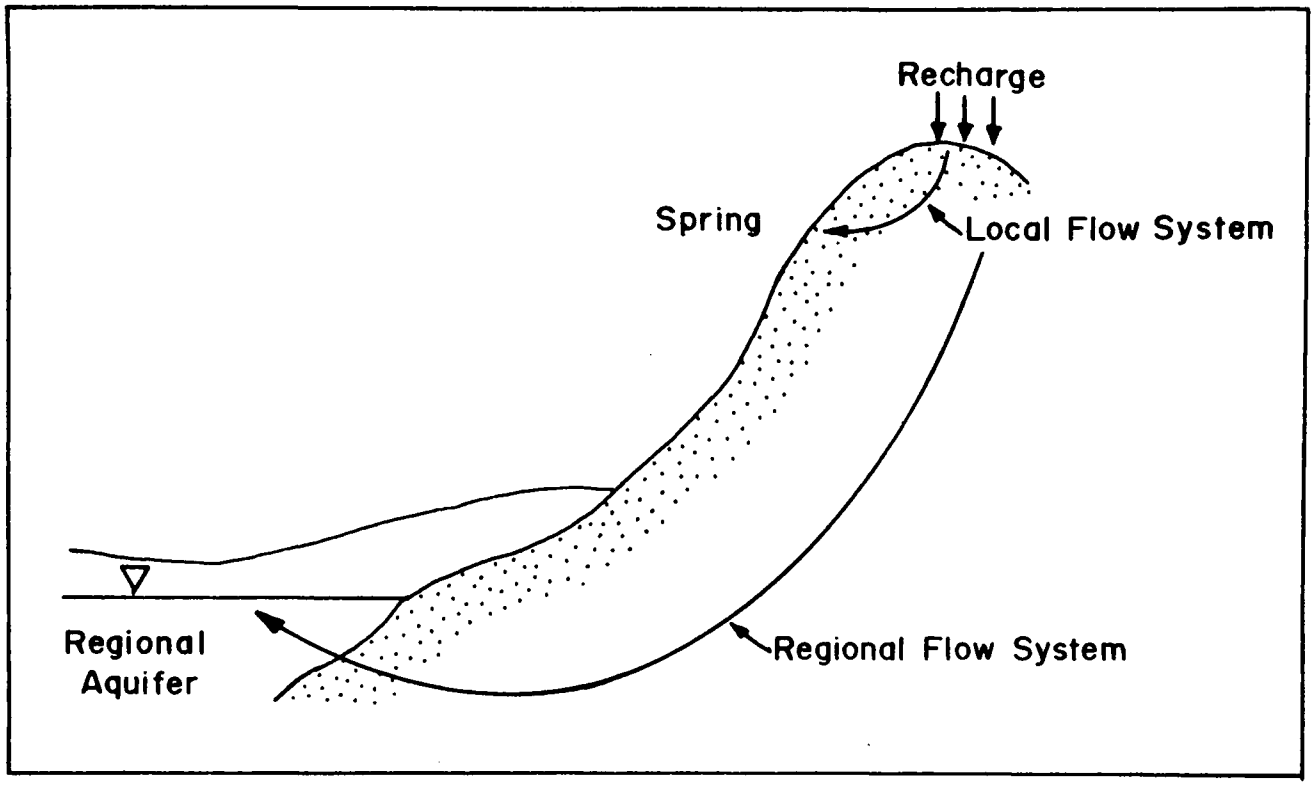

Figure 1.2. Local and regional flow systems. (After Keith, in Wilson and others, 1980).

stream-flow infiltration. Second, precipitation circulates through a regional flow system and recharges the regional aquifer directly.

The purpose of this study is to analyze mountain-front recharge from the Santa Rita Mountains to the Tucson Basin. The study area is approximately 45 miles south of Tucson, Arizona (Fig. 1.3). The mountains are surrounded by the Tucson Basin to the west, the Empire Basin to the east, and the Empire Mountains to the north.

This study has two primary objectives: 1) to qualitatively determine the mechanisms of mountain-front recharge in the study area; and 2) to quantitatively determine the amount of annual mountain-front recharge from the Santa Rita Mountains to the Tucson Basin. Chemical, isotopic, and hydrologic methods will be tested as a means of meeting these goals.

In previous investigations, Feth (1964), in a study of the Weber delta area in Utah, was perhaps the first to emphasize mountain-front recharge as a vital part of ground-water systems in arid regions. Mifflin (1968) considered the role of topography in determining the mechanisms of mountain-front recharge. Kafri and Ben-Asher (1978) studied the roles of soil depth and seasonal precipitation in recharge. Davidson (1960 and 1961) found that significant natural recharge may be limited to coarse-grained materials formed by ancient tributaries, and although the coarse materials near the mountain-front provide an effective channelway, recharge may be inhibited due to the fine-grained material away from the mountain front.

In the Tucson Basin, Simpson, Thourud and Friedman (1970) evaluated seasonal variations in recharge and found that winter

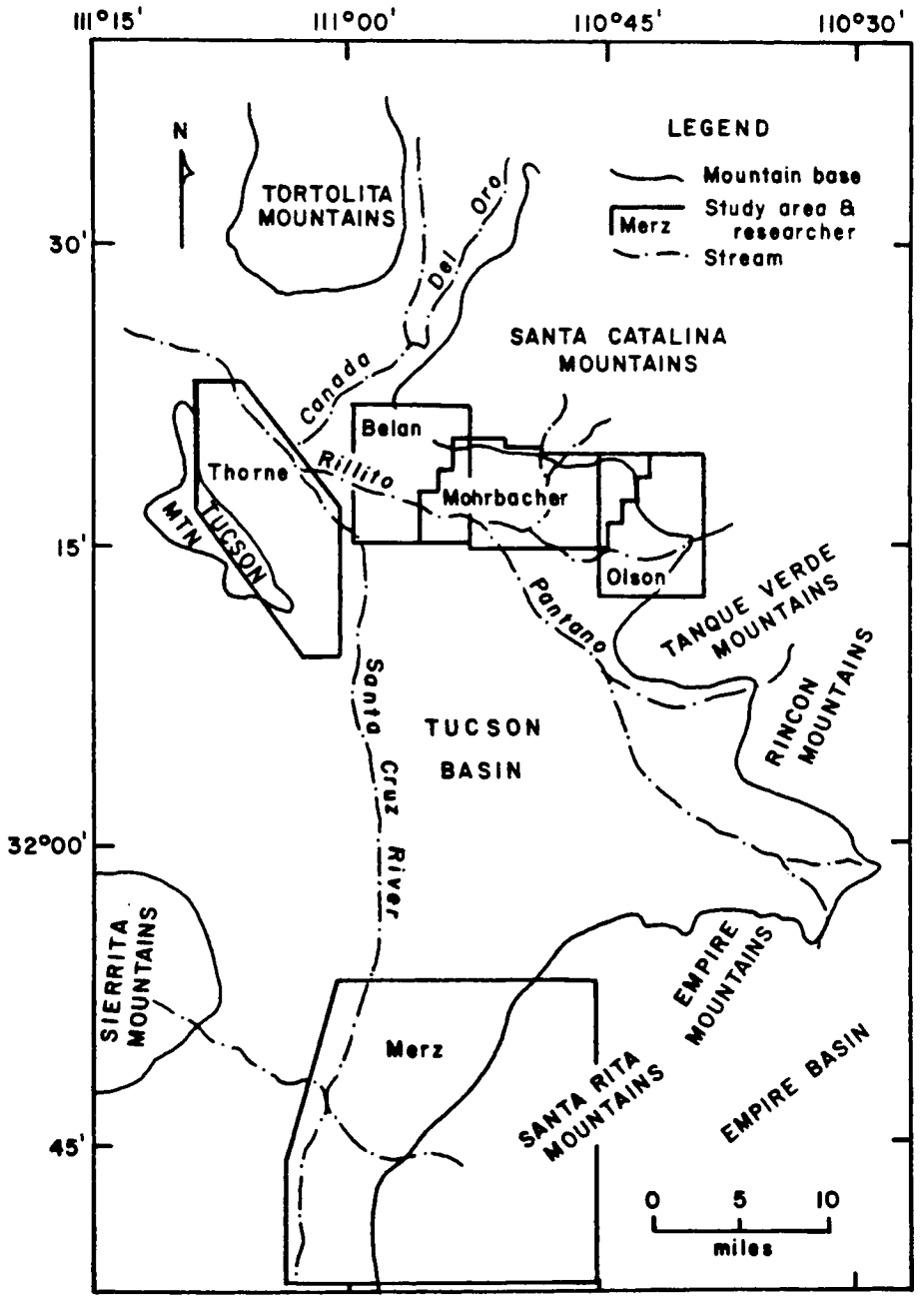

Figure 1.3. Areas where mountain-front recharge has been studied in the Tucson basin. (After Mohrbacher, 1983)

precipitation plays the dominant role in determining annual recharge. Belan (1972) applied Darcy's law to flow nets placed over shoe-string channels in a region of the Santa Catalina Mountains. He estimated recharge to be 336 ac-ft/yr. Anderson (1972) produced an analog model which calculated recharge for all the local mountain fronts to the Tucson Basin. His results appear in Figure 1.4. Thorne (1982) studied recharge from the Tucson Mountains using chemical, isotopic, and hydrologic methods. Mohrbacher (1983) and Olsen (1982) used similar methods to evaluate recharge from the Santa Catalina Mountains. Both researchers found evidence of deep-circulating waters which had recharged at high elevations. Mohrbacher estimated mountain-front recharge to be 24-65 ac-ft/yr/mi and Olsen estimated recharge to be 50 ac-ft/yr/mi. Figure 1.3 shows the study areas of all past researchers in the Tucson area.

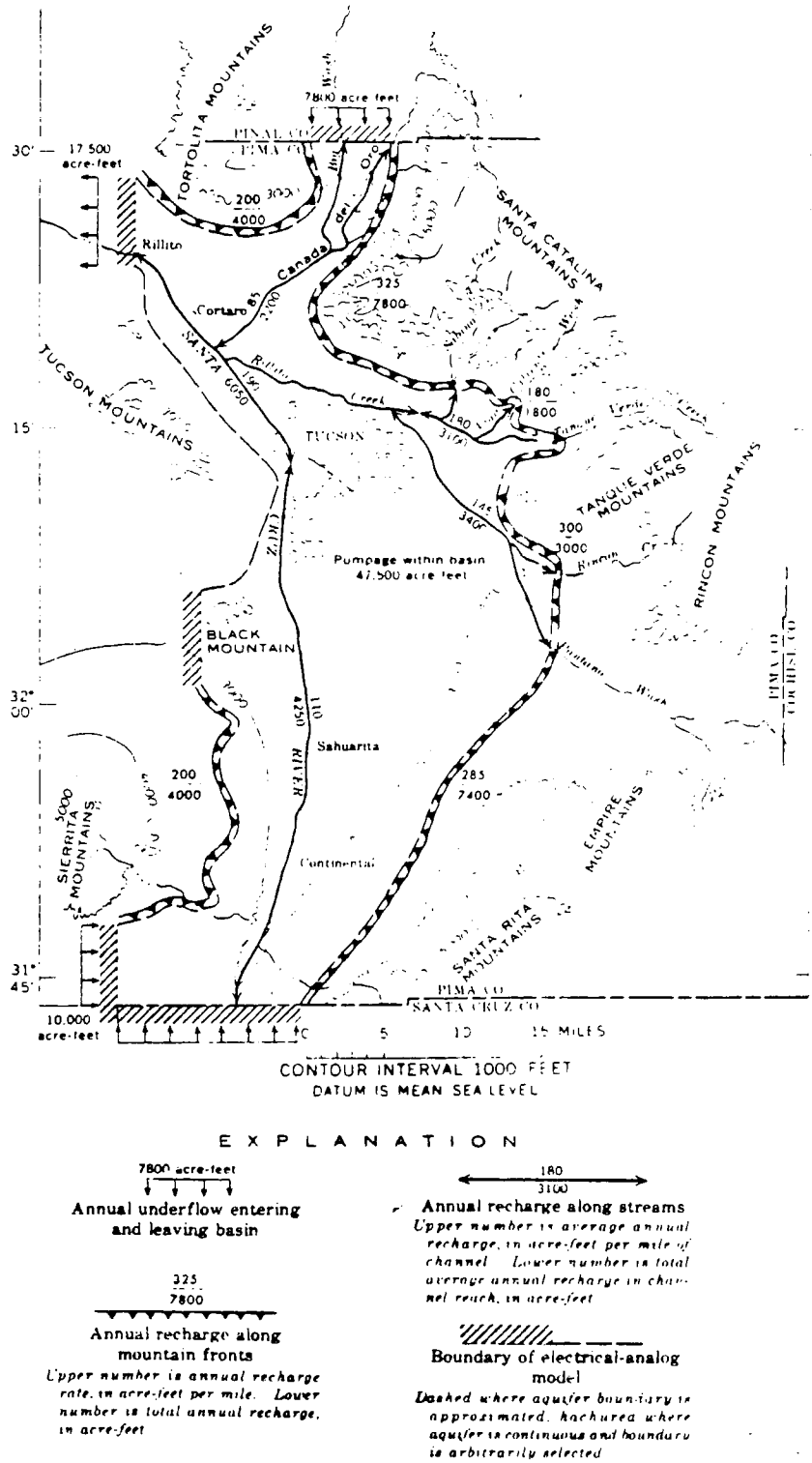

Figure 1.4. Recharge values from Anderson's Analog Model. (Anderson, 1972)

CHAPTER 2

PHYSIOGRAPHY OF THE SANTA RITA MOUNTAINS

This chapter presents the physical setting of the Santa Rita Mountains. The discussion starts with a description of the semi-arid climate of the region. Next, the highly dissected topography and the drainage pattern are described. Finally, the chapter concludes with a detailed outline of the geology of the mountains. The outline covers the rock units, structural features, and depth-to-bedrock characteristics of the study area.

Climate

Southeastern Arizona has a semi-arid to arid climate. Temperatures are hot in the summer, mild in the winter, and cool at high elevations. Relative humidity averages 30% but can be much higher in wet seasons.

Precipitation in the study area occurs predominately in mid-summer and mid-winter. In summer, moisture from the Gulf of Mexico combines with high surface temperatures and orographic lifting to produce intense, short-term storms lasting on the order of hours. These storms are common between July and September. Winter storms originate as Pacific fronts which follow prevailing winds to Arizona. Winter storms are less intense than summer storms but may last several days. They occur between November and March. Summer storms account for an

average of 54% of annual precipitation and winter storms 36% (Kafri and Ben-Asher, 1978).

Topography

The Santa Rita Mountains are dissected by seven deep canyons in the study area (Plate 1, in pocket). Madera Canyon is the largest and the only one with perennial streamflow, indicating that it intersects the water table. Streamflow in other canyons is ephemeral, originating primarily from snowmelt in late winter and spring. Florida Canyon, Chino Canyon, and Agua Caliente Canyon have the largest ephemeral streamflows. Some streamgaging was conducted during this study and results are presented in Chapter 3.

Runoff from the study area drains to the north and west. As can be seen in Plate 1, drainage from Florida Canyon and Faber Canyon connects and trends toward the alluvial fan formed by Madera Canyon. Similarly, drainage from Chino Canyon and Madera Canyon joins and trends toward the Santa Cruz river.

Geology

The Santa Rita Mountains are in the Basin and Range province of the southwestern United States. This province contains north-trending, block-faulted mountain ranges separated by alluvial basins which locally are the Santa Cruz Basin to the west and the Empire Basin to the east of the Santa Rita Mountains (Fig. 1.3).

The Santa Rita Mountains contain volcanic, intrusive, and sedimentary rocks ranging in age from Precambrian to Cenozoic. Mesozoic

volcanics and intrusives form the core of the mountains, and sedimentary rocks of various ages occur in fault zones along the north and west flanks of the mountains. Several mappable terrace and pediment deposits surround the Santa Rita Mountains. Structurally, the mountains contain several zones of faulting and folding produced during various geologic periods.

Plate 2 (in pocket) is a geologic map of the study area and Appendix A presents the entire geologic column with a brief description of lithologies. Inasmuch as only a few of the formations and structures which are listed in Appendix A are present in the study area, only those present will be discussed in detail. However, the Santa Rita Mountains display one of the most complete geologic and structural records in southern Arizona (Drewes, 1972b), and the interested reader is directed to Drewes (1971a, 1971b, 1971c, 1972a, 1972b, and 1976) for a complete analysis.

Geologic Formations

Precambrian and Paleozoic. Five Precambrian and Paleozoic formations are exposed in the study area. The Precambrian Continental Granodiorite crops out in Sawmill Canyon and Santa Rita Ranch Canyon. The Cambrian Abrigo Formation and the Devonian Martin Formation are exposed as fault slices in Sawmill Canyon. To the west, exposed between two faults, are the Permian Scherrer Formation and the Concha Limestone. The following descriptions are based on Drewes (1972a and 1976).

The Continental Granodiorite forms a stock of coarse-grained and porphyritic granodiorite and quartz monzonite. The rock is internally weak and forms gentle slopes and thick layers of grus. Mineralogically, the potassium feldspar is microcline and orthoclase, and commonly weathers intensely to kaolinite. The plagioclase feldspar is 30-50% anorthite and weathers to clay minerals with varying intensity. Biotite, chlorite, and hornblende make up 10-20% of the rock.

The Abrigo Formation contains shale, quartzitic sandstone and thin-bedded limestone. The Martin Formation is a brown dolomite with grey limestone, siltstone, and some mudstone. Finally, the Scherrer Formation consists of quartzite and dolomite, and the Concha limestone is a thin-bedded chert limestone.

Mesozoic Rocks. Mesozoic rocks cover most of the study area. They include sedimentary formations, volcanic flows, and crystalline plutons. The formations include the Triassic Mount Wrightson Formation, Piper Gulch Monzonite, and Quartz Diorite; the early Cretaceous Apache Canyon and Turney Ranch Formations of the Bisbee group; and the late Cretaceous Fort Crittenden Formation, Josephine Canyon Diorite, Madera Canyon Granodiorite, and Elephant Head Quartz Monzonite. The following drescriptions are from Drewes (1971b and 1976).

The Mount Wrightson Formation crops out in an elongate band trending north from Mount Wrightson and in the fault zone on the west flank of the mountains. The formation is predominately volcanic but contains sandstone lenses. Volcanic rocks include andesites, dacites, latites, rhyolites, and welded tuffs. Mineralogically, the rock

contains quartz, albitized plagioclase, potassium feldspar as sanidine, chlorite, epidote, pyroxene, and clay minerals.

The Piper Gulch Monzonite is exposed on the west flank of Mount Hopkins and the east flank of Madera Canyon. The rock grades from monzonite to syenodiorite and forms steep slopes. A thick layer of grus forms in areas of low topography. The mineral assemblage includes plagioclase in the calcic oligoclase to sodic labrodorite phase; orthoclase; amphibole; and quartz, pyroxene and biotite in minor amounts. Plagioclase is strongly to moderately altered to clays and sericite, and orthoclase is strongly altered to kaolinite. The rock has hypidiomorphic-tabular to porphyritic texture.

An unnamed quartz diorite crops out near Florida spring. The rock is porphyritic and contains andesine, plagioclase, amphibole, quartz, and minor amounts of potassium feldspar, biotite, and pyroxene.

The early Cretaceous Bisbee Group is a thick sedimentary sequence exposed along the flanks of the mountains. The Apache Canyon Formation crops out between two faults west of Elephant Head. Siltstone, mudstone, and an arkose containing volcanic fragments of orthoclase and albite comprise the formation. The Turney Ranch Formation is exposed in Sawmill Canyon and consists of red mudstone, siltstone, and intercalated sandstone.

The Fort Crittenden Formation consists of sedimentary and volcanic members. The Brown Conglomerate Member crops out in the Sawmill Canyon fault zone and is composed of a conglomerate with some siltstone and sandstone. The Upper Red Conglomerate Member crops out in the

fault swarm west of Elephant Head and consists of a volcanic conglomerate containing siltstone and sadnstone.

The Josephine Canyon Diorite, the Madera Canyon Granodiorite, and the Elephant Head Quartz Monzonite comprise the principal formations in the study area. Given their large areal extent and presumed extension to depth, these formations probably have the greatest influence on the ground-water chemistry in Madera Canyon. Chemical analyses and mineral modes for each of these formations appear in Table 2.1.

The Josephine Canyon Diorite crops out on the east flank of Mount Hopkins and in Josephine saddle. The formation contains diorite and quartz monzonite. The diorite has a coarse-grained, subophitic to porphyritic texture and consists of slightly albitized andesine plagioclase, ortholcase, quartz, and pyroxene. Slight weathering and alteration of the plagioclase and orthoclase occurs. The quartz monzonite has a fine-grained subophitic to porphyritic texture. Plagioclase, orthoclase, and quartz dominate the rock, but biotite and pyroxene also occur. Heavy alteration of the feldspars to clay minerals is common.

The Madera Canyon Granodiorite is exposed in Madera Canyon. Three rock types comprise the formation: a nonporphyritic granodiorite, a porphyritic granodiorite, and a melanocratic granodiorite. The nonporphyritic granodiorite has a hypidiomorphic granular texture, weathers easily, and contains quartz, orthoclase, plagioclase, biotite, and hornblende. The plagioclase ranges from calcic oligoclase to sodic andesine and secondary clay minerals are scarce. The porphyritic granodiorite is similar to the nonporphyritic rock except it contains

Table 2.1. Average Modes and Chemical Analyses of Mesozoic Plutonics in the Santa Rita Mountains (After Drewes, 1976)

	Modes			Chemistry	
JOSEPHINE CANYON DIORITE					
	Diorite	Quartz Monzonite		Diorite	Quartz Monzonite
Quartz	8.5	19.2	SiO_2	59.9	68.1
Plagioclase	56.1	33.3	Al_2O_3	16.4	15.0
Orthoclase	14	37.9	Fe_2O_3	3.3	2.8
Hornblende	6.6	1.6	FeO	3.2	1.2
Pyroxene	5.3	1.6	MgO	2.9	.45
Biotite	5.6	3.8	CaO	5.1	1.8
Magnetite	3.0	2.1	Na_2O	3.6	3.3
Apatite	.5	.3	H_2O	3.0	4.7
Sphene	.2	.2	H_2O^-	.22	.28
Zircon	.07	.06	H_2O^+	.92	.68
Allanite	Tr.	.04	TiO_2	.76	.56
Rutile	0	Tr.	P_2O_5	.27	.24
Tourmaline	Tr.	Tr.	MnO	.25	.07
Hypersthene	Tr.	0	CO_2	.11	<.05

Table 2.1--Continued

	Modes			Chemistry
ELEPHANT AND QUARTZ MONZONITE				
	Coarse-grained Quartz Monzonite	Fine-grained Quartz Monzonite		Coarse- and fine-grained Quartz Monzonite
Quartz	27.8	29.1	SiO_2	73.0
Plagioclase	34.9	37.9	Al_2O_3	14.1
Orthoclase	20.8	28.8	Fe_2O_3	1.3
Microcline	13.6	.5	FeO	.65
Biotite	1.9	2.4	MgO	.27
Amphibole	.06	.03	CaO	.73
Magnetite	.7	1.0	Na_2O	3.7
Apatite	.07	.2	H_2O	5.2
Sphene	.1	.3	H_2O^-	.09
Zircon	.05	.04	H_2O^+	.58
Allanite	Tr.	Tr.	TiO_2	.34
Morazite	Tr.	0	P_2O_5	.03
Pyrite	Tr.	0	MnO_2	.09
Tourmaline	Tr.	0	CO_2	<.05
	100.0	100.0		100.0

Table 2.1--Continued

Modes				Chemistry		
MADERA CANYON GRANODIORITE						
	Granodiorite	Granodiorite Porphyry	Melanocratic Granodiorite		Granodiorite	Granodiorite Porphyry	Melanocratic Granodiorite
Quartz	20.8	24.9	19.4	SiO_2	66.8	68.1	60.5
Plagioclase	43.7	43.3	43.8	Al_2O_3	16.0	15.2	16.3
Orthoclase	22.6	18.7	21.7	Fe_2O_3	1.9	2.2	2.7
Sanidine	0	0	0	FeO	1.6	1.3	3.3
Hornblende	5.1	3.8	5.1	MgO	1.6	1.1	2.5
Biotite	5.5	7.5	6.1	CaO	3.5	3.6	4.3
Pyroxene	.1	0	0	Na_2O	3.8	3.8	3.8
Magnetite	1.4	1.0	1.4	Ti_2O	3.4	3.3	4.4
Apatite	.2	.3	.3	H_2O^-	.12	.13	.08
Sphene	.5	.6	.6	H_2O^+	.72	.52	.72
Zircon	.03	.06	.05	TiO_2	.49	.62	.99
Allanite	Tr.	Tr.	Tr.	P_2O_5	.18	1.8	.47
Rutile	Tr.	0	Tr.	MnO	.06	.06	.18
Tourmaline	0	0	Tr.	CO_2	.06	<.05	.05
	99.9	100.0	98.45		100.00	100.00	100.00

phenocrysts and weathers less. Finally, the melanocratic granodiorite is porphyritic and contains quartz, orthoclase, calcic andesine plagioclase, boitite and hornblende. Some albitization occurs.

Finally, the Elephant Head Quartz Monzonite crops out near the Elephant Head promontory. The formation contains a friable, coarse-grained quartz monzonite and a resistant fine-grained quartz monzonite. In both rocks, plagioclase, orthoclase, and microcline comprise the major minerals, but biotite, magnetite, and apatite are present in small amounts. The plagioclase contains albite and strong alteration is common. The orthoclase is moderately kaolinized.

Cenozoic Rocks. Cenozoic rocks in the Santa Rita Mountains consist of rhyolite and rhyodacite volcanics and numerous surficial deposits. The rhyolite member of the Oligocene Grosvener Hills Volcanics crops out west of Elephant Head. Tuff or tuff breccia with some tuffaceous sandstone compose the rock (Drewes, 1972b).

Surficial deposits have been divided into six mappable units by Drewes (1972b). They include the gravel of Nogales; the basin fill gravel; the high, intermediate, and low level terrace deposits; and the youngest gravel. Stratigraphic relationships and compositions are given in Figure 2.1.

Finally, the study area contains two Tertiary dike swarms. The first, near Elephant Head, contains short dikes which are cut by small faults. The second, located to the east, consists of long, mostly continuous dikes. Both dike swarms are composed of porphyritic coarse-grained latite and aphanitic rhyolite (Drewes, 1971c).

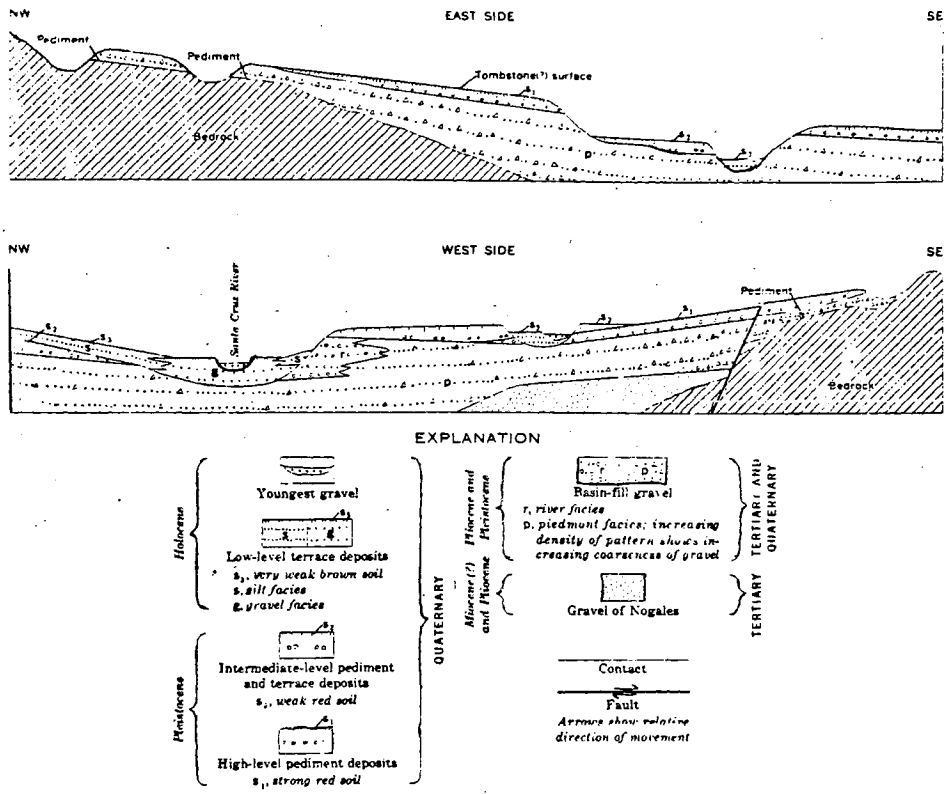

Figure 2.1. Surficial deposits near the Santa Rita Mountains. (Drewes, 1972b)

Structural Geology

Except for Sawmill Canyon and the area west of Elephant Head, structural deformation in the study area is relatively mild. In Sawmill Canyon, faults trending N55°W and dipping northeast and southwest have brought Paleozoic sediments over Cretaceous sediments and Cretaceous sediments over Triassic volcanics. West of Elephant Head high angle reverse faults and thrust faults trending N40°W and dipping southwest have brought Paleozoic sediments over Cretaceous sediments and Cretaceous sediments over Cretaceous plutons (Drewes, 1972a).

Along the front of the mountain range, Elephant Head Fault strikes N35°E and dips 50-65 degrees to the northwest. Near Elephant Head the fault serves as the contact between bedrock and gravel, but to the east the fault confines itself to the surficial deposits (Drewes, 1972a). Recent geophysical evidence indicates that 60 to 80 feet of normal offset occurs along the fault and demonstrate that the Tertiary deposits along the mountain front have been displaced by the fault (Rutledge, 1984).

Depth-to-Bedrock Data

Depth-to-bedrock data provide information about potential aquifer thickness. Geophysical data, geologic maps, and drillers' logs were compiled to construct the contour map of the bedrock surface (Fig. 2.2). The map shows that the depth to the bedrock surface increases from 0 to 60 feet near the mountain front to approximately 500 feet near Elephant Head Fault. Thus, the bedrock surface dips at between 3 and 4 degrees to the north.

CHAPTER 3

METHODS AND RESULTS

Data for this study were collected between March 1982 and September 1983. This chapter describes the methods of data collection and presents the results. Data fall into two classifications: chemical and hydrologic. The possible significance of the data is discussed in the two chapters which follow.

Chemical Data

Water samples were collected from a total of 53 sample sites, including 24 wells, 18 springs, 7 mineshafts, and 4 streams. Figure 2.1 shows sample locations and types. Note that nine locations fall outside the study area or on the far side of the topographic divide. These samples are included to benefit future researchers but are not used in the analysis of mountain-front recharge. The chemical analyses of the water samples are presented in Appendix B and discussed in Chapter 4.

Sample Analysis

At each site, a sample was collected in a plastic bottle for a chemical analysis. Temperature, pH, specific conductance, and flow rate were measured as soon as possible, usually in the field. Additionally, 31 of the sites were sampled for deuterium and oxygen-18 isotopes. These samples were collected in 2-ounce amber bottles and wrapped with paraffin paper to prevent evaporation.

Major Constituents. Each sample was analyzed for bicarbonate, nitrate, sulfate, fluoride, calcium, magnesium, sodium, potassiam, iron, silica, and hardness. Concentrations were measured by several methods. Bicarbonate, chloride, calcium, magnesium, and hardness were analyzed by digital titration. Nitrate, sulfate, iron, and silica concentrations were analyzed by spectrophotometry. Titration and spectrophotometer analyses were conducted with a Hach Direct Reading Engineer's Laboratory Model DR-EL/4. Sodium and potassium were analyzed by atomic absorption with an Electromark Analyzer. Finally, fluoride was determined with an Orion Fluoride Electrode Model 94-09 specific-ion electrode.

Accuracy of the chemical analyses was checked by the cation-anion balance formula:

$$\left(\frac{\Sigma\text{Meq anions} - \Sigma\text{Meq cations}}{\Sigma\text{Meq anions} + \Sigma\text{Meq cations}}\right) \times 100 = \text{percent error} \qquad (3.1)$$

In this study 90% of the analyses were within 10% error and 96% were within 15% error. Percent error for each analysis is included in Appendix B.

Isotopic Analysis. Deuterium and oxygen-18 analyses were made at the Isotope Laboratory in the Department of Geosciences at the University of Arizona. Results appear in Table 3.1. The delta symbol (δ) designates the relative difference in concentration with units of per mil ($^{o}/_{oo}$) according to the formula:

$$(\delta)\ \text{Isotope} = \left(\frac{R\ \text{sample}}{R\ \text{standard}} - 1\right) \times 1000 \qquad (3.2)$$

Table 3.1. Isotope Data for the Santa Rita Mountains. Numbers refer to Figure 2.1 and Appendix B.

Name	No.	Type*	Date	Elevation (ft)	δD ±.2 ‰	$\delta^{18}O$ ±3 ‰
Bellow	1	S	4/19/82	8210	-64	-9.0
Sprung	2	S	10/23/82	6970	-72	-9.4
No Name	3	M	4/06/83	6540	-60.6	-9.9
Kent	5	S	6/30/82	6680	-68	-9.4
Sylvester	6	S	3/29/82	6005	-70	-9.5
Bog	7	S	6/30/82	5880	-72	-9.4
Christobal	10	W	3/31/83	4120	-57.5	-8.8
RF3	13	W	3/31/83	4038	-60.7	-8.9
Melendrez	15	W	11/27/83	3683	-54.6	-7.5
County Well	18	W	6/04/83	5018	-56.7	-7.7
County Sp.	19	S	6/04/83	4712	-55.3	-8.6
High Mine	24	M	6/14/83	4810	-57.7	-8.6
Low Mine	25	M	6/13/83	4490	-46.9	-5.1
Armour	28	S	6/06/83	7960	-63.4	-9.8
Robinson	29	S	6/10/83	5070	-69.6	-9.5
Florida	30	S	6/10/83	6835	-70.8	-10.1
Low Well	32	W	6/14/83	4080	-58.3	-8.8
Willow	33	S	6/14/83	5070	-51.6	-8.31
SR1	34	W	6/15/83	4435	-58.7	-8.6
SR2	35	W	6/15/83	4530	-55.6	-8.5
SR3	36	W	6/15/83	4535	-55.7	-8.3
Chino Mine	37	M	1/09/83	4600	-61.7	-8.2
Quantrell Mine	39	M	1/14/83	5120	-54.5	-8.8
Quantrell Cr.	40	St	1/14/83	3760	-51.2	-7.8
Hermit	41	M	5/19/82	6580	-61	-8.4
Agua Caliente	42	S	3/31/82	3880	-66	-8.2
Sawmill	50	S	6/07/83	6960	-67.1	-10.4
Rock Lady	51	M	6/06/83	6160	-67.7	-9.2
Baldy Sp.	52	S	10/23/82	8640	-77	-10.0
Macbeth	53	S	10/23/82	7130	-74.5	-10.5

*S = spring, M = mine, W = well, St = stream.

where R = the ratio D/H or $^{18}O/^{16}O$ (Toran, 1983). The standard is Standard Mean Ocean Water (SMOW).

Hydrologic Data

Hydrologic data for this report consist of well and aquifer data, streamflow measurements, precipitation records, and evapotranspiration estimates.

Well and Aquifer Data

Twenty-four sampling sites in the study area are wells. At each well, if possible, the water level was measured with a steel tape or an electric sounder. Water levels at some wells were taken several times, but no systematic schedule was kept. Water level and general well data, including drillers' logs, are presented in Appendix C.

At five wells, a time-drawdown test was conducted to determine aquifer properties. Transmissivities were approximated by using the well's specific capacity and Logan's empirical equation (1964):

$$T = \frac{2.43\ Q\ M}{S(2\ M-S)} \qquad (3.3)$$

where T = transmissivity [L^2/T], Q = well discharge [L^3/T], M = aquifer thickness [L], and S = drawdown [L]. Table 3.2 lists transmissivities in the study area. Calculations appear in Appendix D.

At Proctor Ranch, data from the time-drawdown test were sufficient to be analyzed by the Theis method. At site B-1 the data were analyzed by the Thiem method. Results are included in Table 3.2. Note that transmissivity estimates from the specific capacity analyses are

Table 3.2. Transmissivity Estimates for Santa Rita Mountains and Averages for Madera Canyon.

Location	Canyon	Method	T ft^2/d	K ft/d	S
RR3	Madera	Specific capacity	206	4.58	
		Theis	63.5	1.41	.44
Air Force	Madera	Specific capacity	135	5.4	
			151	6.3	
			117	5.8	
		3 Well Average	134	5.8	
B-1	Madera	Specific capacity	149	2.97	
		Thiem	57.8	1.16	
High Well	Sawmill	Specific capacity	164	5.86	
S.R.1	Santa Rita	Specific capacity	60	.4	

Madera Canyon Averages:

Specific capacity - $\overline{T}$ = 151.6 ft^2/day, $\overline{K}$ = 5.0 ft/day

Theis and Thiem method - $\overline{T}$ = 60.7 ft^2/day, $\overline{K}$ = 1.28 ft/day

2 to 3 times higher than from the Theis or Thiem methods. The values range between 57.8 and 206 ft^2/day and all estimates fall within the range for fractured granitic rocks and silty to clean sands (Freeze and Cherry, 1979, p. 29).

Streamflow Data

With the exception of Madera Canyon, streams in the Santa Rita Mountains are ephemeral, flowing only in the winter and spring. Discharge measurements were made on four streams using a Pygmy current meter. No systematic schedule of stream-gaging was kept, but flow in Madera Canyon was measured several times. Discharge measurements range from 0.23 to 6.26 ft^3/s and are listed in Table 3.3.

On most streams, the discharge was measured at two or more locations in an attempt to estimate stream loss or gain. In a losing stream, discharge decreases downstream and the ground-water system is recharging. The opposite is true for a gaining stream.

The rate of streamflow loss or gain can be calculated by the formula:

$$I = \frac{Q_u - Q_d}{L} \qquad (3.4)$$

where I = discharge or recharge of the ground water along the measured length [L^3/T], Q_u = stream discharge at the upstream station [L^3/T], Q_d = stream discharge at the downstream station [L^3/T], and L = the length of the reach [L]. Stream gain and loss estimates are given in Table 3.3. Streams gain between 0.45 and 1.30 cfs/mi. Note that although evaporation is not considered in the formula, it may play a role in reducing discharge.

Table 3.3a. Discharge Measurements for Creeks in the Santa Rita Mountains (in ft^3/sec).

Date	Agua Caliente 1	Agua Caliente 2	Madera 1	Madera 2	Madera 3	Madera 4	Madera 5	Madera 6	Robinson
2/12/83	6.26	5.81							
2/20/83				.84	1.12	3.97			1.38
3/21/83						4.5			
3/30/83							6.13	4.8	
4/06/83			.233		2.53	4.24			

Table 3.3b. Stream Gain or Loss (in CFS/mile). Reach numbers refer to Plate 1.

Canyon	Reach	Date	$Q_u - Q_d$ (cfs)	L (mile)	Gain (cfs/mi)
A.C.	AC 1-2	1/12/83	.45	1	.45
Madera	MC 2-3	2/20/83	.28	.45	.62
Madera	MC 3-4	2/20/83	2.85	2.39	1.2
Madera	MC 4-5	3/21/83 and 3/30/83	1.63	1.25	1.3
Madera	MC 5-6	3/30/83	-1.33	2.88	.46

Precipitation Data

Precipitation data have been collected at the Santa Rita Experimental Range for 60 years. Eight raingages are close enough to the mountain front to be useful in a water balance. Additionally, the Smithsonian Institution has been measuring precipitation on the top of Mount Hopkins for three years. Figure 3.1 shows raingage locations, yearly averages, and total precipitation from September 1982 through August 1983. Monthly data are included in Appendix E.

The linear relationship between precipitation and elevation has been established by Duckstein, Fogel, and Thames (1973). On the Santa Rita Experimental Range, the relationship is 1.5 inches increase per 1000 feet (Green and Martin, 1967). For the period from September 1982 through August 1983 the slope, including data from Mount Hopkins, is a 2-inch increase per 1000 feet. From this estimate, additional data may be generated by the formula:

$$E(h_1) - E(h_2) = a\Delta h \tag{3.5}$$

where E = rainfall at a given elevation [L], h = elevation [L], and a = the slope of the rainfall-elevation line (Ben-Asher, Randall, and Resnick, 1976). Data at seven locations were generated for computing volumetric rainfall in this study.

From the actual and generated data, volumetric rainfall was calculated for Madera and Robinson Canyons by the Thiessen polygon method. Table 3.4 presents the results.

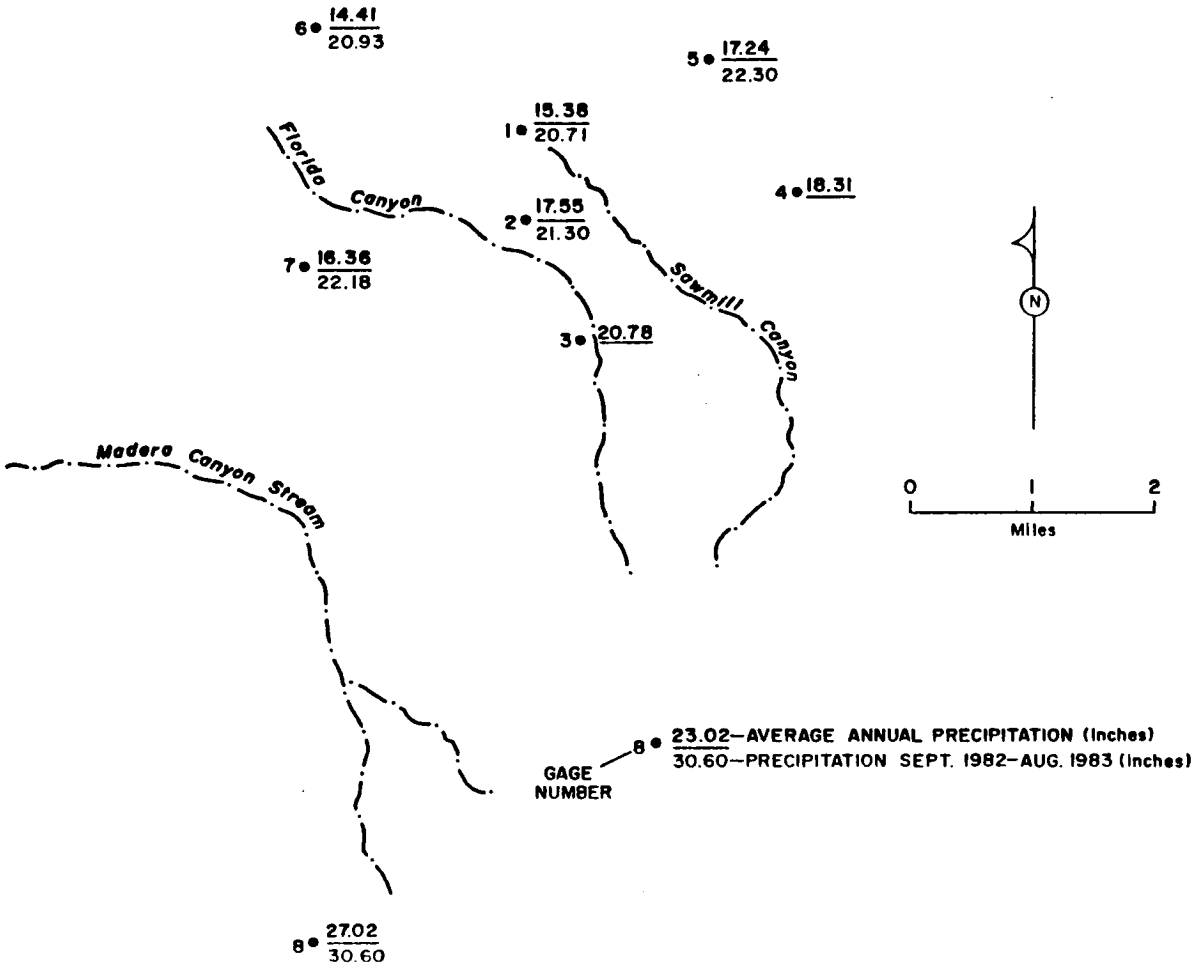

Figure 3.1. Raingage locations and annual data.

Table 3.4. Volumetric Precipitation and Evapotranspiration for September 1982 - August 1983 in Madera and Florida Canyons. Values in acre-feet, calculated using Thiessen method.

Location	Precipitation		Evapotranspiration	
Madera Canyon	Winter	6,333	Winter	2,912
	Summer	5,847	Summer	3,800
	Total	12,180	Total	6,712
Florida Canyon	Winter	2,079	Winter	961
	Summer	1,919	Summer	1,241
	Total	3,988	Total	2,202

Evapotranspiration Data

Evapotranspiration is extremely difficult to measure directly, and water balances using traditional techniques often predict no groundwater recharge: a result which often disagrees with observed water level fluctuations (Kafri and Ben-Asher, 1978). These two researchers developed a computer model to simulate recharge through mountain soils near the Santa Rita Mountains. They estimate that 54% of winter and 30-40% of summer precipitation is recharged. The summer value may be high, perhaps due to an artifact in the model. These figures imply that evapotranspiration amounts to approximately 46% of winter and 60-70% of summer precipitation. Evapotranspiration estimates based on these figures are listed in Table 3.4.

CHAPTER 4

HYDROGEOCHEMISTRY FOR THE SANTA RITA MOUNTAINS

This chapter evaluates the ground-water chemistry of Madera Canyon. Graphical methods, equilibrium considerations, and stable isotopes are tested as a means to determine if recharge occurs by deep circulation or by shallow circulation and streamflow infiltration. Additionally, the ground-water chemistry of water from minor canyons in the study area is described.

Madera Canyon

Chemical data from ground-water samples in Madera Canyon suggest the circulation of two types of water. Alternative interpretations are: 1) that both systems are shallow-circulating and may be interconnected, or 2) that one system is shallow-circulating and the other is deep-circulating but that the two systems may be interconnected.

Graphical Methods

Trilinear Diagrams. Figure 4.1 is a trilinear diagram of water samples from Madera Canyon. The diagram shows one water type to be high in calcium and bicarbonate and the other water type to be high in calcium and sulfate. Figure 2.1 demonstrates that sample location controls water type. The calcium bicarbonate water comes from sites on the east wall of Madera Canyon and on the alluvial fan far from the

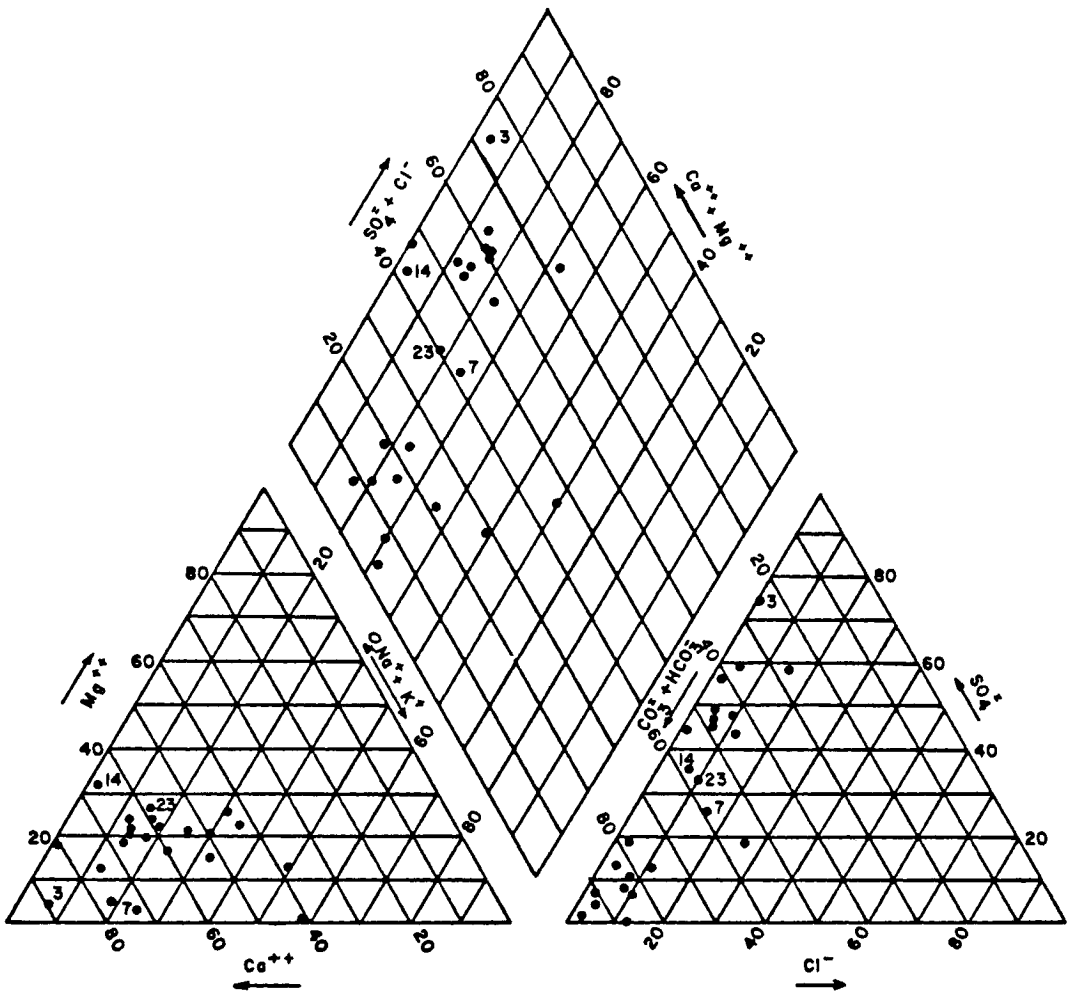

Figure 4.1. Trilinear diagram of analyses of water samples from Madera Canyon.

stream. The calcium sulfate water comes from No Name Mine (site #3) near the headwaters of Madera Canyon and from sites on the alluvial fan near the stream.

The calcium bicarbonate samples may come from either a deep- or shallow-circulating system. The relatively high sodium and potassium percentages may suggest deep circulation, but also may result from shallow circulation through the alluvial materials which presumably contain the same mineral assemblage that occurs in the bedrock at depth. Also, the high bicarbonate percentage is more indicative of shallow circulation.

The calcium sulfate samples come from No Name Mine which discharges water directly into Madera Canyon stream. At No Name Mine, calcium comprises 95% of the cations and sulfate comprises 75% of the anions in solution. As the stream flows onto the alluvial fan, the relative concentrations of calcium and sulfate have dropped to 87% and 58%, respectively, and a corresponding increase in sodium and potassium and bicarbonate is present. This suggests that in the stream the calcium sulfate water is mixing with and being diluted by the calcium bicarbonate type water. The flowlines in Figure 5.1 support this interpretation.

Mixing would be indicated further by intermediate points between the two water types on the trilinear diagram. In the central field of Figure 4.1, the Lucky Ledge (site #23) and the Bog Springs (site #7) samples plot between the calcium bicarbonate and the calcium sulfate water types, but due to their geographic location they more likely represent local, independent systems.

Evidence for mixing does appear on the anion triangle. The calcium bicarbonate samples are clustered toward the lower left corner, and the calcium sulfate samples are clustered near the upper corner. The sample from Madera Canyon Well (site #14) plots in between. Additionally, the well is at the head of the fan, a location where mixing would occur. A reasonable interpretation is that high sulfate water infiltrates at the western turn of the stream and continues to flow north underground where it mixes with the calcium bicarbonate water, thus lowering the percentage of sulfate and moving the datum point to its intermediate position.

Finger-Print Diagrams. Finger-print diagrams of samples from Madera Canyon lead to similar interpretations as the trilinear diagrams. Figure 4.2 is a finger-print diagram of analyses of water from sites located on the east flank of Madera Canyon. Calcium and bicarbonate are the dominant ions. The subparallel nature of the plots suggest that the waters have a similar origin. Also, the increase in concentration of all ions suggests that water chemistry is evolving along an underground flow path.

Figure 4.3 is a finger-print diagram of No Name Mine and sites near the Madera Canyon stream. The strongly parallel plots suggest that the samples come from the same source. Note that the calcium and sulfate concentrations decrease with distance traveled along the stream, indicating solution and mixing.

Figure 4.4 is a finger-print diagram of wells on the alluvial fan. These plots vary widely in terms of parallelism and

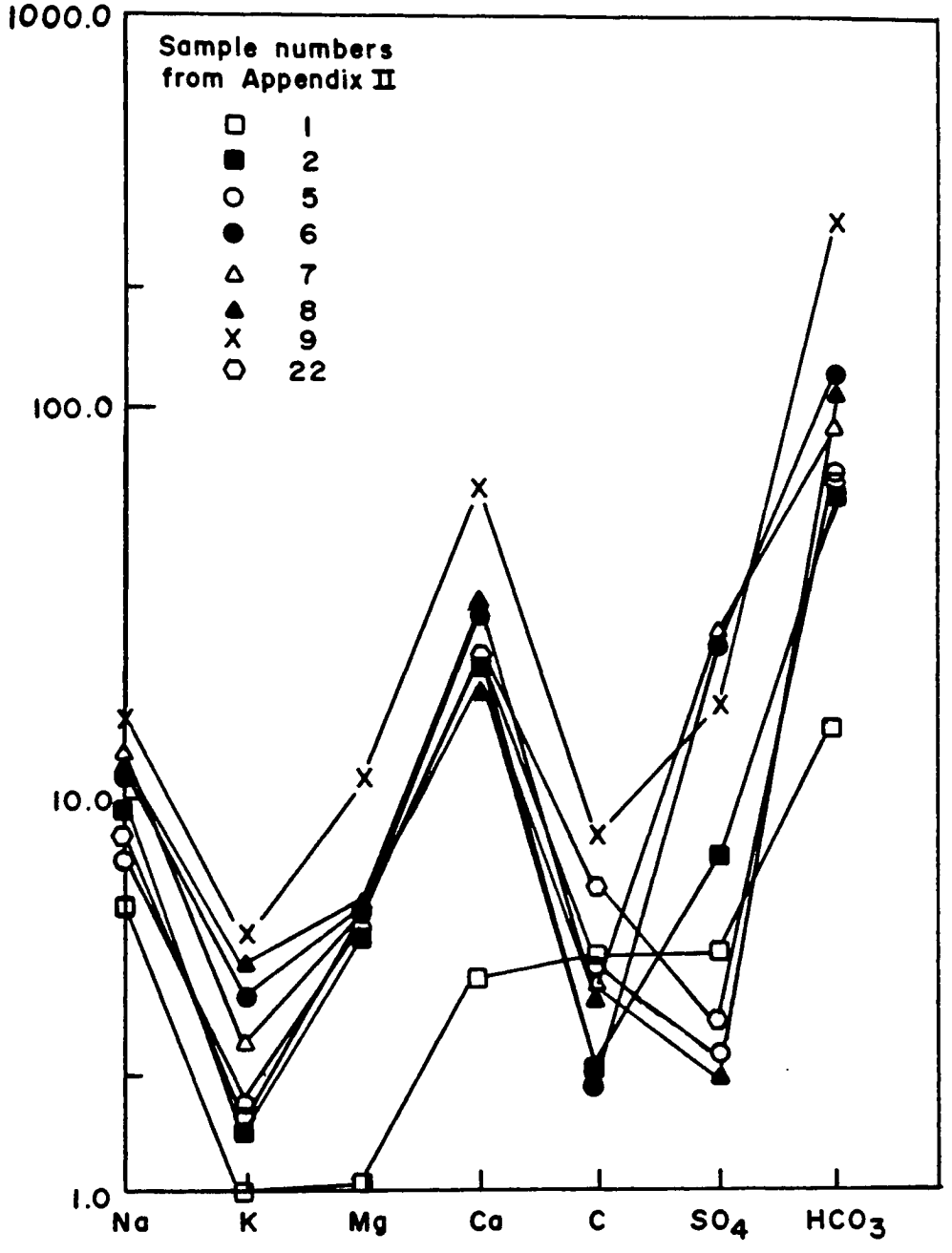

Figure 4.2. Finger-print diagrams of analyses of water samples from the east flank of Madera Canyon.

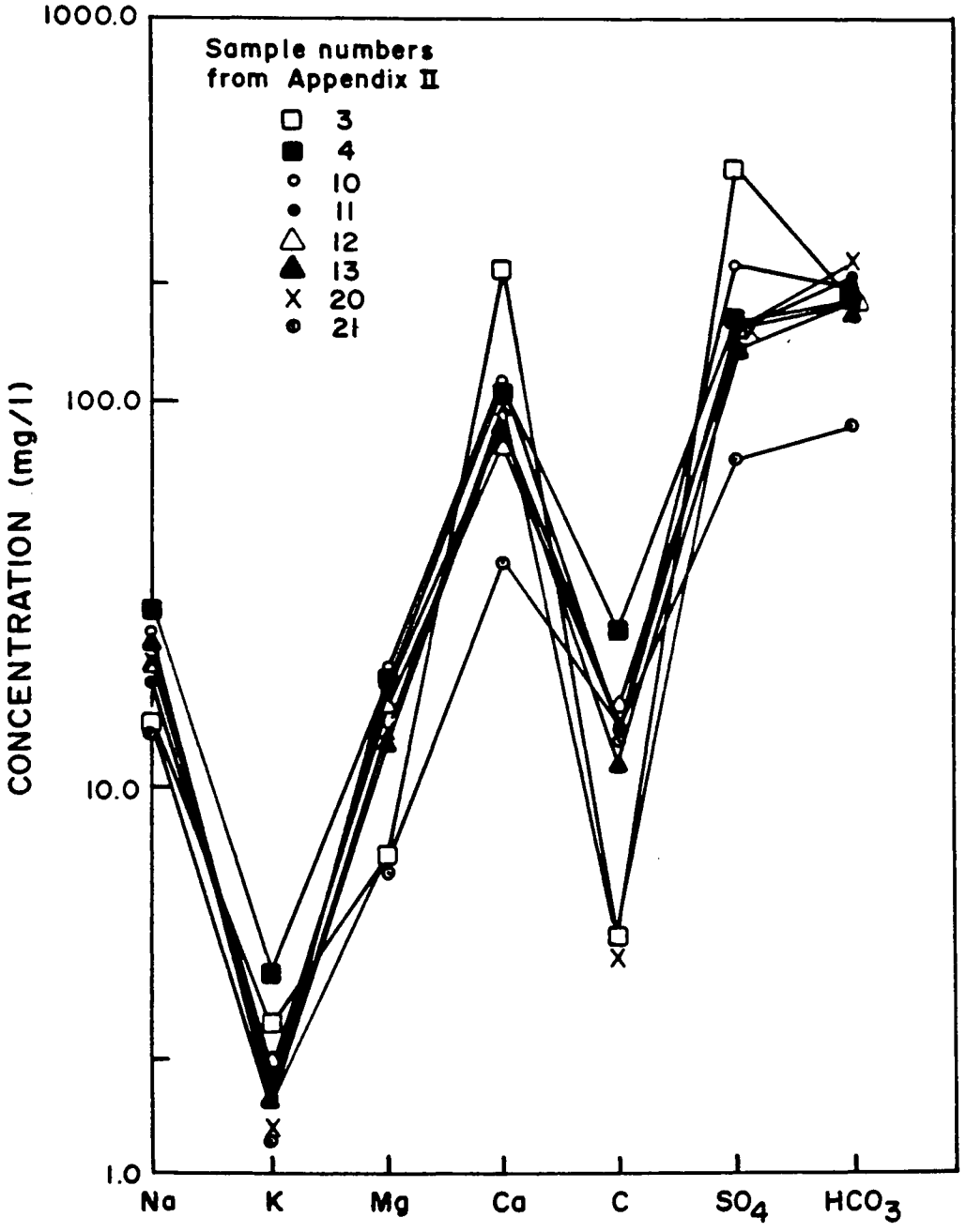

Figure 4.3. Finger-print diagrams of analyses of water samples from No Name Mine and near Madera Canyon stream.

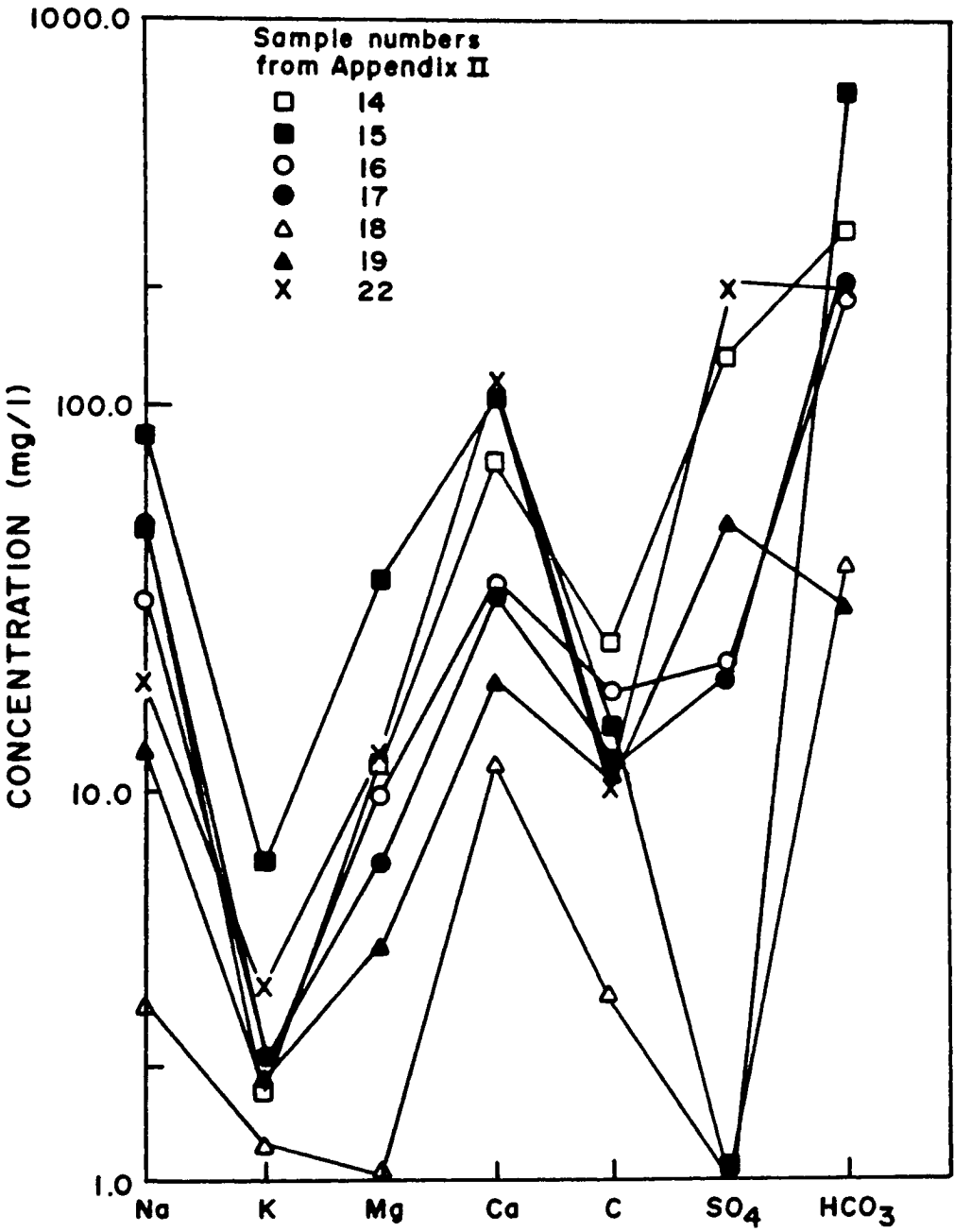

Figure 4.4. Finger-print diagrams of analyses of water samples from Madera Canyon fan.

concentrations of ions. Calcium and sodium are the dominant cations and sulfate and bicarbonate are the dominant anions.

If the two dominant water types in Figures 4.2 and 4.3 are taken as endmembers, intermediate points would suggest mixing. Madera Canyon Well, B1 (#16), and B2 (#17) are on the alluvial fan where mixing might occur. Figure 4.4 illustrates that water from these sites has intermediate concentrations of calcium and sulfate.

The finger-print diagrams lend insight into possible deep circulation or shallow circulation question. In Figure 4.3, the narrow range of concentrations imply that the flow path is relatively short or that water flows quickly through the system. The short path from the mine to the alluvial fan on the surface and from the stream to the wells in the subsurface meets both conditions. Thus, shallow circulation is again demonstrated for the calcium sulfate waters.

The wider concentration range in Figure 4.2 may indicate either deep or shallow circulation. In general, the concentration of each ion increases with distance from the top of the mountains. This is particularly noticeable in the sodium and potassium concentrations. Two probable explanations present themselves: 1) water may be circulating slowly through deep fractures allowing enough time to dissolve the large concentrations, or 2) water may be circulating quickly through the shallow alluvial material. Because the alluvial material presents a greater surface area for chemical reactions to occur, less time is needed for equal concentrations to develop.

Note two additional features from the finger-print diagrams. First, the calcium sulfate system contains higher concentrations of

most ions than the calcium bicarbonate system. This appears contradictory because one would assume lower concentrations in a shorter, shallower system. However, the high concentrations begin at No Name Mine and are diluted thereafter. The high concentrations of sulfate presumably occur from the oxidation of pyrite and other metallic sulfides which have been observed at the mine.

The second feature is the finger-print of Melendrez Well (site #15). This well is farthest from the alluvial fan and contains the largest concentrations of sodium, potassium, magnesium, chloride, and bicarbonate in the canyon. However, the sample contains no sulfate. This cannot result from precipitation of gypsum because both the sulfate and calcium concentrations are well below saturation. Plus, no corresponding reduction in calcium occurs. An explanation is that the well is not connected with the two systems and represents an entirely different flow regime. If this is the case, then all interpretations dependent on this well are brought into doubt.

Scattergrams. Scattergrams of several combinations of ions are presented in Figures 4.5-4.8. The scattergrams support the interpretations presented so far. For major ions, the scattergrams reveal a consistent pattern wherein the analyses of water from calcium bicarbonate sites plot on one relatively straight line and the water from calcium sulfate sites on another. The regression lines and correlation coefficients are included in the figures. Note that the calcium sulfate plots are less spread out due to the narrow range of concentrations.

In the plots of sodium plus potassium versus total dissolved solids, the calcium bicarbonate samples plot above the calcium sulfate

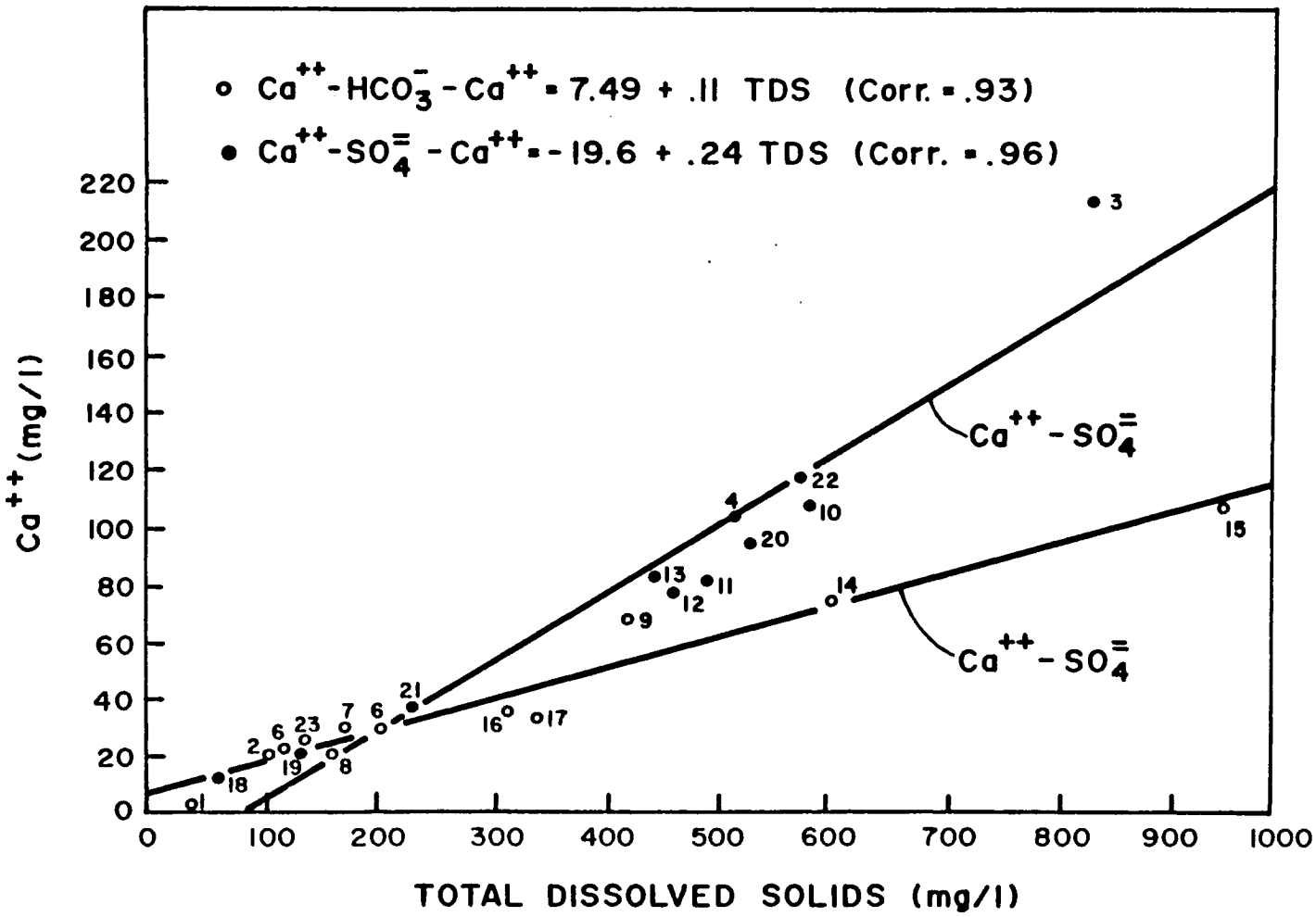

Figure 4.5. Scattergram of analyses of water samples from Madera Canyon showing regression lines for each water type, Ca^{++} vs. TDS.

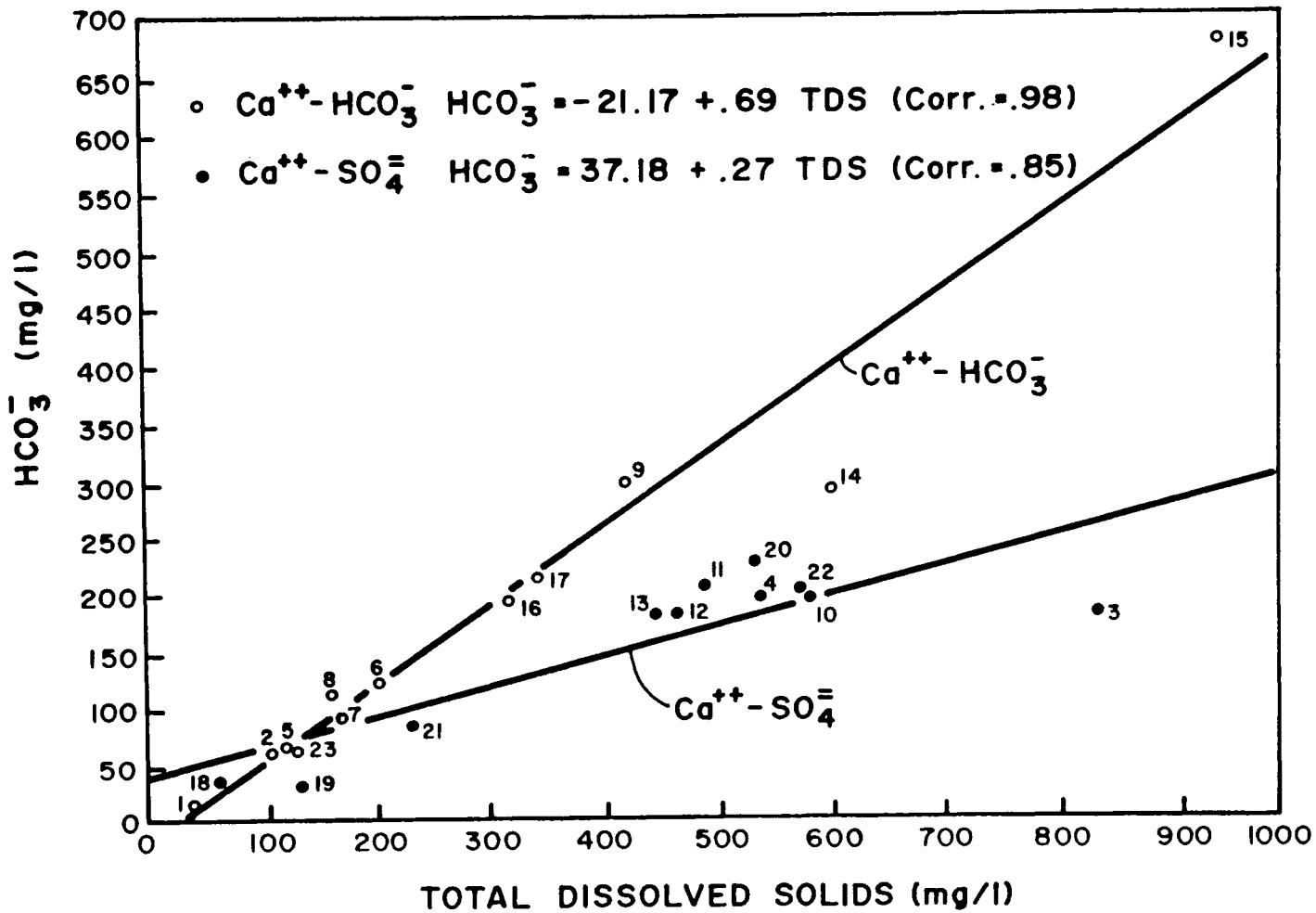

Figure 4.6. Scattergram of analyses of water samples from Madera Canyon showing regression lines for each water type, HCO_3^- vs. TDS.

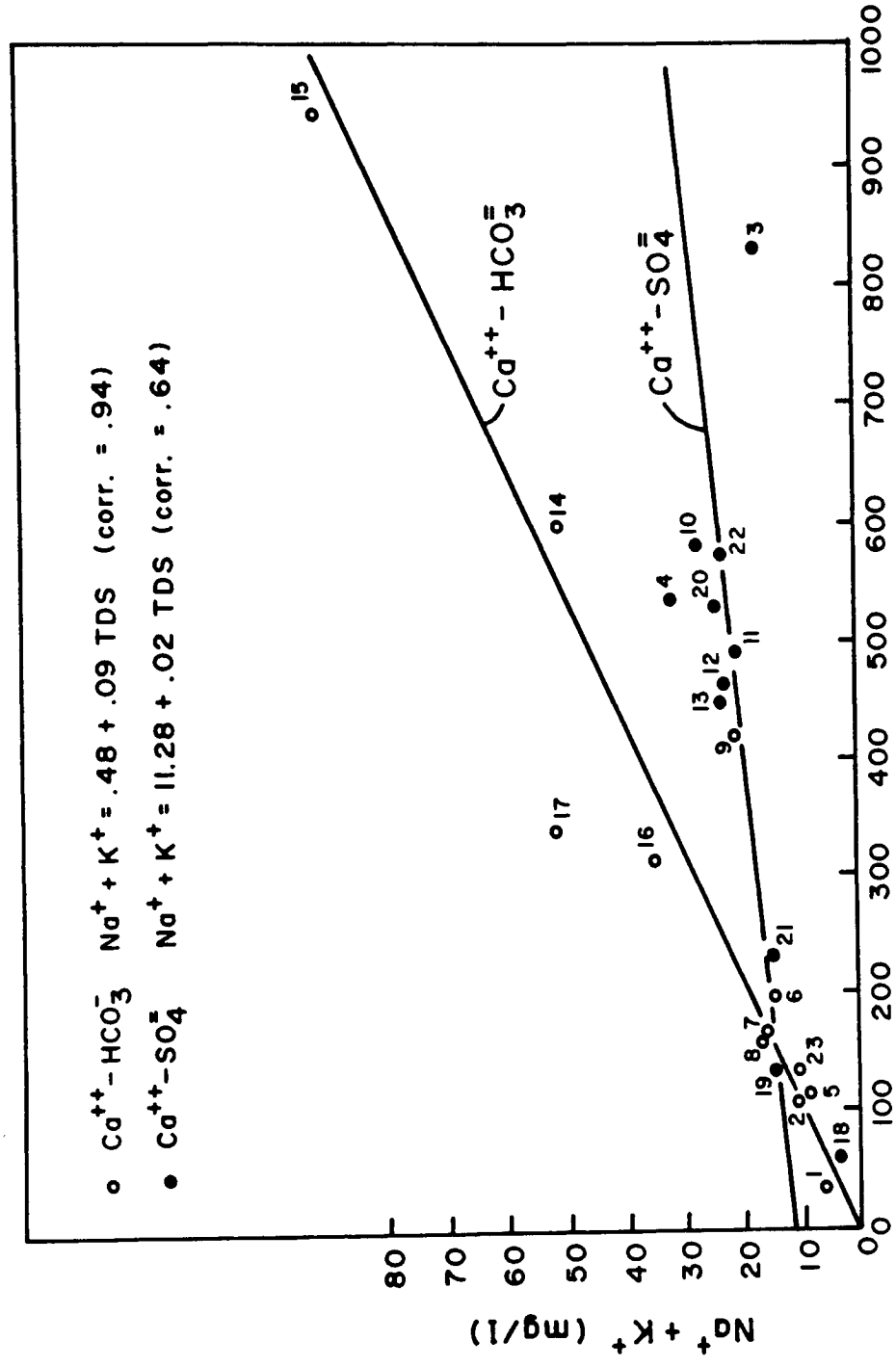

Figure 4.7. Scattergram of analyses of water samples from Madera Canyon showing regression lines for each water type, $Na^+ + K^+$ vs. TDS.

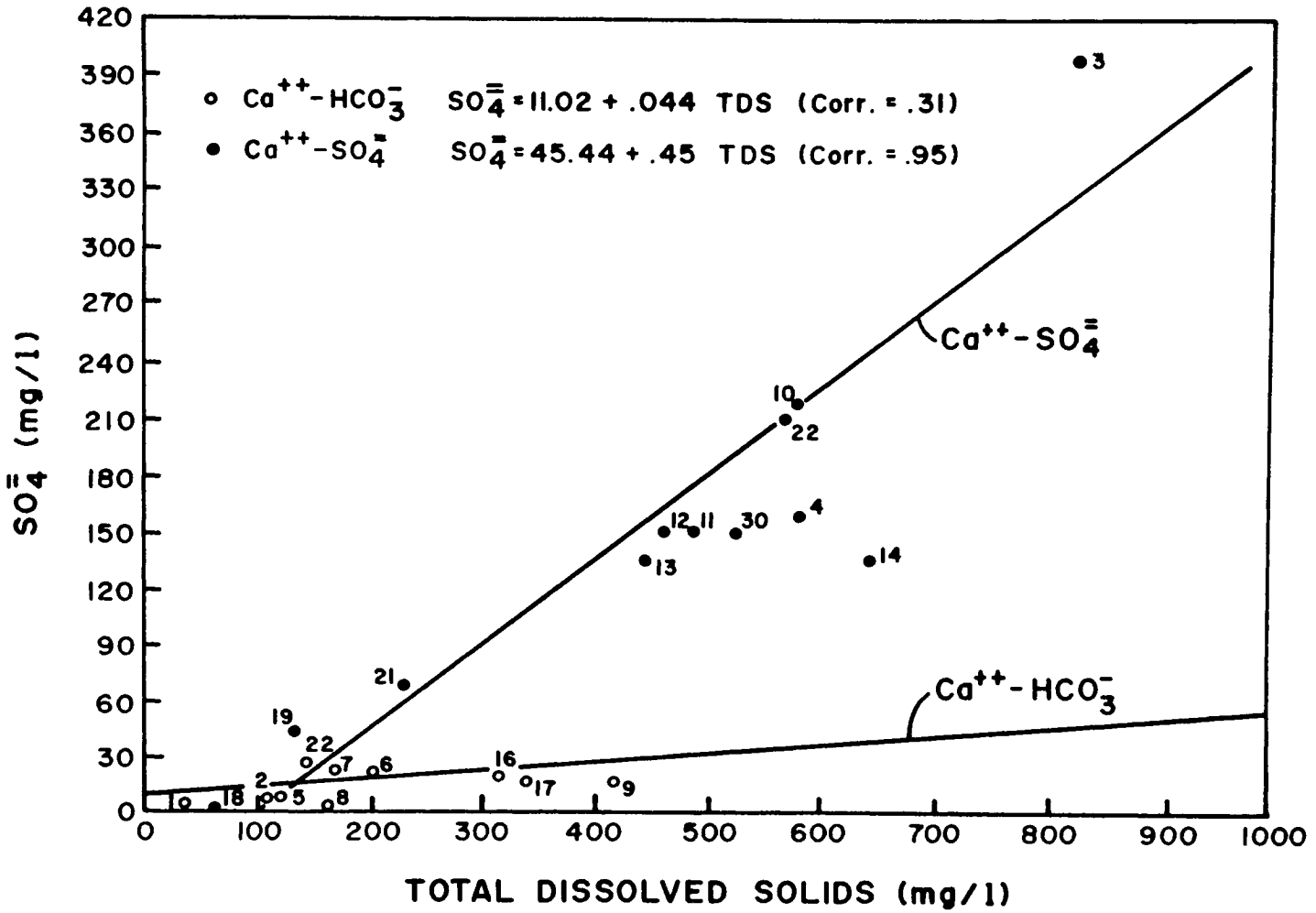

Figure 4.8. Scattergram of analyses of water samples from Madera Canyon showing regression lines for each water type, $SO_4^{=}$ vs. TDS.

samples; but in the calcium and sulfate versus total dissolved solids plots, the calcium sulfate samples plot above the calcium bicarbonate samples. This is predictable given the chemistry of the two water types.

Mixing is suggested by the scattergrams. In every plot the cluster of points from the calcium sulfate wells on the alluvial fan is shifted toward the calcium bicarbonate line. The sodium plus potassium versus total dissolved solids plot shows this trend most clearly. Thus, the calcium sulfate water appears to be mixing with the calcium bicarbonate water resulting in intermediate concentrations. In every case, Madera Canyon Well is the point that shifts the most.

In three of the diagrams the regression line intercepts the y-axis at a negative value. This is not logical and seems to result from the influence of the sites with the highest concentrations, Melendrez Well for the calcium bicarbonate samples and No Name Mine for the calcium sulfate samples. If these sites are removed, the regression lines intercept the y-axis much closer to zero.

Equilibrium Analysis

Theoretical Considerations. Chemical equilibrium considerations aid interpretation of ground-water movement. As precipitation infiltrates through the soil zone, it dissolves carbon dioxide (CO_2) which originates from the decay of organic matter and the respiration of roots. The process produces carbonic acid (H_2CO_3). The carbon dioxide charged water continues to infiltrate and the carbonic acid begins to dissolve the minerals that it contacts. The water therefore

becomes concentrated with cations contained in the minerals, and the mineral surfaces become altered, generally to clay minerals. Note that organic acids in the soil also play a minor role in dissolving mineral surfaces.

The extent to which dissolution and alteration continue depends on the chemical equilibrium thermodynamics of the specific water-mineral reactions. If the equilibrium constants of particular mineral-water reactions are known, diagrams can be drawn which plot the ratios of the activities of calcium, sodium, and potassium to the hydrogen ion activities against SiO_2. Stability diagrams can then be drawn to indicate which mineral will be in equilibrium with a given solution.

As recharging water comes into contact with feldspars calcium, sodium and potassium cations are released. In general, the feldspar is altered first to gibbsite, then to kaolinite, and finally to muscovite or montmorillonite. When the solution reaches equilibrium with the host feldspar, muscovite or montmorillonite is the only remaining secondary mineral.

These properties suggest that an estimate of the relative residence time of a water sample may be made from where its analysis plots on the stability diagram. For example, an analysis plotting in the gibbsite field may be relatively younger than an analysis plotting in the muscovite field.

Note that several factors may lead to errors in interpreting chemical equilibrium data. For example, the model presented above assumes the water reacts with only one feldspar with a known composition. However, in nature the water encounters several feldspars of

varying compositions, as well as many accessory minerals. Furthermore, to be most accurate in interpreting chemical equilibrium data, an analysis for aluminum concentration should be made, and this is rarely done. Also, pressure and temperature conditions should be known but rarely are. All these complications may lead to misleading plots on the stability diagrams. Therefore, conclusions based on equilibrium considerations may supplement those derived from other techniques, but should not be given too much weight by themselves.

Garrels and Christ (1965), Drever (1982), and Hem (1970) discuss the theoretical details of water-mineral equilibria, and Tardy (1971) and Feth, Robertson, and Polzer (1964) discuss granitic rocks in particular.

Equilibrium and Madera Canyon Samples. In Madera Canyon, rock-forming minerals include anorthite, albite, orthoclase, microcline, and quartz. Accessory minerals include biotite, amphiboles, pyroxenes, and chlorite. Kaolinite and montmorillonite dominate as weathering products. Table 4.1 presents common reactions involving these minerals and the equilibrium constant for each reaction. Figures 4.9-4.11 present stability diagrams for each major cation. Both Table 4.1 and Figures 4.4-4.11 are based on Tardy (1971).

The stability diagrams present some very interesting relationships. In general samples taken from springs have analyses which plot in the kaolinite field, and samples taken from wells along the mountain front have analyses which plot in the montmorillonite or microcline field. This finding suggests that the ground-water chemistry is evolving toward equilibrium with the host feldspars.

Table 4.1. Possible Reactions and Equilibrium Constants for Common Minerals Found in the Study Area (Tardy, 1971).

Mineral	Reaction
Microcline-kaolinite	$2\log[H_4SiO_4] + \log[K^+]/[H^+] = -2.45$
Microcline-gibbsite	$3\log[H_4SiO_4] + \log[K^+]/[H^+] = -7.28$
Microcline-muscovite	$3\log[H_4SiO_4] + \log[K^+]/[H^+] = -5.93$
Muscovite-kaolinite	$\log[K^+]/[H^+] = 4.52$
Muscovite-gibbsite	$3\log[H_4SiO_4] + \log[K^+]/[H^+] = -9.96$
Albite-montmorillonite	$5\log[H_4SiO_4] + 3\log[Na^+]/[H^+] = +7.90$
Albite-kaolinite	$2\log[H_4SiO_4] + \log[Na^+]/[H^+] = +0.93$
Albite-gibbsite	$3\log[H_4SiO_4] + \log[Na^+]/[H^+] = -3.90$
Anorthite-montmorillonite	$4\log[H_4SiO_4] + 3\log[Ca^{+2}]/[H^+] = +65.37$
Anorthite-kaolinite	$\log[Ca^{+2}]/[H^+] = +16.41$
Anorthite-gibbsite	$2\log[H_4SiO_4] + \log[Ca^{+2}]/[H^+] = +6.78$
Montmorillonite-Na-kaolinite	$4\log[H_4SiO_4] + \log[Na^+]/[H^+] = -9.31$
Montmorillonite-Na-gibbsite	$11\log[H_4SiO_4] + \log[Na^+]/[H^+] = -43.11$
Montmorillonite-Ca-kaolinite	$8\log[H_4SiO_4] + \log[Ca^{+2}]/[H^+] = -15.70$
Montmorillonite-Ca-gibbsite	$22\log[H_4SiO_4] + \log[Ca^{+2}]/[H^+] = -83.28$
Kaolinite-gibbsite	$\log[H_4SiO_4] = -4.82$

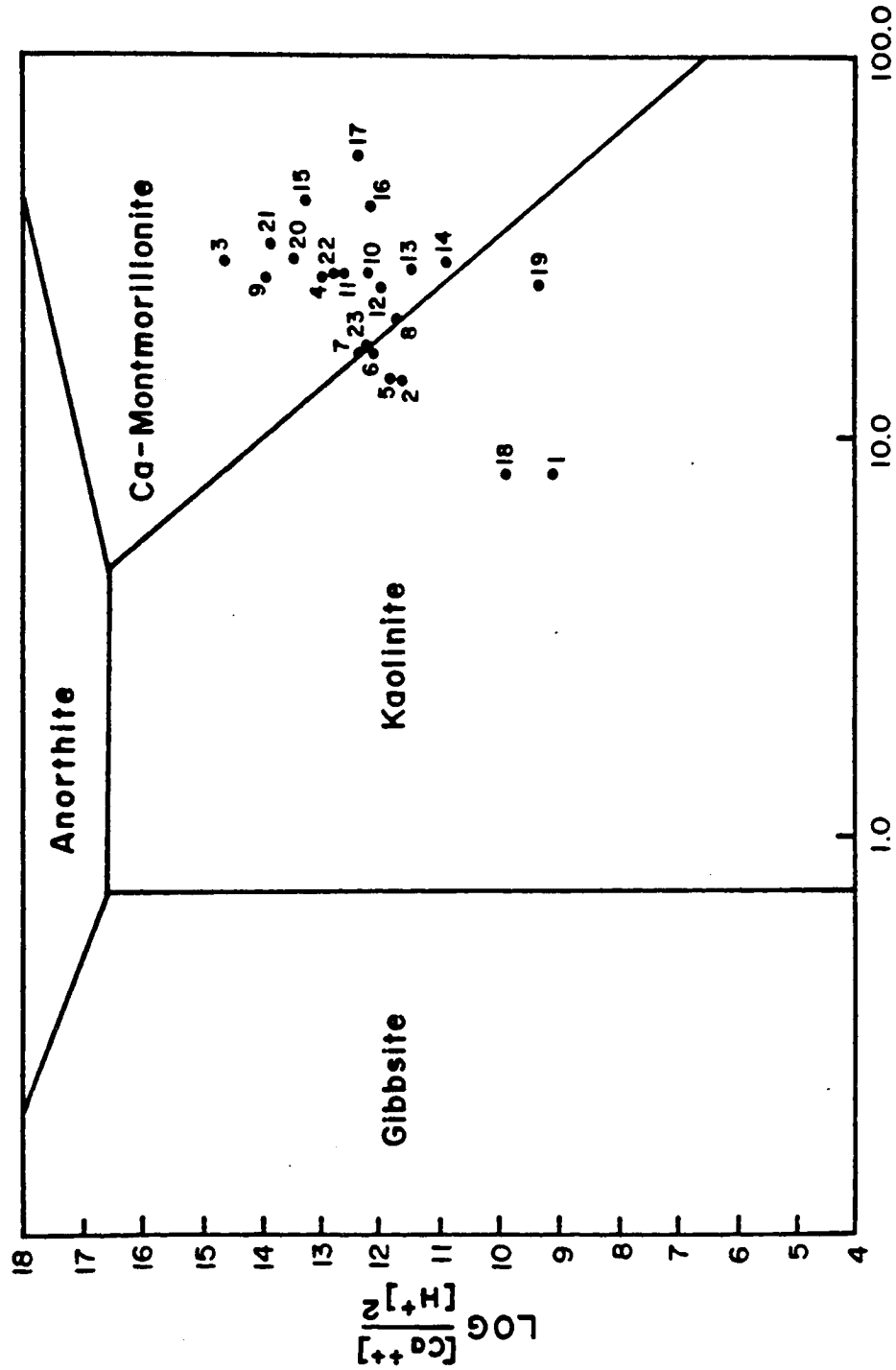

Figure 4.9. Stability diagram of log $[Ca^{++}]/[H^+]^2$ versus log $[SiO_2]$ for analyses of water samples from Madera Canyon (Tardy, 1971).

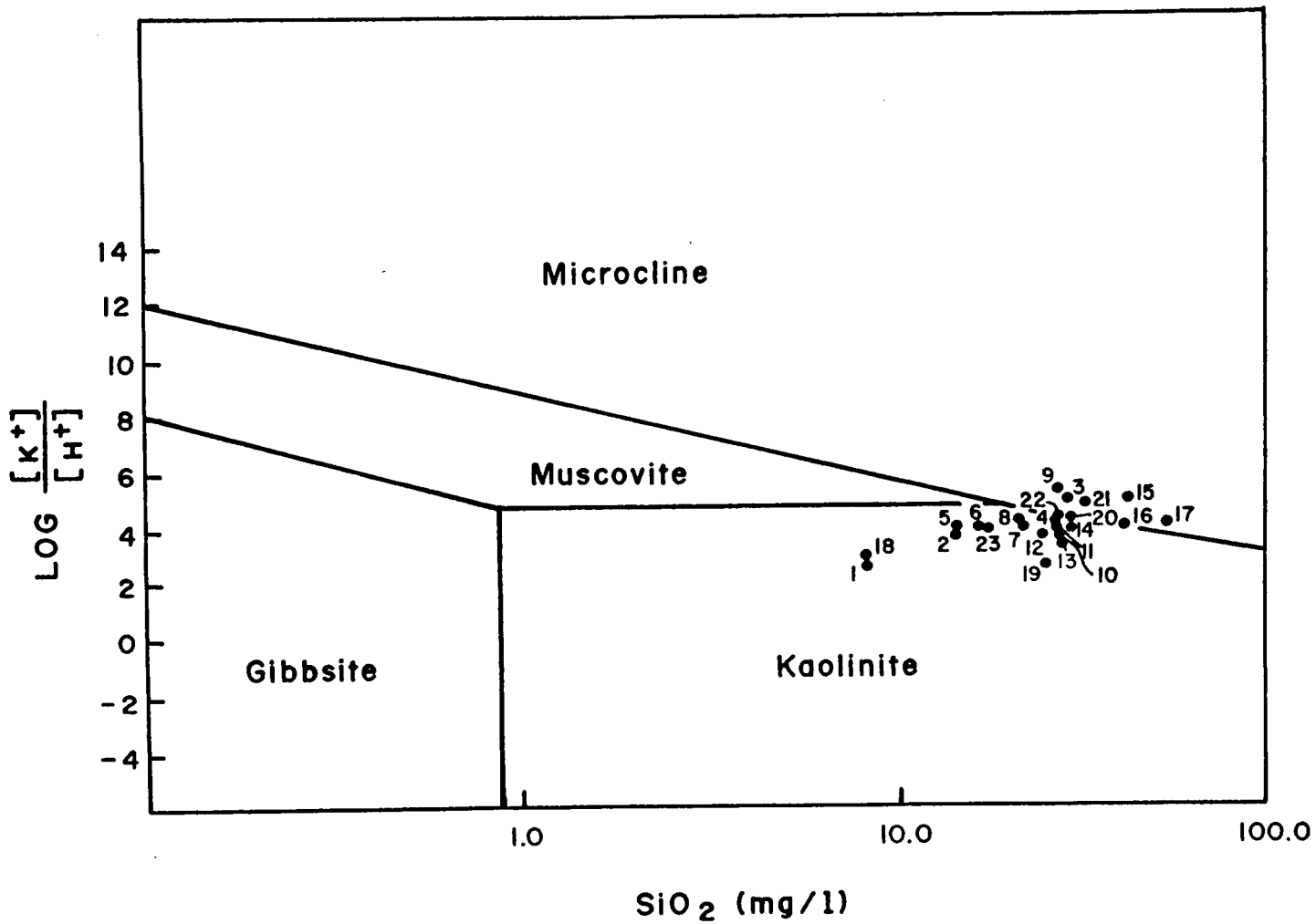

Figure 4.10. Stability diagram of log $[K^+]/[H^+]$ versus log $[SiO_2]$ for analyses of water samples from Madera Canyon (Tardy, 1971).

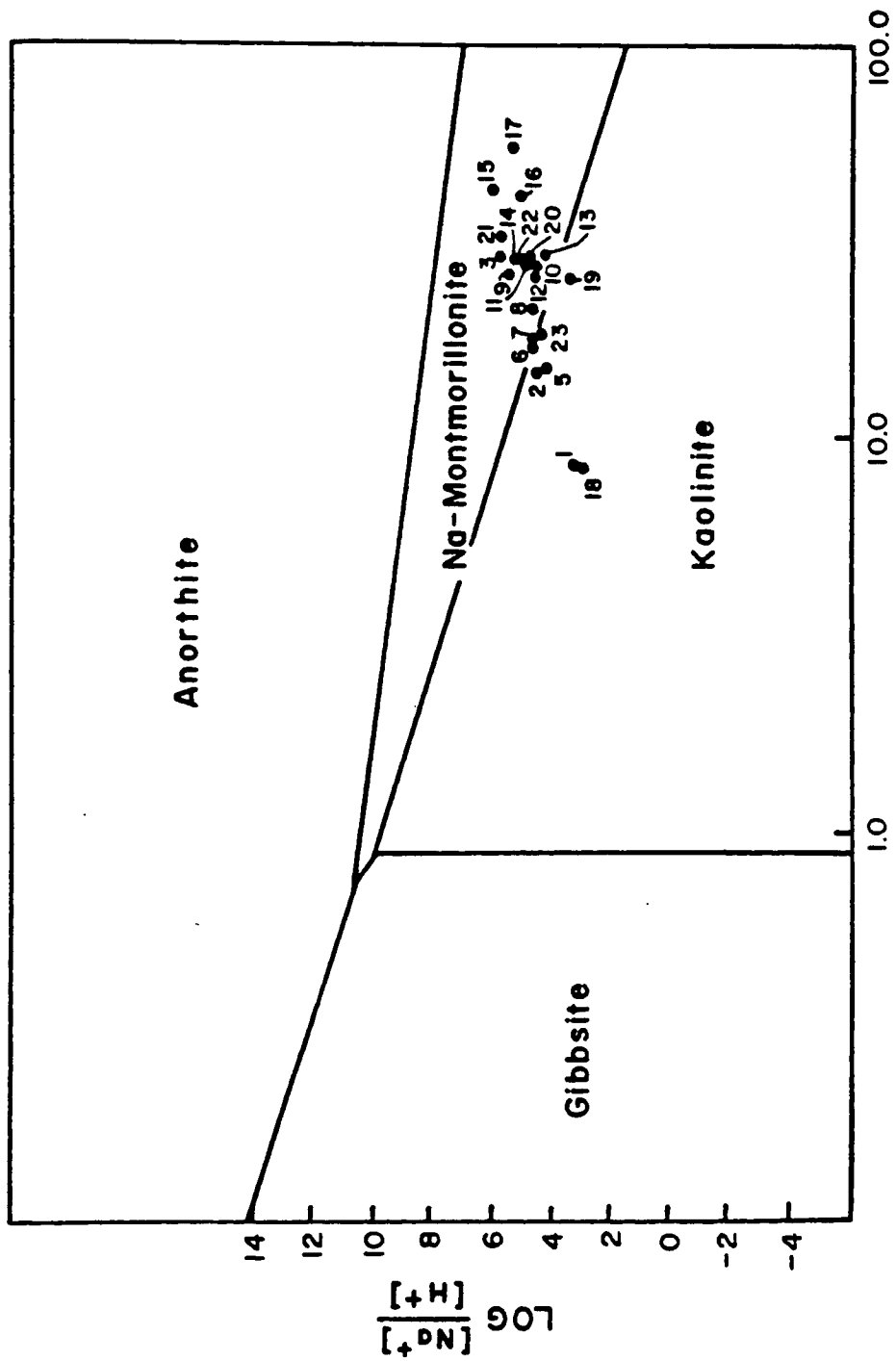

Figure 4.11. Stability diagram of log $[Na^+]/[H^+]$ versus log $[SiO_2]$ for analyses of water samples from Madera Canyon (Tardy, 1971).

Several particular analyses are worth noting. First, in each figure, the plot from the analysis of Bellows Spring (#1), which is the highest spring in the canyon, suggests that it is least evolved. Similarly, the plot from the analysis of Melendwrez well (#15), which is located farthest out on the alluvial fan, suggests that it is most evolved toward chemical equilibrium. Also, the analysis from Madera Canyon Stream (#22) plots in an intermediate position between these two extremes in each figure.

Analyses from the samples from Kent (#5), Silvester (#6), Bog (#7), and Below Dutch John (#9) springs plot along a path leading from the kaolinite field to the montmorillonite field in Figures 4.9 and 4.10, and in Figure 4.10 the path remains in the kaolinite field. This is strong evidence that the ground-water chemistry is evolving toward equilibrium because the springs occur in close proximity along a line with a loss of elevation between each (Plate 2).

The stability plots support the interpretations given so far. Water may either be circulating slowly through deep fractures resulting in the relatively high concentrations of cations, or it may be circulating through shallow alluvial materials whose greater surface area promotes more rapid dissolution.

Isotopic Analysis of Mountain-Front Recharge

Theoretical Considerations. Isotopes of an element have different numbers of neutrons in their nuclei and thus have different masses. Because of the mass differences, the lighter elements have higher vibrational frequencies and thus form weaker chemical bonds than

the heavier isotopes. The weaker bonds cause the lighter isotopes to be segregated under certain thermodynamic processes. The segregation of lighter isotopes from heavier isotopes is known as fractionation.

Fractionation takes place in the atmosphere separating deuterium from hydrogen and oxygen-18 from oxygen-16. Processes in the atmosphere which fractionate hydrogen and oxygen include evaporation and condensation. Due to the weaker bonds, the lighter isotopes evaporate more readily than the heavier isotopes and thus the lighter isotopes enrich the vapor phase. Similarly, during condensation, the heavier isotope enriches the liquid phase.

Inasmuch as air temperature affects evaporation and condensation, temperature gradients in the atmosphere also cause fractionation. Warmer temperatures cause the lighter isotope to stay in the vapor phase and lower temperatures cause the heavier isotope to condense preferentially. These properties suggest that precipitation which falls at high elevations will have a higher concentration of the lighter isotope than that precipitation which falls at low elevations. Also, because temperatures are cooler in the winter, precipitation will falls during the winter will tend to be isotopically lighter than that which falls during the summer. Note from equation (3.2) that the isotopic value of a sample becomes more negative as the ratio of the light isotope to the heavy isotope increases.

Two final factors which influence the isotopic content of water in an area must be addressed. First, the "continental" effect occurs as a mass of moist air moves across a continent. Inasmuch as the heavier isotopes condense and precipitate more readily than the lighter

isotopes, the moisture will tend to be enriched in the lighter isotopes as the air mass moves across a continent. Similarly, the same effect occurs as an individual storm proceeds along its course. Namely, the moisture remaining in the vapor phase becomes isotopically lighter.

The fractionation properties of hydrogen and oxygen have made them useful as environmental tracers. Craig (1960) studied world-wide rainfall data and found a linear correlation between the concentrations of deuterium and oxygen-18. Ground-water data which plot near his regression line suggest that the water has a meteoric origin and subsequently infiltrated before appreciable evaporation took place. Except for unusual thermal or geochemical conditions, isotope values remain constant after the water has infiltrated. Therefore, because isotope concentrations are dependent on elevation and remain constant after infiltration, they may be used to estimate the recharge elevation.

Studies on several continents have documented the isotope-elevation relationship. For example, in Nicaragua, Payne and Yurtsever (1974) found the average gradient of oxygen-18 to decrease 0.87% per 1000 ft (2.6% per 1000 m) increase in elevation. Fontes and Zuppi (1974) calculated the isotope gradient of oxygen-18 in central Italy to be between -1.65% and 0.52% per 1000 ft (-5.38% and -1.7% per 1000 m) increase in elevation. Their values were seasonally dependent.

In the Tucson basin Olsen (1982) and Mohrbacher (1983) used isotopic data and major ion data to distinguish between deep-circulating and shallow-circulating recharge. They discovered isotopically light water to be associated with major faults and high concentrations of sodium and sulfate, which suggests deep circulation. Also,

isotopically heavy water was associated with stream channels and high concentrations of calcium and bicarbonate, suggesting shallow circulation. Their values for deuterium and oxygen-18 range approximately from -60 $^{o}/_{oo}$ to -80 $^{o}/_{oo}$ and -7.5 $^{o}/_{oo}$ to -11.8 $^{o}/_{oo}$.

Thorne (1981) studied recharge in the Tucson Mountains and concluded that recharge cannot be traced with stable isotope data because the Santa Cruz river is too close and masks any significant associations. His oxygen-18 values range from -7.3 $^{o}/_{oo}$ to -8.6 $^{o}/_{oo}$. Turner (1984) collected oxygen-18 data from several mountain ranges in the Tucson basin. His results appear in Table 4.2 and Figure 4.12. He took his samples from springs at approximately 2000 feet and 7000 feet in elevation. His values range from -8.4 $^{o}/_{oo}$ to -13.0 $^{o}/_{oo}$. At each elevation, the more negative values suggest a high elevation of recharge, but the wide spread of the data bring their usefulness into doubt.

Gallaher (1979) studied the distribution of oxygen-18 in the Tucson basin. He concluded that the distribution was due to the location of recharge zones and the ground-water flow patterns. Concerning recharge, his data suggested that mountain-front recharge occurs along the Santa Catalina, Tanque Verde, and Rincon mountain fronts. Furthermore, winter precipitation is the predominant source of ground-water recharge in the basin.

Smalley (1984) studied isotope data from near Safford, Arizona and calculated the isotope-elevation gradient for deuterium to be -2.8 $^{o}/_{oo}$ per 1000 feet increase in elevation (-9.1 $^{o}/_{oo}$ per 1000 m) and for oxygen-18 to be -0.32 $^{o}/_{oo}$ per 1000 ft increase in elevation (-1.05

Table 4.2. Unpublished Isotope Data from the Tucson Basin (Turner, 1983).

Location	$\delta^{18}O$ (‰)	Elevation (ft)	Mountain Range
Manning Camp	-12.2	7920	Rincon
Italian	-13.0	8000	Rincon
Unnamed	-11.1	8160	Rincon
Devil's Bathtub	-10.0	7540	Rincon
Spud Rock	-11.4	7700	Rincon
Deer Head	-11.7	7540	Rincon
Bell	- 9.2	6480	Santa Rita
Bellows	- 8.7	8240	Santa Rita
Baldy	-11.2	8800	Santa Rita
Macbeth	-10.2	7120	Santa Rita
Sprung	- 9.9	6960	Santa Rita
Stilb	-11.1	2740	Santa Catalina
Stillwell	- 8.8	2880	Santa Catalina
Barrel	-11.1	2800	Santa Catalina
Gibbon	-10.2	2800	Santa Catalina
Agua Caliente	- 9.5	2780	Santa Catalina
Madrona	- 9.1	3680	Santa Catalina
Box	-10.3	7120	Santa Catalina
Pigeon	-10.5	8240	Santa Catalina
Lemman	-10.4	8400	Santa Catalina
Bill Williams	-10.2	8640	Santa Catalina

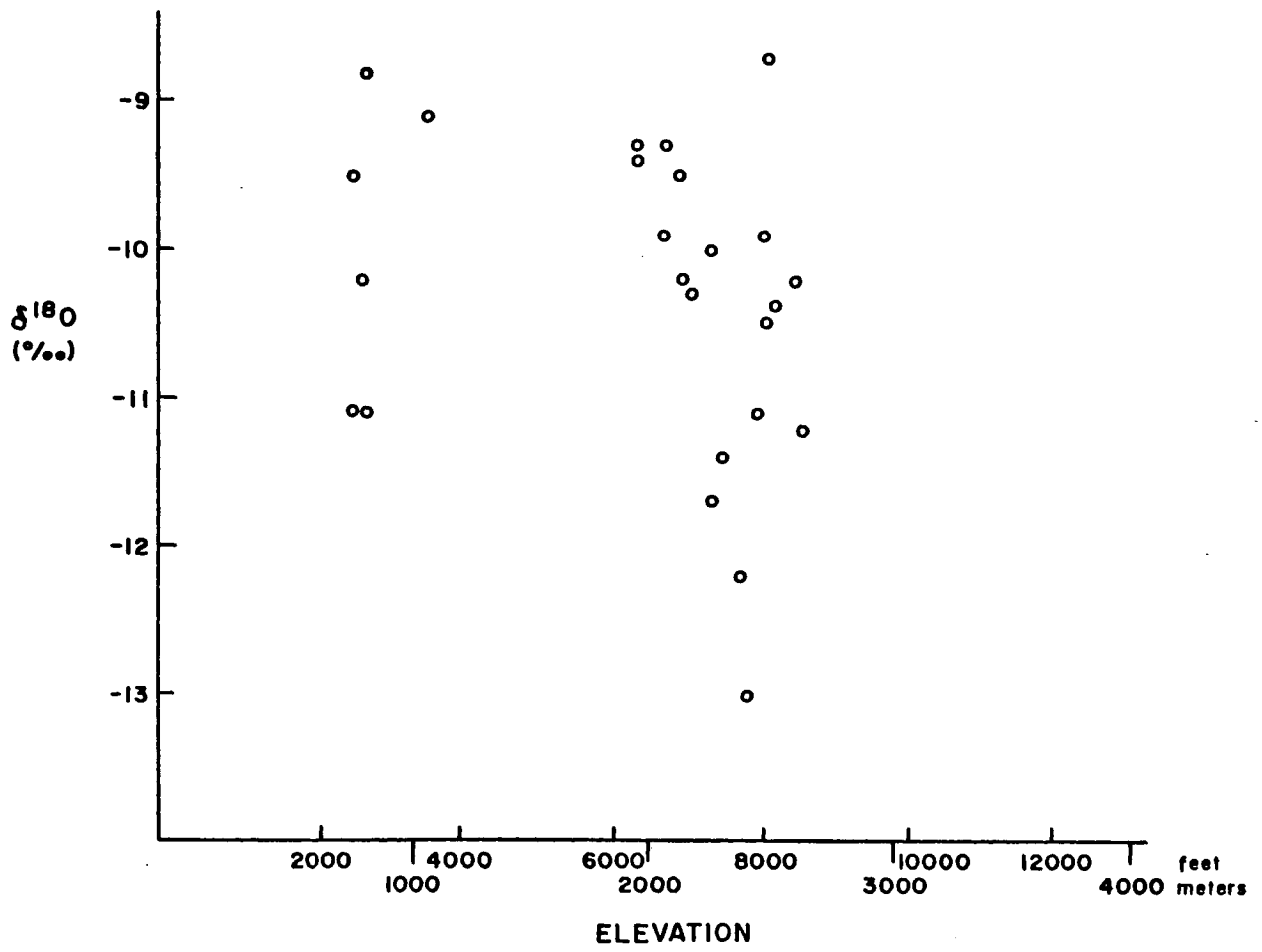

Figure 4.12. Unpublished isotope data from the Tucson basin. (Turner, 1983)

‰ per 1000 m). His values range from -60 ‰ to -85 ‰ for deuterium and from -9.5 ‰ to -12.5 ‰ for oxygen-18.

Finally, the general relationships presented here have several exceptions. Although isotope content is related to elevation, the concentration at a given location represents an average value of precipitation which has fallen over a range of elevations. And, although no evaporation takes place in the subsurface, other circumstances can influence the isotopic content of the ground water. Water-mineral reactions, unusually high pressures and temperatures, climatic dependent factors which change through time, all effect the isotopic content of the ground water.

Isotopic Analysis of the Santa Rita Mountain Samples. Thirty-one samples were taken from wells, springs, mines, and streams in the Santa Rita Mountains for isotopic analysis. A plot of oxygen-18 versus deuterium is shown in Figure 4.13. Note that the data fall near the meteoric line of Craig (1960) which suggests that the water originated as rainfall.

Figures 4.14 and 4.15 present plots of oxygen-18 and deuterium versus elevation and include regression lines and correlation coefficients. The isotope values range from -54.6 ‰ to -77.0 ‰ for deuterium and -5.1 ‰ to -10.5 ‰ for oxygen-18. The regression lines show the isotope-elevation gradient is -2.6 ‰ for deuterium and -0.3 ‰ for oxygen-18 for every 1000 foot increase in elevation (-8.54 ‰ and -0.98 ‰ per 1000 m, respectively). The lines are drawn only for the samples taken from springs because samples from wells necessarily have their source in higher elevations, and give

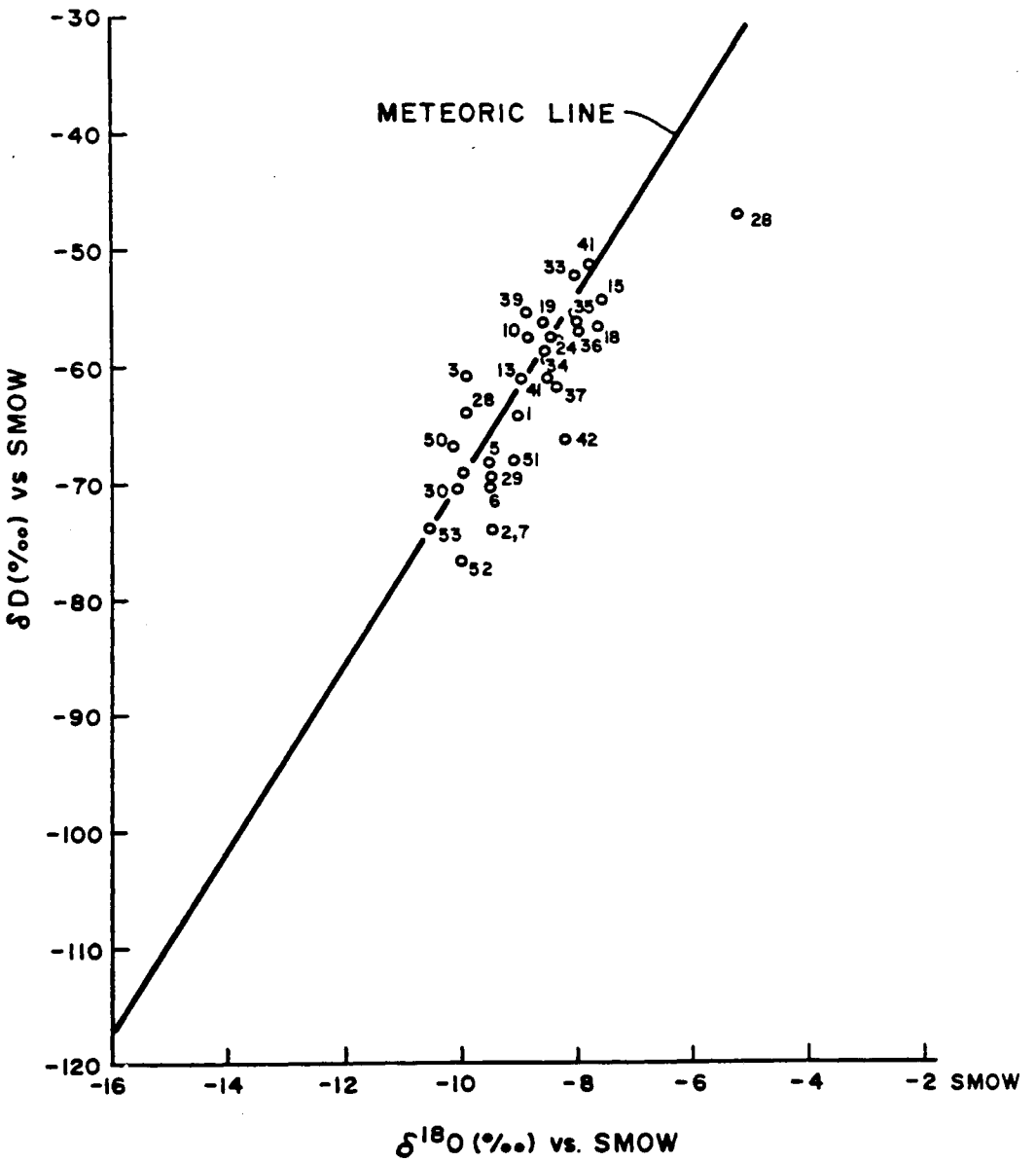

Figure 4.13. Isotope values compared with meteoric line of Craig (1960).

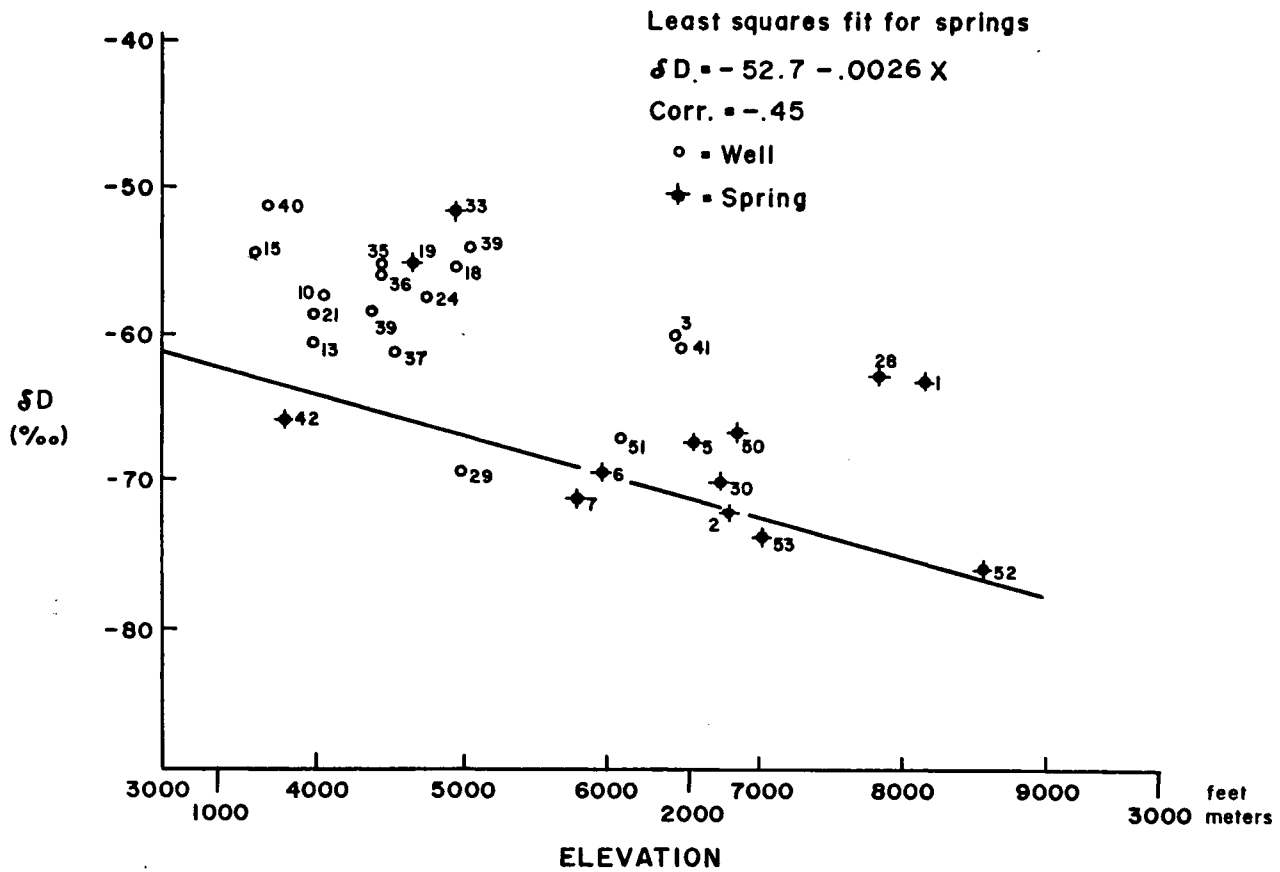

Figure 4.14. δD (^{o}/oo) vs. elevation.

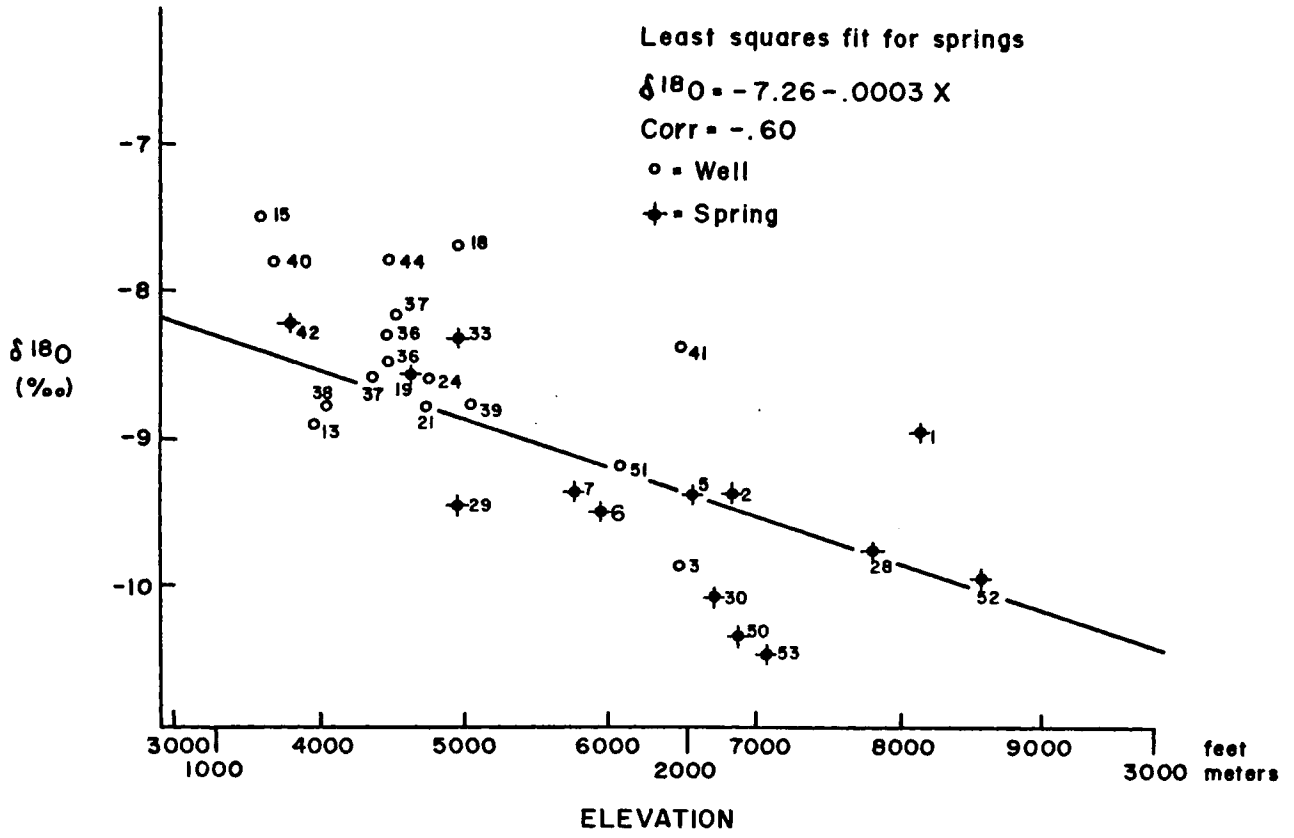

Figure 4.15. $\delta^{18}O$ ($^{o}/oo$) vs. elevation.

misleading results. The relatively wide scatter of the data about the regression lines results in correlation coefficients of -0.45 and -0.66. However, several of the sample sites discharge over large areas and are subjected to evaporation. If these samples were removed, the isotope-elevation relationship would improve.

None of the plots demonstrates evidence of deep circulating recharge: All ground-water samples from low elevations have low negative values and all ground-water samples from high elevations have high negative values. The broad range of values suggests that recharge takes place at several elevations and thus results from shallow circulation. Because some of the samples were taken from large diameter wells, the water may have been subjected to evaporation. In this event, any recharge which does occur at high elevations may be masked.

Comparison of Isotopic Data. As mentioned above, Smalley (1984) studied isotope-elevation relationships near Safford, Arizona. Figures 4.16 and 4.17 present his data and the data from this study as well as the respective regression lines. For both deuterium and oxygen-18, the Safford values are more negative than the Santa Rita values at all elevations. Several possibilities may explain this. First, if the Safford area is uniformly cooler than the Santa Rita study area, then samples from there should have more negative values. Second, because most of his samples were collected between late winter and early summer, they probably represent cooler winter precipitation and are thus enriched in the lighter isotope. Samples from the Santa Ritas were collected throughout the year and any seasonal effect is therefore masked. Finally, as rainfall in an area increases, less of

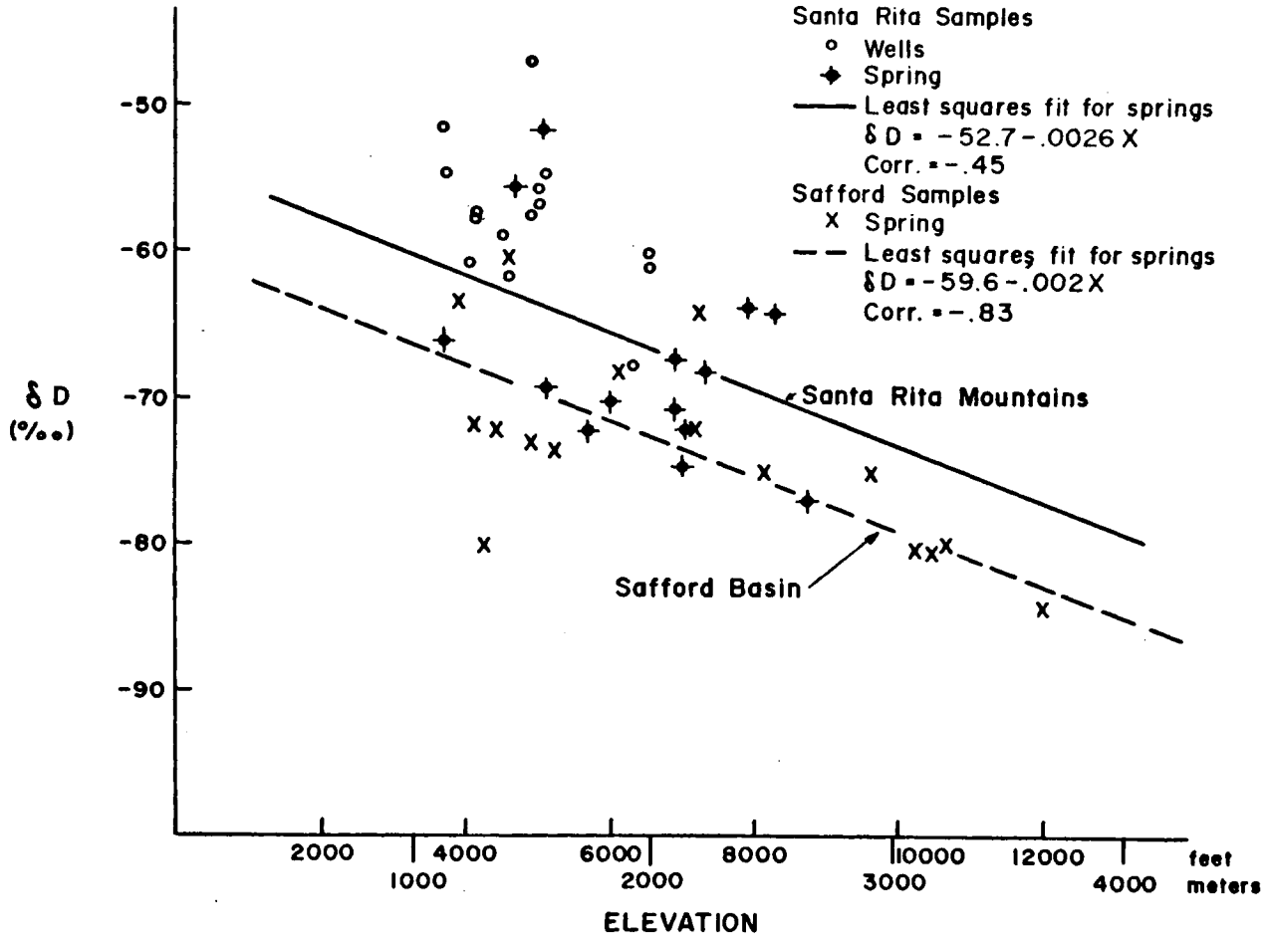

Figure 4.16. Comparison of deuterium vs. elevation for Safford basin and Santa Rita Mountains.

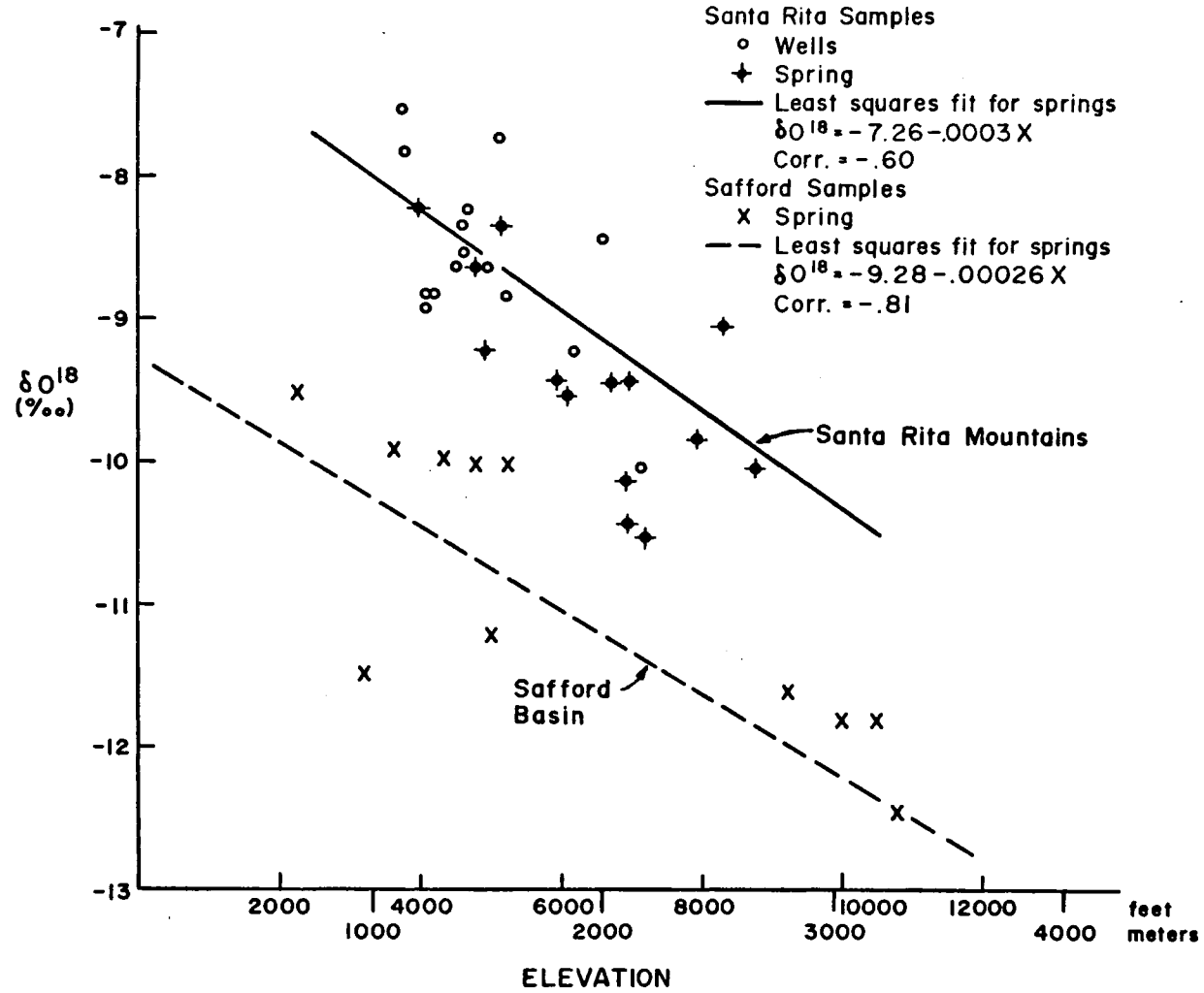

Figure 4.17. Comparison of oxygen-18 vs. elevation for Safford area and Santa Rita Mountains.

the heavy isotope is available and therefore the concentration of the lighter isotope increases making the water isotopically lighter. Therefore, because the Safford area receives more precipitation than the Santa Ritas, the water should again be relatively enriched in the lighter isotopes.

Note that although the values from the Safford basin are uniformly lighter than those from the Tucson Basin, the gradients are nearly identical. This is a significant finding and suggests that at least in southeastern Arizona the isotope-elevation gradient is relatively constant.

The isotope data taken from studies in the Tucson basin indicate that the isotope content from the Santa Catalina mountains and Santa Rita mountains are lighter than isotopic content from the Tucson mountains. This may be due to the higher elevations and cooler temperatures in the Santa Catalina mountains and Santa Rita mountains than the Tucson mountains. Also, they receive more precipitation which may result in lighter isotopic values. Finally, along the Santa Catalina mountain-front, isotopically light water containing high concentrations of sodium and sulfate is associated with major faults. Thus faults may be the conduits for deep-circulation recharge. Wells in the Santa Rita area are not near the major fault so a direct comparison cannot be made.

Summary

Chemical data from Madera Canyon reveal the circulation of a calcium sulfate type water and a calcium bicarbonate type water.

Whereas the calcium sulfate water almost certainly recharges the basin by streamflow infiltration, some question remains as to the mechanism of recharge of the calcium bicarbonate water. Most likely the calcium bicarbonate water occurs as a shallow regional flow system or local, independent systems which are influenced but not controlled by streamflow infiltration. This interpretation is favored over a deep-circulating regional system because of the chemical and isotopic data presented in this chapter and the geologic data presented in Chapter 2. Remember, no major faults occur in Madera Canyon to provide channelways for water to circulate at depth. Furthermore, inasmuch as none of the wells in the study area appears to penetrate deeply into the bedrock, any deep-circulating water is undetectable. Chapter 6 compares the results of this study with the results of other recent studies in the region.

Ground-water Chemistry in the Minor Canyons

Water samples were taken from wells, springs, mines, and streams in each of the side canyons. Chemical analyses appear in Appendix B. Figure 4.18 is a trilinear diagram of analyses of water samples from the sites and Figures 4.19-4.24 present finger-print diagrams. Due to the lack of data in the side canyons, little can be said about the source, evolution, and movement of the waters, and the discussion can only be descriptive.

Santa Rita Ranch contains three wells and one spring. The trilinear plot and finger-print diagram (Fig. 4.19) show that the water is dominated by calcium and bicarbonate ions, but also high in sodium

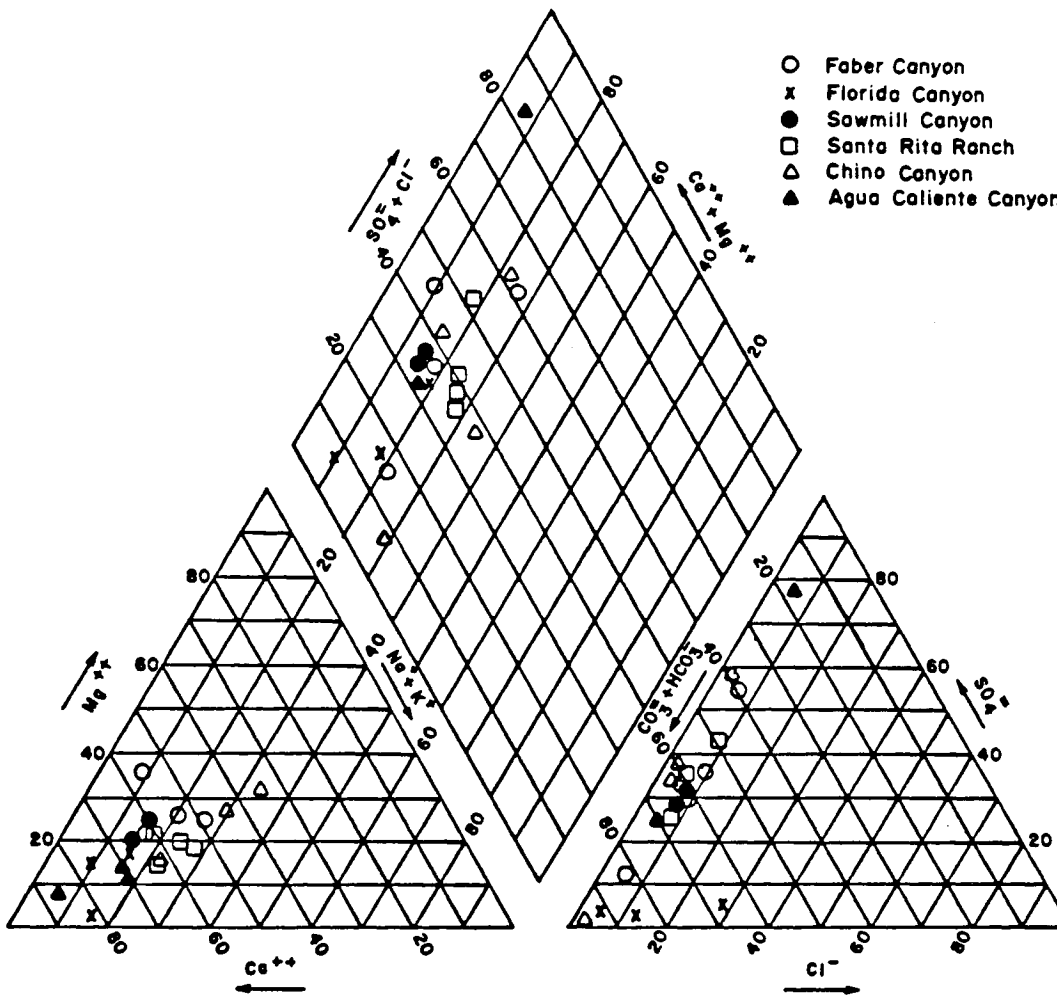

Figure 4.18. Trilinear diagram of analyses of water samples from from minor canyons.

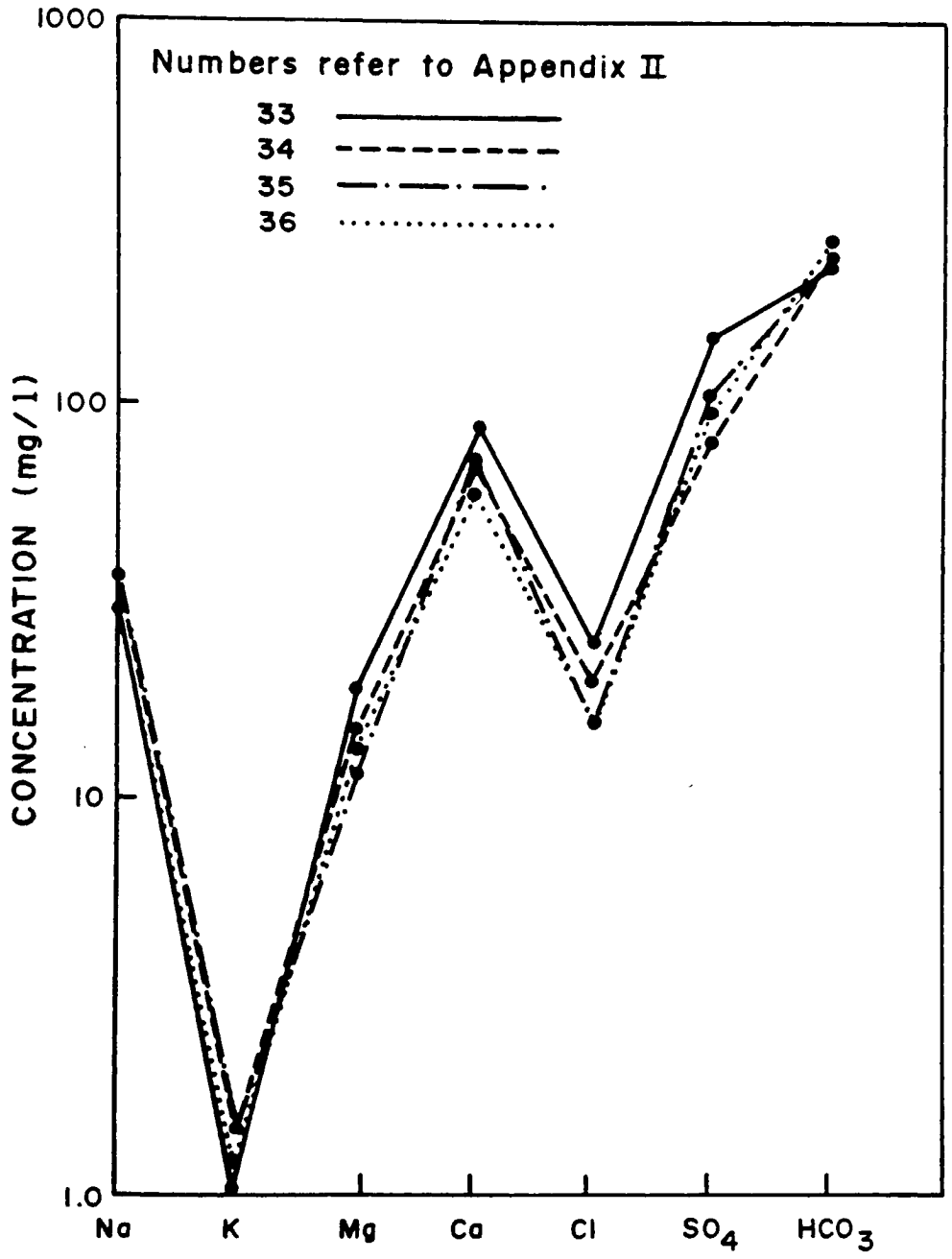

Figure 4.19. Finger-print diagrams of analyses of water samples from Santa Rita Ranch.

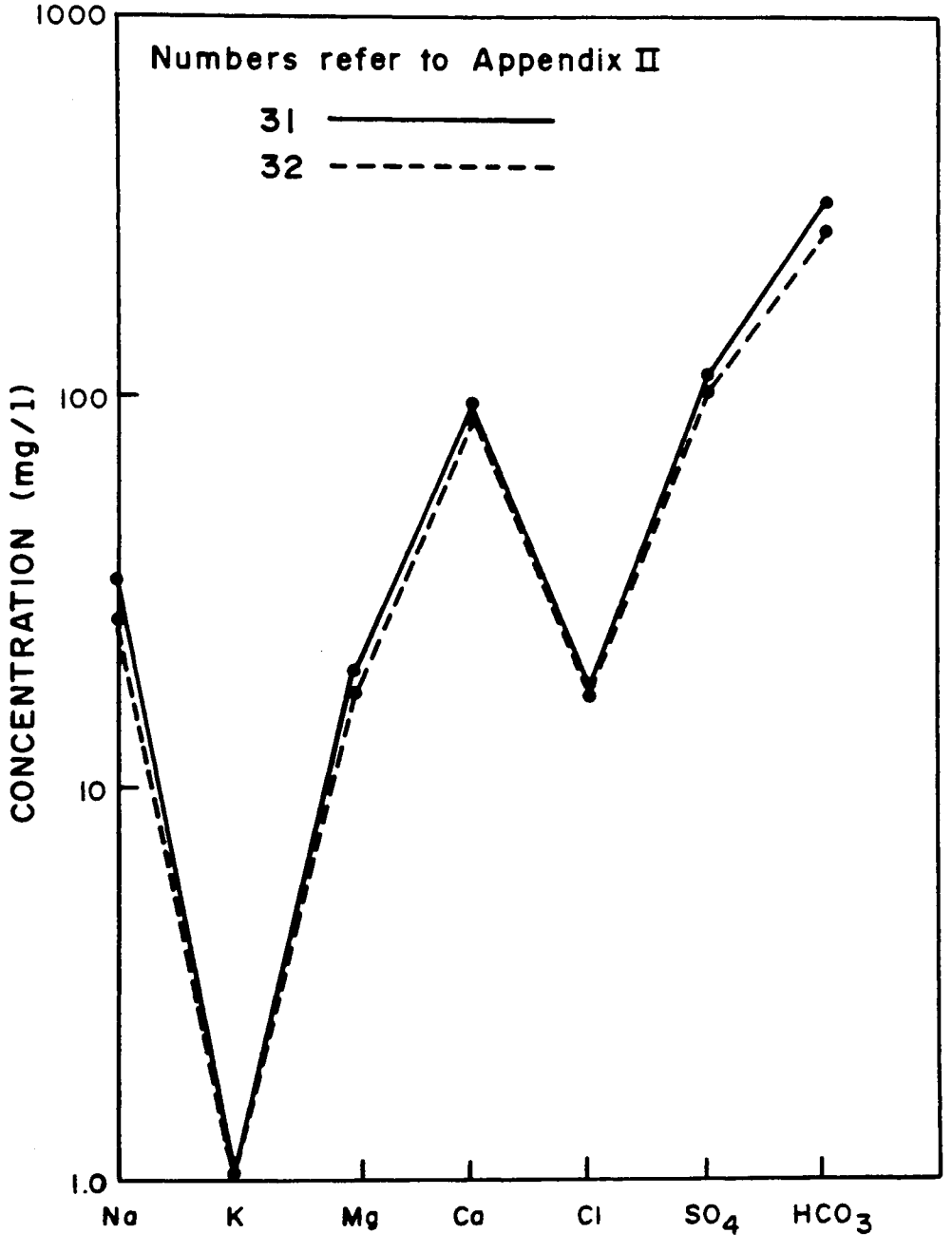

Figure 4.20. Finger-print diagrams of analyses of water samples from Sawmill Canyon.

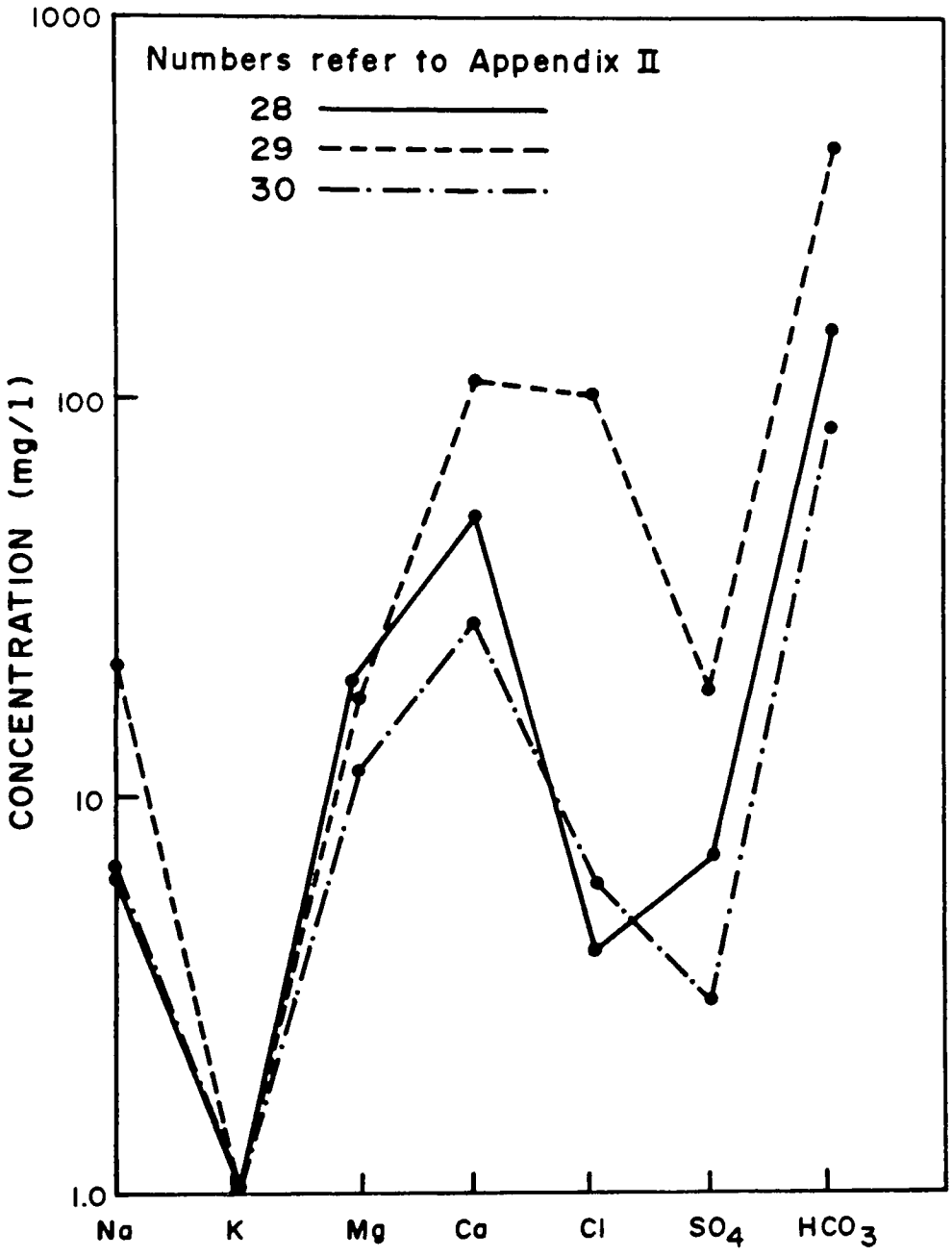

Figure 4.21. Finger-print diagrams of analyses of water samples from Florida Canyon.

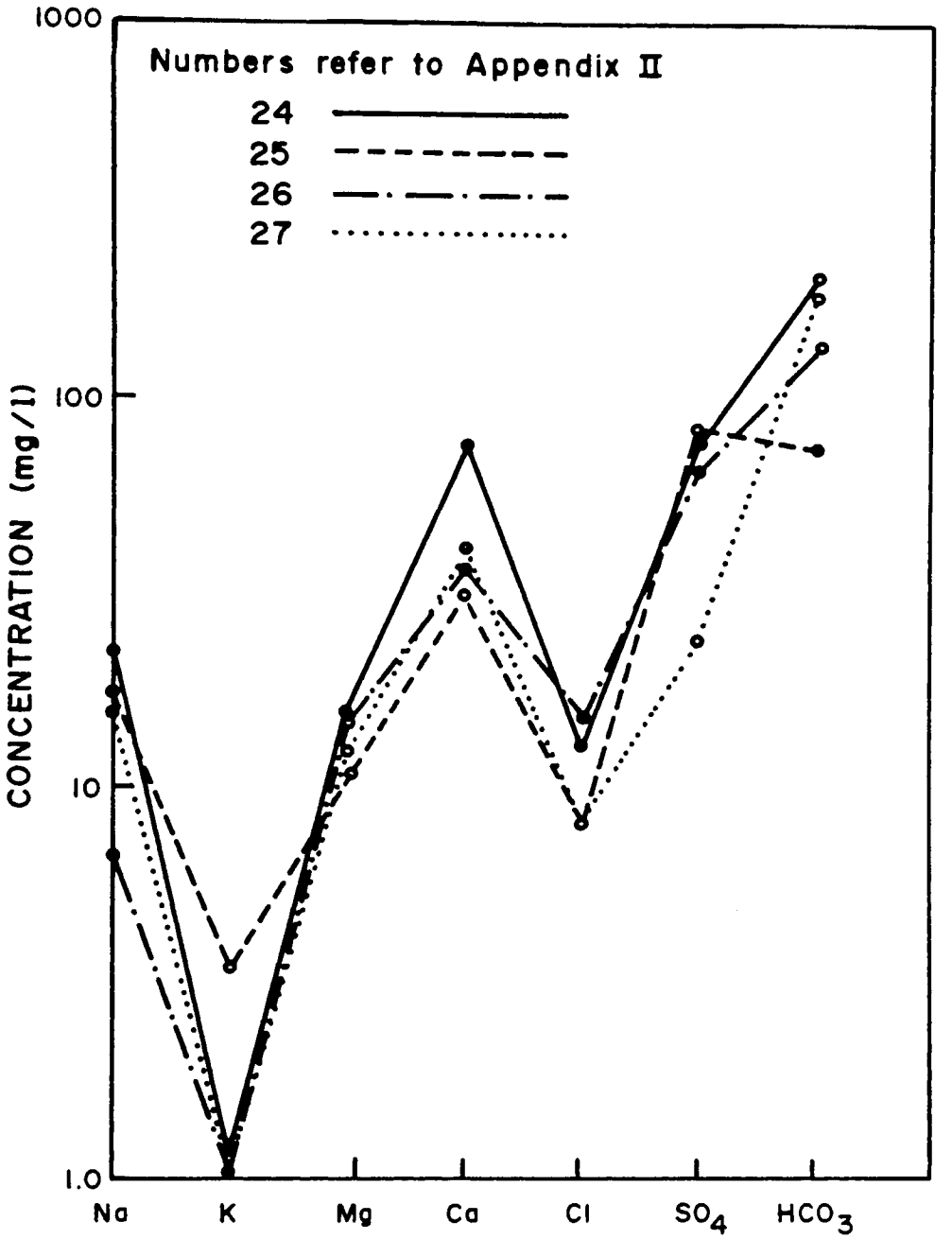

Figure 4.22. Finger-print diagrams of analyses of water samples from Faber Canyon.

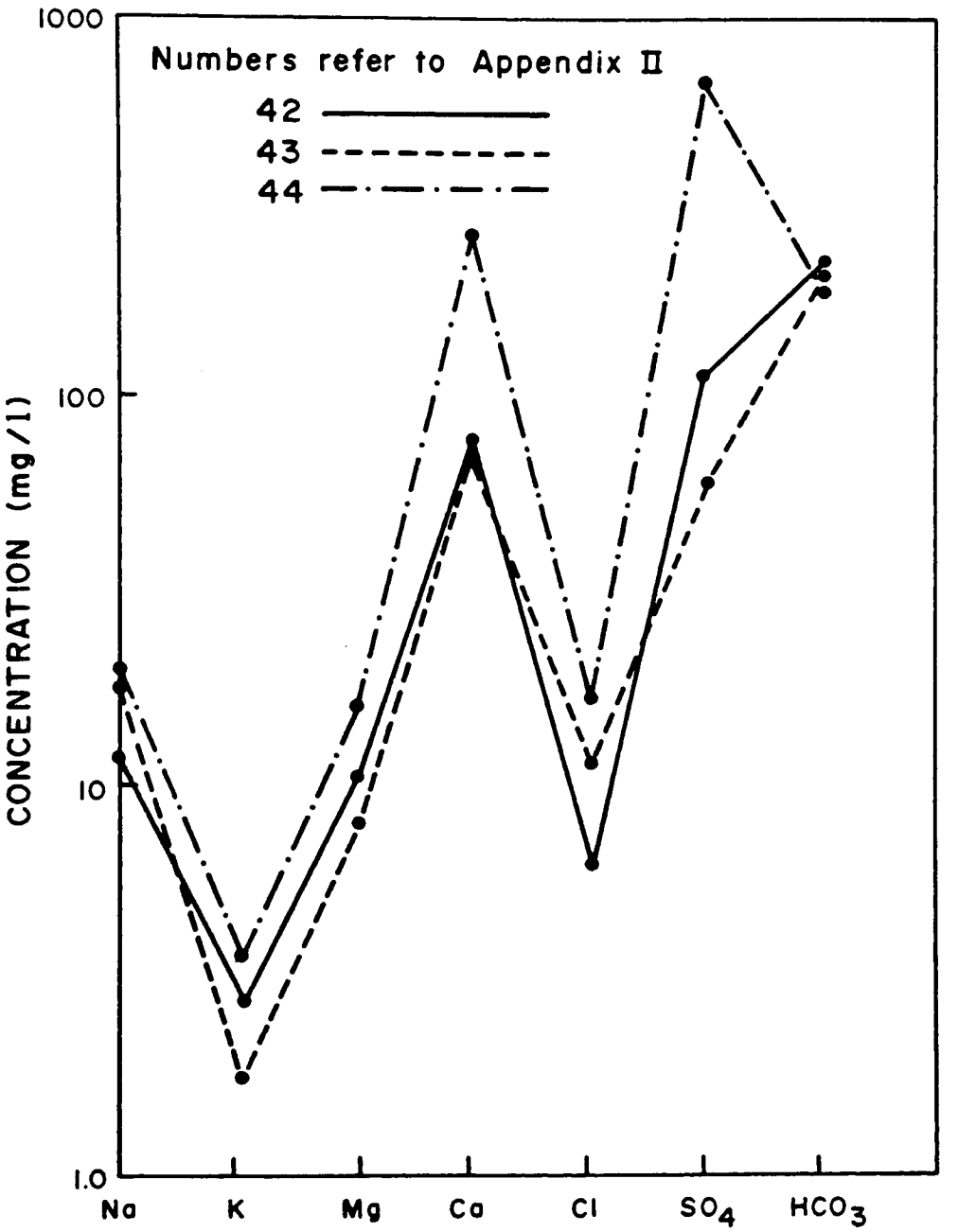

Figure 4.23. Finger-print diagrams of analyses of water samples from Agua Caliente Canyon.

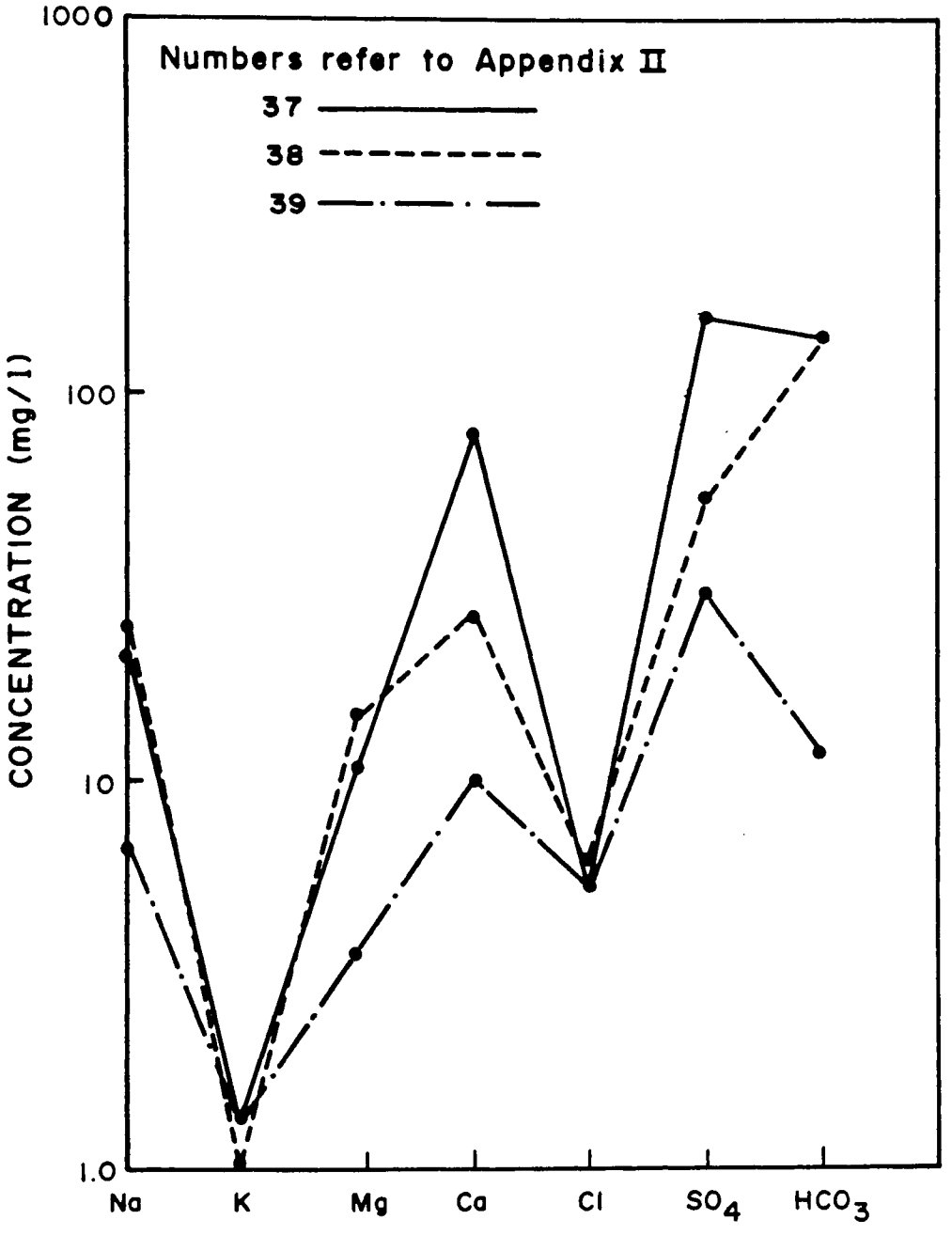

Figure 4.24. Finger-print diagrams of analyses of water samples from Chino Canyon.

and sulfate. The close grouping of the samples in both plots and their geographic proximity indicate that the samples are connected hydrologically. The concentrations of ions are relatively high suggesting a long flow path or residency time in the subsurface.

Sawmill Canyon contains two wells. Plots of analyses of water samples from the wells (Fig. 4.20) are nearly identical to those of the Santa Rita Ranch samples. However, there is probably not a hydrologic connection between the two wells, nor between Sawmill Canyon and Santa Rita Ranch. The two wells in Sawmill Canyon are 2.5 miles apart, separated by several faults, and occur in separate geologic formations. Sawmill Canyon is separated from Santa Rita Ranch by a topographic divide.

Three springs were sampled in Florida Canyon. They are dominated by calcium and bicarbonate but the wide scatter on the trilinear diagrams and the subparallel graphs on the finger-print diagram (Fig. 4.21) suggest that the springs result from local flow systems.

Faber Canyon contains two mines and a spring. Additionally, Old Hickory Well is included because of its proximity. The canyon is small and Figure 4.21 suggests that the sites are connected hydrologically. Calcium and bicarbonate are the dominant ions, but high sulfate concentrations occur in all the samples.

Only eight sample sites from which samples could be taken were found on the western flank of the Santa Rita mountains. Similar to the Madera Canyon samples, these were dominated by calcium and either sulfate or bicarbonate (Figs. 4.23-4.24). The calcium sulfate samples are predominately from mines. Aqua Caliente (site #42) presents the best

evidence for deep circulation in the study area. The temperature of 27 degrees Celsius suggests a deep source, and the high negative isotope value indicates a high elevation of recharge. The geology of the western flank is structurally and stratigraphically the most complex in the study area making a comprehensive analysis of ground-water movement impossible without more data.

CHAPTER 5

MOUNTAIN-FRONT RECHARGE

An attempt to estimate mountain-front recharge for Madera Canyon and Florida Canyon is given in this chapter. Depending on the types of data available for each canyon, a flow-net analysis, a water balance, or both will be used. An equipotential map of Santa Rita Ranch is also included, but due to insufficient data, no attempt to estimate recharge is made at the ranch. Recharge calculations appear in Appendix F.

Methods of Analysis

Flow-net Analysis

A flow-net analysis combines Darcy's Law with an equipotential map to evaluate ground-water flow. The flow net is constructed by first drawing an equipotential map based on available water level data. Next, streamlines are drawn perpendicular to the equipotential lines to indicate the ground-water flow pattern. The region between adjacent streamlines is called a streamtube.

Ground-water recharge is indicated by convex equipotential lines in the direction of flow and diverging streamlines. Recharge is calculated by applying Darcy's Law to a streamtube. The formula:

$$Q = TW \frac{dh}{dl} \tag{5.1}$$

is used where Q = total flow through the streamtube [L^3/T], T = transmissivity [L^2/T], W = width of the streamtube [L], dh = change in head between two equipotentials [L], and dl = length between two equipotentials [L]. For the canyons in the study area, two or more equipotential drops will be averaged for each streamtube.

The largest source of error in the flow-net analysis lies in the transmissivity estimate. Recharge values vary greatly depending on the method used to estimate transmissivity. Additional error results from insufficient water level data and from drawing an equipotential map over areas which may not be connected hydrologically.

Water Balance Analysis

A water balance analysis assumes water entering an area equals water leaving the area plus or minus changes in storage. In the Santa Rita Mountains the only input is precipitation (P). Output consists of evapotranspiration (ET), surface runoff (RO), and ground-water outflow (GR). Knowing any three of the variables allows the fourth to be calculated by the principle of mass balance, if a steady-state system can be assumed.

For the Santa Rita Mountains, precipitation, runoff, and evapotranspiration have been estimated by other means and ground-water outflow from the canyons, which equals ground-water recharge to the basin, is calculated by the formula:

$$GR = P - ET - RO. \qquad (5.2)$$

Mountain-front Recharge Calculations

Madera Canyon

Madera Canyon is the largest canyon in the Santa Rita Mountains. Wells and springs supply the necessary data for a flow-net analysis. Precipitation, runoff, and evapotranspiration data allow a water balance to be calculated.

Flow-net Analysis. Figure 5.1 is an equipotential map of Madera Canyon. Two interesting features are present in the map. First, in the direction of flow, the equipotentials change from concave at high elevations to convex at low elevations. This indicates that at high elevations the ground-water system is discharging and the stream is gaining; therefore, it is not a recharge system. Conversely, at low elevations the ground-water system is recharging and the stream is losing, indicating recharge. The runoff data presented in Table 3.3 support this conclusion.

The second interesting feature is the decrease in hydraulic gradient at lower elevations. This may be explained by an increase in cross-sectional areas. As the saturated thickness increases and the canyon widens at low elevations, less gradient is necessary to drive the same volume of water. Also, the transmissivity is presumably greater in alluvial materials at the foot of the mountain than in the fractures at high elevations. Based on both these features, recharge appears to occur predominately through shallow circulation.

Recharge estimates are calculated for two streamtubes shown in Figure 5.1. Because of the difficulty in obtaining a consistent value

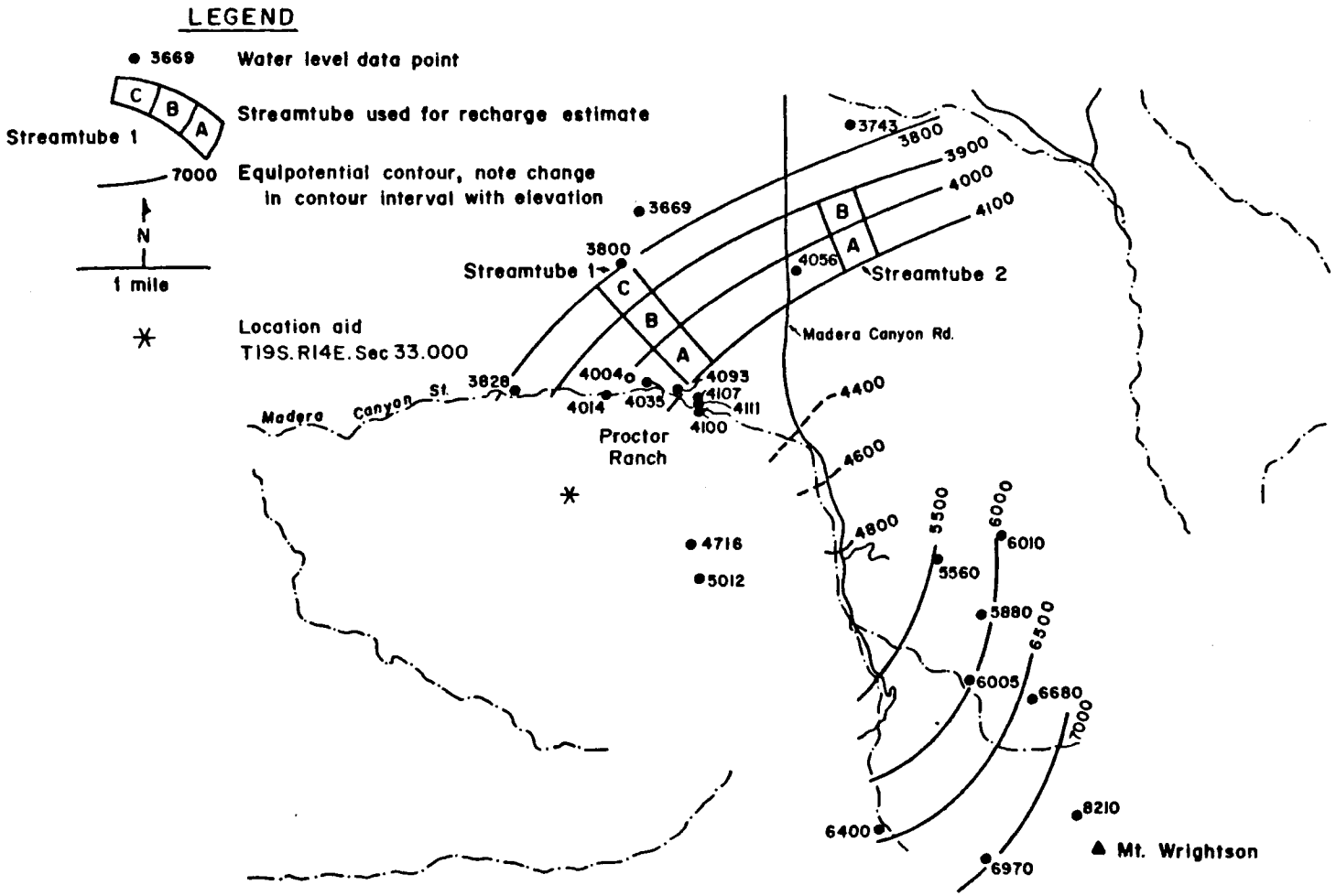

Figure 5.1. Equipotential map of Madera Canyon showing streamtubes used in recharge calculations.

for transmissivity, values of 63 and 130 ft/day are used in the calculations. Yearly ground-water recharge in ac-ft/yr/mi is calculated to be:

Transmissivity	Streamtube #1	Streamtube #2
63	205	154
130	424	318

Water Balance Analysis. The water balance for Madera Canyon is illustrated in Appendix E. The catchment area equals 7.94 mi^2. Volumetric rainfall from September 1982 through August 1983 equals 12,132 ac-ft and 6687 ac-ft, respectively. Surface runoff was approximately 3040 ac-ft.

Based on these values and equation (5.2), the total annual recharge equals 2405 ac-ft. Dividing this by 4.6 miles of mountain-front yields a recharge value of 523 ac-ft/yr/mi.

Comparison of Results. The recharge values calculated by the flow-net analysis are between 50% and 85% of those calculated for the water balance. But, the technique used to estimate the parameter values in the water balance would tend to be overestimated. For example, Madera Canyon Stream was gaged between February and April when streamflow is seasonally high. Thus, extrapolating these streamflows throughout the entire year would overestimate runoff. Similarly, equation (5.2) assumes a steady-state system. Therefore, any water taken into storage is not accounted for and erroneously presumed to recharge the regional aquifer.

Considering these uncertainties and those associated with measuring precipitation, evapotranspiration and transmissivity, the differences between the mountain-front recharge results are not unreasonable, and at least the order of magnitude of the results appears plausible.

Faber Canyon

Figure 5.2 is an equipotential map and flow-net of the canyon. Two mines, Faber Canyon Spring, and Old Hickory Well provide water level data. The chemical analyses indicate that the system is connected hydrologically. No transmissivity data are available, but the canyon floor is composed of fractured igneous rock with virtually no alluvial cover, suggesting low permeabilities. Also, the catchment area of the canyon is relatively small, and the canyon receives very little runoff. Therefore, the canyon probably does not contribute significantly to mountain-front recharge.

Florida Canyon

A water balance was used to calculate mountain-front recharge in Florida Canyon. A flow-net analysis is not feasible because there are no wells or mines in the area, and the chemical data from the springs indicate that they are not connected hydrologically.

The catchment area in Florida Canyon equals 2.88 square miles. Volumetric precipitation and evaporation equal 4070 ac-ft and 2232 ac-ft, respectively. Surface runoff is approximately 698 ac-ft/yr. These values result in a recharge value of 1140 ac-ft/yr. Dividing this by

yields a result of 633 ac-ft/yr/mi.

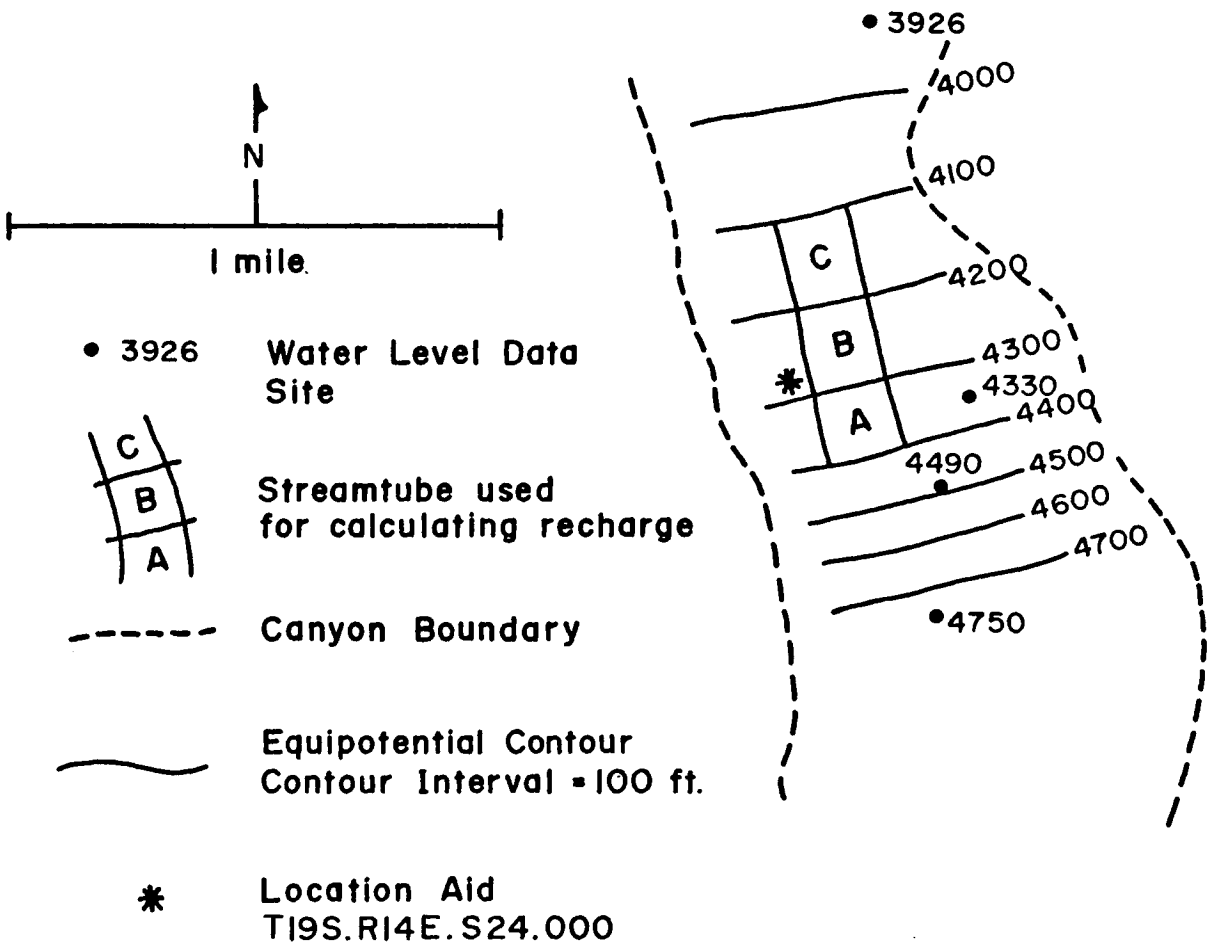

Figure 5.2. Equipotential map of Faber Canyon.

This value is close to the result for the water balance in Madera Canyon. Additionally, the similar topography and elevations lend credibility. However, Madera Canyon opens onto a broad alluvial fan but Florida Canyon drains into a relatively narrow channel. The effect of this morphology cannot be determined.

Santa Rita Ranch

Santa Rita Ranch has four wells allowing an equipotential map to be drawn. Unfortunately, pumping has disturbed the natural regime and a flow-net analysis cannot be made. Also, no runoff data are available and no record of pumping has been kept so a water balance cannot be made either. Figure 5.3 is the equipotential map of the canyon.

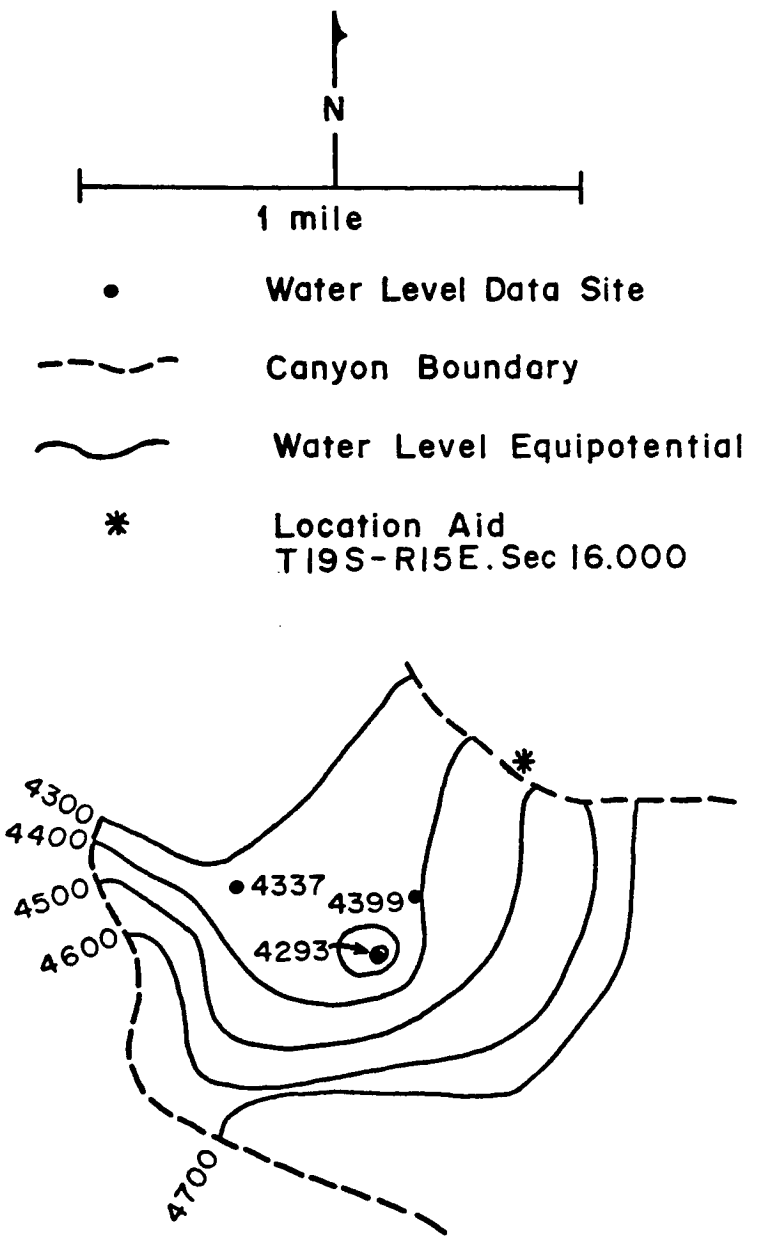

Figure 5.3. Equipotential map of Santa Rita Ranch.

CHAPTER 6

COMPARISON OF RESULTS

The techniques used in this study have been used by Mohrbacher (1983) and Olsen (1982) in the Tucson Basin. Although the areas are similar in geology and climate, important differences are present in the results. The purpose of this chapter is to compare the results from the Santa Rita Mountains with the results from the other areas and investigate possible reasons for any differences.

Summary of Results

Mohrbacher and Olsen studied recharge along adjacent sections of the Santa Catalina Mountains (Fig. 1.3). Geologically, the mountains are composed of a layered gneiss containing quartz, plagioclase, orthoclase, muscovite, and biotite. The Tertiary Rillito Formation and the Cenozoic basin fill abut the mountain front. The Rillito beds contain conglomerate, sandstone, and mudstone which are cemented by calcium carbonate. The basin fill contains poorly sorted gravel, sand and silt. Note that no large alluvial fan is present in the area.

The Catalina Fault is the major structure in the area. The fault parallels the mountain front and dips 30-55 degrees to the south. Also, several normal faults run parallel and perpendicular to the mountain front.

Olsen's data reveal the presence of three water types. The first is associated with local faults and contains high concentrations

of sodium and sulfate. The sodium is most likely derived from the weathering of plagioclase in the mountain mass, and the sulfate is most likely derived from the dissolution of gypsum as recharge rises along the fault zone. The data further suggest that this water type is the product of deep circulation.

The second water type comes from wells tapping the basin fill sediments and Rillito beds. The water is dominated by sodium, calcium and bicarbonate which come from the dissolution of calcite cement. This water type appears to be the result of shallow circulation.

The third water type is unclassified but Olsen's scattergrams suggest it to be the result of mixing between the sodium sulfate water and the sodium calcium bicarbonate water.

Olsen concluded that the contribution of the deeply-circulating sodium sulfate water to basin recharge was minimal compared to the shallow-circulating sodium-calcium bicarbonate water.

Olsen's isotopic analysis supported and refined his analysis of recharge. The sodium sulfate water had isotopically light, a proximity to major faults, and tightly clustered concentrations indicating a high elevation of recharge. The sodium-calcium bicarbonate water was isotopically heavier, located near stream channels, and had a broad range of concentrations indicating it was recharged over a range of elevations.

Olsen used a flow-net analysis to obtain his mountain-front recharge estimate of 50 ac-ft/yr/mi. The flow-net had one streamtube drawn along Tanque Verde Creek in the highly permeable basin fill and one streamtube drawn on each side of the creek in the highly

impermeable Rillito beds. Olsen averaged the values from each streamtube to obtain his recharge estimate.

Mohrbacher's results were consistent with Olsen's. His data also revealed the circulation of three types of water. The first contained high concentrations of calcium and bicarbonate and is associated with both the gneiss and the sedimentary Rillito beds and the basin fill. This water appears to be recharged by streamflow infiltration.

The second type of water contained high sulfate or chloride. The sulfate concentrations increase linearly with total dissolved solids which suggest the Rillito units to be the source of the water. Recharge from this water type is small.

The third type of water is high in sodium, potassium, and sulfate but low in calcium and magnesium. This type is associated with wells in the gneiss and the fault zones. The sodium and potassium come from the dissolution of albite, potassium feldspar, muscovite, and their alteration products. The sulfate may come from oxidation of pyrite or other metallic sulfides. Mixing is indicated between the first and third type but not between the first and second or the second and third type.

Mohrbacher's isotope data reveal that water samples from wells and springs in the gneiss and fault zones are isotopically light compared to samples from other locations. This, plus the major ion chemistry, suggests a high elevation of recharge for these sites. Similarly, isotopic values for wells in the alluvium suggest that recharge is from Sabino Creek or Rillito Creek. Furthermore, the

isotope data suggested that winter precipitation is the dominant source of recharge for both the gneissic sites and the alluvial sites.

Mohrbacher used a flow-net analysis to calculate his recharge values of 25-65 ac-ft/yr/mi. He ignored recharge near the stream and drew his flow-nets over the low permeable Rillito units.

Discussion

The similarity of the results of Mohrbacher's and Olsen's studies with this study can be traced to the similarity of the geology of the two mountain ranges and the fact that the same techniques were used in each investigation. The differences between the studies can be traced to subtle differences in geology and the lack of available data in the Santa Rita Moutnains.

The Santa Catalina and the Santa Rita Study areas contain large crystalline blocks bounded by sedimentary units. The mineral assemblage in each area contains quartz, plagioclase, orthoclase, biotite, hornblende, microcline, and their weathering products.

Three important differences in geology distinguish the two areas. First, no major faults are present in the Santa Rita study area. The Elephant Head Fault is present to the north, but all conclusions are based on data collected between the fault and the watershed divide. Second, Madera Canyon opens onto a broad alluvial fan which is much more permeable than the Rillito units. Third, the presence of No Name Mine in Madera Canyon provides a glut of sulfate to Madera Canyon Creek.

In terms of data, the Santa Catalina study areas have a much better data base than the Santa Rita study area. Not only are more sites available for sampling but streams have been gaged systematically and several deep wells penetrate the bedrock.

The results of each study are that recharged water is dominated by calcium, sodium, bicarbonate, and sulfate. Also, each study demonstrates that streamflow infiltration is the dominant source of mountain-front recharge in the study areas.

Although the water chemistry in each area is similar, the source of the constituents is different. In Madera Canyon, sulfate originates in No Name Mine, probably as the oxidation product of pyrite or other sulfur-bearing minerals. In the Santa Catalina mountains sulfate originates from dissolution of gypsum along fault planes and in the Rillito units. Whereas sulfate is used to trace shallow circulating water in Madera Canyon, it is used to trace deeply-circulating water in the Santa Catalina area.

Another similarity is that the high sulfate waters in each study contain large amounts of total dissolved solids. However, the high concentrations in the Santa Ritas begin at No Name Mine and are reduced along the flow path due to dilution and mixing with other water types. Conversely, the high concentrations in the Santa Catlina mountains result from slow movement through a long flow path.

Isotopically, Mohrbacher's and Olsen's data fall into consistent groups wherein the deeply-circulating waters have lighter isotopic values than the shallow circulating waters. In the Santa Rita study no such separation was detected.

Finally, the comparatively low values of recharge for the Santa Catalina Mountains result from the fact that most recharge occurs through the low permeability Rillito beds. In Madera Canyon recharge occurs through the large, permeable alluvial fan. For example, if Olsen's transmissivity value for his basin fill streamtube were taken over his entire flow-net he would have calculated more recharge than occurs in Madera Canyon. Mohrbacher intentionally drew his streamtubes away from any stream to avoid the effect of streamflow infiltration.

CHAPTER 7

CONCLUSIONS AND RECOMMENDATIONS

This study has evaluated mountain-front recharge from the Santa Rita Mountains to the Tucson Basin. Two objectives were sought. The first was to qualitatively determine the mechanisms of recharge in the study area, and the second was to quantitatively determine the annual amount of mountain-front recharge. Essentially, both objectives were met. Chemical data indicate the presence of two flow systems in the area, and the hydrologic data were sufficient to estimate recharge from Madera Canyon, Florida Canyon, and Faber Canyon. The purpose of this chapter is to summarize the major findings of the study, to evaluate the techniques, and to make recommendations for future researchers.

Conclusions

Chemical data collected in Madera Canyon reveal the circulation of two types of water. The first contains high concentrations of calcium and sulfate. This water originates in No Name Mine near the upper reaches of Madera Canyon Stream. The mine discharges water into the stream where it is diluted until it flows onto the alluvial fan. At this point, the stream water begins to recharge the ground-water system by streamflow infiltration.

The second water type contains high concentrations of calcium and bicarbonate. In this type concentrations increase between sample sites at high elevations and sample sites at low elevations. This fact,

combined with evidence obtained from graphs, chemical equilibrium considerations, and isotopic data indicate that the calcium bicarbonate water is part of a shallow circulating regional flow system. Note, however, that independent flow systems could conceivably give similar plots and interpretations.

Mixing of the two water types appears to occur in the stream and in the ground. This is evidenced by the chemical data from sites where mixing would be expected to occur.

The three techniques that were tested to evaluate the mechanisms of mountain-front recharge met with varying degrees of success. The major ion chemistry was the most useful. Trilinear diagrams, finger-print diagrams, and scattergrams provided plots on which consistent and realistic interpretations could be based. The chemical equilibrium methods were limited by insufficient chemical, pressure, and temperature data. The isotope data provided a correlation between isotopic content and elevation and were useful in supporting interpretations based on the major ion chemistry.

Hydrologically, annual mountain-front recharge was calculated to be in the 200-400 ac-ft/yr/mi range for Madera Canyon. This result was obtained by a flow-net analysis and supported by a water balance. In Faber Canyon, a flow-net analysis could not be made because no transmissivity data were obtained, and in Florida Canyon a water balance predicted recharge to be 633 ac-ft/yr/mi. The flow-net is limited by inconsistent transmissivity values, and the water balance is limited by a lack of runoff and evapotranspiration data.

In conclusion, the methods tested in this study are valid techniques to be used in the study of mountain-front recharge and lead to meaningful results.

Recommendations

To further refine the knowledge of mountain-front recharge in the Santa Rita Mountains, the following recommendations are made to future researchers.

First, each site should be sampled several times over a period of at least a year. This would reveal any seasonal effects on recharge and particularly pertains to isotope data and Madera Canyon Stream. Also, sampling precipitation at several elevations would aid the isotopic analysis. Finally, water samples should be tested for aluminum to aid the equilibrium analysis.

Next, water levels and streams should be monitored on a systematic schedule to refine both the flow-net and the water balance analysis. Also, this would provide information on the time lag between a surface water event and a corresponding ground-water event. More aquifer tests should also be conducted to produce a more accurate transmissivity value. A raingage on top of Mount Wrightson and a couple of strategically located evaporation pans would add more control to the water balance analyses.

Finally, if enough money were available, observation wells far out on the alluvial fan would greatly aid investigations. They would provide information on aquifer thickness, transmissivities,

deeply-circulating waters, and the role of the Madera Canyon Fault in determining recharge.

APPENDIX A

GEOLOGIC FORMATIONS OF THE SANTA RITA MOUNTAINS

(Drewes, 1972a)

Age			Groups, formations, and members			Description	Estimated thickness (ft)
Quaternary	Holocene		Youngest gravel and low-level terrace deposits			Gravel and intercalated sand; infantile gray soil on low-level terrace gravel.	0–300 ±
	Pleistocene	Late Pleistocene	Intermediate-level pediment and terrace deposit			Gravel and sand; capped by weakly developed red soil.	0–400 ±
		Middle Pleistocene	High-level pediment deposits			Gravel and sand; capped by well-developed red soil.	0–50 ±
	Pleistocene and Pliocene		Basin-fill gravel			Gravel, sand, and silt, commonly pinkish-gray and slightly indurated; locally includes tuffaceous beds.	0–2,000 ±
	Pliocene and Miocene(?)		Gravel of Nogales			Gravel, sand, and silt; rich in volcanic clasts; commonly pale red, poorly sorted, and slightly indurated.	0–1,000 ±
Tertiary	Late(?) Oligocene		Rhyolite intrusives of the northern Santa Rita Mountains			Rhyolite porphyry of a plug and of the Gardner Canyon and Box Canyon dike swarms.	
			Igneous complex of the southern Santa Rita Mountains	Dikes and stock of the San Cayetano Mountains		Rhyodacite porphyry dike swarm and medium-coarse-grained light-gray granodiorite.	
				Dikes and laccoliths in the Grosvenor Hills area		Rhyodacite vitrophyre, medium-gray to light-gray.	
				Grosvenor Hills Volcanics	Rhyodacite member	Rhyodacite lava flows, agglomerate, tuff, and welded tuff.	150–2,200
					Rhyolite member	Rhyolite tuff; a little welded tuff and lava.	500+
					Gravel and silt member	Gravel and silt; a little limestone and shale.	0–200
	Oligocene to Paleocene		Quartz vein swarm			Mineralized quartz veins of the southern Santa Rita Mountains.	
			Rhyolitic volcanics			Rhyolitic tuff and lava of Wasp Canyon.	0–100
			Olivine andesite plugs			Vesicular and amygdaloidal plugs at Deering Spring.	
			Andesite dikes and sills			Small andesite intrusives; include some dacite and diorite intrusives.	
	Paleocene		Greaterville intrusives			Quartz latite porphyry dikes and plugs, light-gray to grayish-orange-pink; contains stubby bipyramidal quartz phenocrysts; associated with mineralization.	
			Helvetia stocks			Granodiorite to quartz monzonite stocks and a quartz diorite stock, medium coarse grained.	
			Cottonwood Canyon dike swarm			Quartz latite porphyry, finely porphyritic to coarsely porphyritic.	
			Gringo Gulch plugs			Hornblende dacite porphyry; partly very coarsely porphyritic; microgranodiorite in core of one plug.	

	Paleocene(?)	Volcanics of Red Mountain		Rhyolitic and andesitic pyroclastic rocks, intensely altered.	
		Gringo Gulch Volcanics	Upper member	Rhyolitic to dacitic tuff, sandstone, and a capping andesite lava.	900+
			Lower member	Rhyolitic and dacitic pyroclastic rocks and some flows; contains intercalated epiclastic rocks.	700+
Cretaceous	Late Cretaceous	Elephant Head Quartz Monzonite		Stocks of coarse-grained quartz monzonite and an aplitic phase.	
		Madera Canyon Granodiorite		Stock of coarse-grained hornblende granodiorite, and porphyritic and leucocratic phases.	
		Josephine Canyon Diorite		Large stock of fine-grained diorite and quartz diorite and a late quartz monzonite phase.	
		Salero Formation	Upper member	Sedimentary and volcanic rocks.	3,500±
			Arkose member	Arkose and conglomerate; largely facies of welded tuff member.	500±
			Welded tuff member	Rhyodacite welded tuff.	1,200+
			Exotic block member	Dacitic volcanics containing large exotic blocks.	1,000±
			Lower member	Dacitic volcanics.	400±
		Fort Crittenden Formation	Upper red conglomerate member	Volcanic conglomerate; some sandstone and siltstone.	1,400+
			Rhyolitic tuff member	Tuff, in part intercalated in upper red conglomerate member.	0–650
			Brown conglomerate member	Arkosic conglomerate; some sandstone and siltstone.	2,000+
			Lower red conglomerate member	Volcanic conglomerate; some sandstone and siltstone.	800–1,200
			Shale member	Fossiliferous gray shale; some sandstone and conglomerate.	4,550+

Age		Groups, formations, and members		Description	Estimated thickness (ft)
Cretaceous	Early Cretaceous	Bisbee Group	Turney Ranch Formation	Sandstone and red siltstone.	1,500+
			Shellenberger Canyon Formation	Siltstone and arkose.	1,600+
			Apache Canyon Formation	Arkose and siltstone; some limestone lenses.	1,500–2,000
			Willow Canyon Formation	Arkose and conglomerate.	2,200+
			Glance Conglomerate	Limestone- and granite-cobble conglomerate.	0–1,500+
		Bathtub Formation	Upper member	Dacitic volcanics and tuffaceous sandstone.	0–1,500
			Middle member	Rhyolitic to andesitic volcanics.	800–1,500
			Lower member	Conglomerate and volcanic sandstone.	700±
		Temporal Formation	Upper member	Conglomerate and rhyolitic volcanics.	600–1,000
			Middle member	Rhyolitic to latitic volcanics and conglomerate.	100–400
			Lower member	Rhyolitic to dacitic volcanics and fanglomerate.	200–1,800
Jurassic		Squaw Gulch Granite		Large stock of coarse-grained pink rock ranging in composition from granite to quartz monzonite.	
Early Jurassic and Late Triassic		Canelo Hills Volcanics		Arkosic sandstone and conglomerate, tuff and tuffaceous sandstone, and quartzite.	600+
		Piper Gulch Monzonite		Stock of very coarse grained dark-gray rock ranging in composition from monzonite to quartz monzonite.	
Triassic		Gardner Canyon Formation	Upper member	Red mudstone, dacitic volcanics, and conglomerate.	1,800+
			Lower member	Red siltstone and chert-pebble conglomerate.	200
		Mount Wrightson Formation	Upper member	Eolian sandstone and andesitic to rhyodacitic volcanics.	2,000+
			Middle member	Rhyolitic to latitic volcanics; some sandstone and conglomerate.	5,000±
			Lower member	Dacitic to andesitic volcanics and sandstone.	1,500+

Permian	Early Permian	Naco Group	Rainvalley Formation		Limestone and dolomite; a little sandstone.	0–800
			Concha Limestone		Limestone, thick-bedded, cherty, dark-gray.	400–575
			Scherrer Formation	Upper quartzite member	Quartzite, pale-reddish-gray, fine-grained.	140 ±
				Middle dolomite member	Dolomite, light- to medium-gray.	120 ±
				Lower quartzite and basal siltstone members	Quartzite, pale-yellowish-gray, fine-grained; basal reddish-gray siltstone.	460 ±
			Epitaph Dolomite	Upper member	Limestone, moderately thick bedded, medium-gray, slightly cherty.	880 ±
				Lower member	Mainly light-brownish-gray marlstone and dolomitic siltstone; locally contains some argillite and gypsum; basal 180 ft contains intercalated dark- to medium-gray medium-thick-bedded dolomite.	620 ±
			Colina Limestone		Limestone, dark-gray, medium-thick-bedded.	850 ±
Pennsylvanian	Early Permian and Late Pennsylvanian		Earp Formation		Siltstone and shale, reddish-gray; contains some sandstone and chert-pebble conglomerate.	800 ±
	Late and Middle Pennsylvanian		Horquilla Limestone		Limestone, fine-grained, thin-bedded to moderately thick bedded, medium- to light-gray; contains siltstone beds in upper half and two thin conglomerate beds near base.	1,000 ±
Mississippian		Escabrosa Limestone			Limestone, coarse-grained, thick-bedded, cherty, medium-gray, crinoidal.	560 ±
Devonian		Martin Formation			Brown dolomite, gray limestone, siltstone; some sandstone.	400 ±
Cambrian	Late and Middle Cambrian	Abrigo Formation			Shale, quartzitic sandstone, and thin-bedded limestone.	740–900
	Middle Cambrian	Bolsa Quartzite			Quartzite, coarse-grained, thick-bedded, light- to brownish-gray and purplish-gray; thin basal conglomerate.	460 ±
Precambrian		Continental Granodiorite			Granodiorite porphyry and quartz monzonite porphyry; contains aplite and fine-grained quartz monzonite intrusives.	
		Pinal Schist			Hornblende gneiss, granite gneiss, and schist.	

APPENDIX B

CHEMICAL DATA FROM SANTA RITA STUDY AREA

Concentrations in mg/l.

(Note: S = spring, W = well, M = mine, St = stream.)

Number	Name Location	Type Elevation (ft)	Land Owner	Date	Discharge (cfs)	Sp. Con. (m mhos)	T (°C)	pH	HCO_3^-	$NO_3^=$	Cl^-	$SO_4^=$	F^-	Ca^{++}	Mg^{++}	Na^+	K^+	Fe^{++}	Hard	SiO_2	% Error
	MADERA CANYON																				
1 (B)	Bellows 20.15.	S 8210	Forest Service	4/19/83	.009	46		5.8	15	3.52	4	4	0	3.6	T	5.5	1	0	13	8.5	5.4
2 (S)	Sprung 20.14.13.abd	S 6970	Forest Service	3/26/82	.07	160	10	6.7	60	3.52	2	7	-46	21.6	4.5	10	1.4	0	64	15	-21.4
3 (NN)	No Name 20.14.14.aad	M 6540	Forest Service	5/24/82		1120		7.7	183	1.76	4	400	4.4	213.6	6.5	15	2.4	.12		30	-1.7
4 (AF)	Air Force 19.14.27.cda	W	Air Force	1981		630	16	7.1	197	.88	24	160	-6	104.4	18.5	28.9	2.4	.281		28.00	0.0
5 (K)	Kent 20.14.12.aaa	S 6680	Forest Service	3/29/82		150	10	6.8	68	2.2	4	7	.36	23.2	4.8	7.3	1.6	0		15	-16.4
6 (SY)	Slyvester 20.14.1.dcc	S 6005	Forest Service	3/29/82	.035	300	13	6.8	122	1.76	2	23	-60	31.2	5.4	12	3.2	0		17.2	-.62
7 (BG)	Bog 20.14.1.acc	S 5880	Forest Service	3/29/82	.035	250	15	7.0	90	0	4	23	.33	31.2	5	13.7	2.4	0		17.6	-12
8 (DJ)	Dutch John 19.14.36.dca	S 6010	Forest Service	4/17/82		230		6.8	111	2.2	4	2	.32	21.6	5.3	12.5	3.85	0		21.8	-3.5
9 (BDJ)	Below Dutch John 19.14.36.cdc	S 5560	Forest Service	4/17/82		580		7.7	296	1.32	8	17	.38	64	11.5	16.5	4.5	.78		28.0	4.6
10 (CH)	Christobal 19.14.27.cac	W 4120	Redondo	3/31/83		620	20	6.7	194	1.76	14	220	.4	108	18.23	25.0	1.51	.12	345	28.6	.73
11 (RF1)	RF1 19.14.27.cbc	W 4038	Laos	7/16/82		523		7.0	202	2.64	14	150	.34	82.4	18.23	18.9	1.64	.12	281	28.0	3.01
12 (RF2)	RF2 19.14.27.cbd1	W 4060	Laos	7/16/82		500		6.6	180	2.2	14	150	.26	78.4	16.04	21.09	1.75	.12	262	26.0	2.56
13 (RF3)	RF3 19.14.27.cbde	W 4038	Laos	3/31/83	.096	500	20	6.4	179.2	2.64	11	135	.28	83.20	13.12	22.1	1.51	.22	262	29.0	-1.11
14 (MC)	Madera Well 19.14.23.cac	W 4050		1/24/83		600	14.4	6.8	289	3.52	24	135	1.1	74.00	22.36	48.5	1.75	.07	227	30.0	3.80
15 (ML)	Melendrez 19.14.22.bcc	W 3683		1/24/83		970	15	7.3	678	12.32	15	1	1.15	108	36.21	84.2	6.67	.12	419	44	-1.87
16 (B1)	Benson #1 19.14.14.dca1	W 3797	McGibbon	8/17/82	.27	340	23	6.9	192	.9	18	22	2.7	35.2	10.21	32.7	1.98	.12	130	42	1.12
17 (B2)	Benson #2 19.14.14.dca2	W 3797	McGibbon	6/28/83		360		7.0	213	2.2	12	20		34	6.8	50.0	1.98	.02	113	56	-1.99
18 (CW)	County Well 20.14.3.abc	W 5018		6/04/83		75		5.9	39	3.08	3	0		12.00	.50	2.99	1.28	0	41	8.6	-1.59
19 (CS)	County Spring 19.14.34.cdd	S 4712		6/04/83		210		5.6	30.48	3.52	11	51		20.50	4.00	13.1	1.86	.05	80	26	-1.07
20 (MR)	Marcos 19.14.28.cbd	W 3840	Laos	3/31/83		530		7.3	224.3	3.52	4	150	.32	95.20	14.34	22.5	1.57	0	297	31.2	-12
21 (LW)	Laos West 19.14.30.dcc	W 3495	Laos	3/30/83		270		7.85	85.3	2.20	14	70	.32	38	6.3	14.9	1.51	.12	122	34	2.59
22 (MS)	Madera Stream 19.14.35.dca	St 4740	Forest Service	5/24/82		830		6.90	200	1.76	11	210	1.8	113.6	12.25	20	3.2	0		29	2.55
23 (LL)	Luck Ledge 20.14.12.baa	St 5840	Forest Service	3/24/82		210	9	7.0	63	1.32	6	27	.48	23.2	5	8.3	1.6	0	72	18	-4.7
	FABER CANYON																				
24	High Mine 19.14.24.ddc	M 4810		6/14/83		470	17.8	6.5	212	4.0	13	80		78	16	23.9	1.17	.02	260	31	-5.7
25	Low Mine 19.14.24.dac	M 4490		6/13/83		280	20	6.5	76	2.2	8	85		32	11	18.4	3.39	.06	124	13	-1.27
26	Faber Sp. 19.14.24.dab	S 4330		6/13/83		360		7.2	140	3.5	15	67		38	15	6.98	.83	.08	155	4.5	9.45
27	Old Hickory 19.14.13.dca	W 3985	McGibbon	8/17/82	.022	320	23	6.4	192	2.2	8	24	1.15	41.6	12.88	17.6	.93	.38	157	32	.06

Number	Name Location	Type Elevation (ft)	Land Owner	Date	Discharge (cfs)	Sp. Con. (m mhos)	T (°C)	pH	HCO_3^-	$NO_3^=$	Cl^-	$SO_4^=$	F^-	Ca^{++}	Mg^{++}	Na^+	K^+	Fe^{++}	SiO_2	Hard	% Error
	FLORIDA CANYON																				
28	Armour Sp. 19.15.	S 7960	Forest Service	6/06/83	.022	230	7.8	6.8	150	.9	4.2	7		51.6	6.07	6.56	.81	0	137	23.3	-9.67
29	Robinson Sp. 19.15.29.cbb	S 5070	Forest Service	6/09/83	.069	610	17	7.1	440	3.52	10.4	18		114.4	7.98	27.50	.93	.03	360	46	-3.00
30	Florida Sp. 19.15.	S 6835	Forest Service	6/09/83	.034	145	11.1	6.6	85	5.28	6	3		28	.73	6.77	.93	0	71/119	17.4	-.44
	SAWMILL CANYON																				
31	High Well 19.15.20.ddb	W	McGibbon	7/11/82		620		7.2	317	3.96	17	115	1.6	96.8	20.65	34.80	1.04	.09	327	30	.50
32	Low Well 19.15.18.ddd	W	McGibbon	6/15/83		530	20	6.4	268	0	17	105		92	17.2	27.8	.58	.11	300	26	-1.05
	SANTA RITA RANCH																				
33	Willow Sp. 19.15.22.bbc	S 5070	McGibbon	6/14/83	.022	560	17.8	6.8	238	11.9	25	155		91	20	31.90	.58	.02	312	23	3.1
34	SR1 19.15.16.cbc	W 4435	McGibbon	7/19/82		540		7.2	249	17.6	20	85	2.7	72.8	15.55	39.2	1.40	0	246	30	.15
35	SR2 19.15.16.cca	W 4530	McGibbon	7/19/82		550		7.3	249	7.92	17	110	2.9	87.2	11.66	34.8	1.40	0	266	30	.87
36	SR3 19.15.16.cac	W 4535	McGibbon	7/19/82		497		7.2	273	7.04	17	100	6.5	64	14.09	34.8	1.28	0	218	28	9.59
	CHINO CANYON																				
37	Chino Mine 20.14.8.caa	M 4600		1/09/83		460		7.7	142.7	5.28	5	160	2.55	79.20	10.94	23.9	1.28	0	243	44.4	-.21
38	Chino Basin Sp. 20.14.8.cbb	S 4175		1/09/83		300		7.9	140	3.96	6	52	.69	27.6	14.58	26.5	.34	.03	129	10.8	-1.85
39	Quantrell Mine 20.14.8.aad	M 5120		1/14/83		106	14.4	5.6	12.2	3.08	5	32	0	10	3.65	6.98	1.28	.4	40	16.2	-3.2
40	Quantrell Cr. 20.14.6.dab	St 3760		1/14/83		106	14.4	6.0	17.1	3.08	8	27	0	10.40	2.1	10.2	1.04	.01	.35	19.6	-2.6
	AGUA CALIENTE CANYON																				
41	Hermit Mine 20.14.10.ddd	M 6580	Forest Service	5/19/82		1500		7.8	183	0	16	650	1.0	256	16.7	19.5	3.6	.12	725	30	5.8
42	A.C. Sp. 20.13.13.aab	S 3880		3/31/82		640	27	6.8	216	4.84	6	110	.25	77.6	10.5	12	2.7	0		27	6.1
43	Far West 20.13.9.ddd	W 3428		1/30/83		400		8.0	200	5.72	11	58	.43	70	7.78	18.1	1.75	.12	207	32	-.81
44	A.C. Stream 20.14.17.abd	St 4580		1/09/83		210		7.0	73.2	1.32	7	52	.35	30.40	5.1	11.3	.93	0	97	21.6	1.03
45	Nat. 1 18.15.34.add1	W 4860	McGibbon	3/06/82		780	19	7.1	313	7.92	26	58	3.0	73.6	8.5	33	4.2	0	238	27	13.11
46	Nat. 2 18.15.34.add2	W 4830	McGibbon	3/06/82		940	15	7.1	382	1.32	26	82	4.6	88.8	18.75	35	5.4	.25	350	23	16.68
47	Nat. 3 18.15.34.daa2	W 4880	McGibbon	3/06/82		960		7.1	384	7.92	36	78		96	20	13	3.85	.4	370	29	16.14
48	Nat. 4 18.15.34.daa1	W 4875	McGibbon	3/06/82		760	17	6.7	337	5.72	36	140		96	14.25	35	4.2	2	296	25.6	17.12
49	Nat. 5 18.15.34.baa	W 4600		8/20/82		485	25	7.1	258.4	2.64	14	52		39.2	6.81	68.33	2.22	0	126	1.7	3.54
50	Sawmill Sp. 20.15.	S 6960		6/07/83	.007	260		6.8	167	3.96	5	3		56.8	3.16	8.75	.58	.12	155	21	-7.4
51	Rock Candy 20.15.	M 6160		6/06/83		680		7.1	498.6	3.52	4	17		134	18.23	32.7	1.51	.30	410		-5.3
52	Baldy Spring 20.15.	S 8640	Forest Service	4/19/82	T	36		5.0	0	5.28	2	2	0	2.4	T	2.5	1	0	8	8.9	-14.9
53	Macbath 20.14.13.daa	S 7130	Forest Service	3/26/82		320	10	5.9	146	0	2	31	.70	44.8	5.2	12.5	1.04	0	136	18	-2.2

APPENDIX C

GENERAL WELL INFORMATION

Name: Air Force, 3 wells
Location: 19.14.27.dca
Sample Number: 4

Well #1

Elevation: 4147

Water level (ft):	Date:
41.5	8/62
43.6	2/63
26.8	1/64
20.7	4/71
46.0	2/76
44.0	2/77
46.0	2/78
43.0	2/79
45.0	2/80

Depth (ft): 57.0

Driller's Log (ft):
0-25: over burden, boulders
25-26: hard weathered granite
56-57: hard granite

Perforated: 30-55 ft

Driller: Roscoe Moss

Well #2

Elevation: 4132

Water level (ft):	Date:
17.9	8/62
9.7	2/63
7.0	1/64
8.0	4/71
45.3	2/76
44.0	2/77
45.0	2/78
43.0	2/79
45.5	2/80
20.6	2/81

Depth (ft): 50.0

Driller's Log (ft):
0-20: gravel, sand, boulders
20-48: weathered granite
48-50: hard granite

Perforated: 25-49 ft

Driller: Roscoe Moss

Well #3

Elevation: 4147
Water level (ft): 13.5 Date: 1/64
13.8 4/71
35.4 2/76
22.4 2/81
40.8 12/81
Depth (ft): 43.0

Driller's Log (ft): 0 -27 : over burden
27 -24.5: weathered granite
42.5-43 : hard granite

Perforated: 43 ft

Driller: Weber Well Drilling

Name: Christobal
Location: 19.14.27.cac
Sample Number: 10
Elevation: 4120
Water level (ft): 29.10 Date: 2/26/83
Depth (ft): 95

Driller's Log (ft): 0 - 1 : top soil, boulders
7 -25 : sand, pebbles, boulders
25 -26.5: hard boulders
26.5-95 : sand, pebbles, boulders
95 : granite

Perforated: 35-95 ft

Driller: Tom White

Name: RF1
Location: 19.14.27.cac
Sample Number: 11
Elevation: 4038
Water level (ft): 24.04 Date: 3/26/83
23.42 3/30/83
Depth (ft): 77

Name: RF2
Location: 19.14.27.cbd
Sample Number: 12
Elevation: 4060

Water level (ft):			Date:
	23.02		3/26/83
	22.2		3/30/83

Name: RF3
Location: 19.14.27.cbd2
Sample Number: 13
Elevation: 4038

Water level (ft):			Date:
	33.7		3/27/83
	40.0	(pumping)	3/30/83

Depth (ft): 68

Name: Madera Well
Location: 19.14.23.cac
Sample Number: 14
Elevation: 4050

Water level (ft):		Date:
	15	8/17/82
	17.4	1/24/83
	14.0	3/26/83

Name: Melendrez
Location: 19.14.22.bcc
Sample Number: 15
Elevation: 3683

Water level (ft):		Date:
	13.0	1/24/83
	5	11/14/83

Name: B-1
Location: 19.14.14.dca1
Sample Number: 16
Elevation: 3797

Water level (ft):			Date:
	85.33	(pumping)	8/17/82
	75.4		11/04/82
	53.6	(pumping)	3/26/83
	47.58		3/31/83

Depth (ft): 110

Name: B-2
Location: 19.14.14.dca2
Sample Number: 17
Elevation: 3797

Water level (ft):	Date:
51.11	8/16/82
52.1	11/04/82
47.16	3/26/83
46.61	3/31/83

Name: County Well
Location: 20.14.3.abc
Sample Number: 18
Elevation: 5018
Water level (ft): 6 Date: 6/04/83

Name: Marcos
Location: 19.14.28.cbd
Sample Number: 20
Elevation: 3840
Waater level (ft): 11.85 Date: 3/26/83

Name: Laos West
Location: 19.14.30.dcc
Sample Number: 21
Elevation: 3495

Depth (ft): 360

Driller's Log (ft):
0- 20: clay and boulders
20- 80: soft cemented boulders
80-180: clay and boulders
180-360: sand, gravel and boulders

Name: Old Hickory
Location: 19.14.13.dca
Sample Number: 27
Elevation: 3985

Water level (ft):	Date:
57.0 (pumping)	8/17/82
58.3	11/04/82

Depth (ft): 150

Name: High Well
Location: 19.14.20.ddb
Sample Number: 31
Elevation: 4340
Water level (ft): 12.21 Date: 11/04/82
7.72 3/31/83

Depth (ft): 40

Name: Low Well
Location: 19.15.18.ddd
Sample Number: 32
Elevation: 4050
Water level (ft): ≅10 Date: 6/15/83

Name: SR1
Location: 19.15.16.cbc
Sample Number: 34
Elevation: 4435
Water level (ft): 98.0 Date: 6/13/83

Name: SR2
Location: 19.15.16.cca
Sample Number: 35
Elevation: 4530
Water level (ft): 236.50 Date: 4/02/82

Name: SR3
Location: 19.15.16.cac
Sample Number: 36
Elevation: 4535
Water level (ft): 136.50 Date: 4/02/82

Depth (ft): 250

Name: Far West
Location: 20.13.9.ddd
Sample Number: 43
Elevation: 3428
Water level (ft): 241.6 Date: 3/30/83

Depth (ft): 276

Name: Nat 1
Location: 18.15.34.add
Sample Number: 45
Elevation: 4860

Water level (ft):	34.6	Date:	2/19/82
	33.5		8/02/82
	33.4		8/20/82

Name: Nat 3
Location: 18.15.34.daa1
Sample Number: 47
Elevation: 4880

Water level (ft):	52.62	Date:	8/02/82
	53.0		8/20/82

Name: Nat 4
Location: 18.15.34.daa2
Sample Number: 48
Elevation: 4875
Water level (ft): 63.9 Date: 2/19/82

Name: Nat 5
Location: 18.15.34.daa3
Sample Number: 49
Elevation: 4600
Water level (ft): 290.3 Date: 2/19/82

Name: Near Melendrez
Location: 19.14.21.ddd
Sample Number: none
Elevation: 3839
Water level (ft): 38.2 Date: 1/24/83

Name SR4
Location: 19.15.16.cdd
Sample Number: none
Elevation: 4565
Water level (ft): 145.5 Date: 6/13/83

APPENDIX D

CALCULATIONS OF TRANSMISSIVITY VALUES

RR3

Specific capacity analysis:

Drawdown (S) = 5.15 ft

Discharge (Q) = 4.3 gpm = .01 cfs

Thickness (M) = 51.4 ft

$$T = \frac{2.43\ QM}{S(2M-S)} \quad \frac{24.3 \cdot .01\ ft^3/s \cdot 45\ ft}{5.15\ ft\ (2.45\ ft - 5.15\ ft)} = .0024\ ft^2/s = 206\ ft^2/d$$

$$K = \frac{206\ ft^2/d}{45\ ft} = 4.58\ ft$$

Theis analysis: Data in Table D.1, data plot in Figure D.1.

Q = .576 cfm

S = 10.4 ft

Sd = 10

t = .75 m

$r^2 = .3\ ft^2$

td = .25

$$T = \frac{Q}{4\pi s}\ Sd = \frac{.576\ ft^3/m}{4\pi\ 10.4\ ft}\ 10 = .044\ ft^2/m = 63\ ft^2/d$$

$$S = \frac{Tt}{r^2 td} = \frac{.044\ ft^2/m \cdot .75\ m}{.3\ ft^2 \cdot .25} = .44$$

$$K = \frac{63\ ft^2/d}{45\ ft} = 1.41\ ft/d$$

Air Force

Specific capacity analyses:

	#1	#2	#3
S	13.2 ft	15.1 ft	19.3 ft
Q	.0125 ft^3/s	.0145 ft^3/s	.011 ft^3/s
M	25 ft	24 ft	20 ft

#1: $T = \frac{2.43 \cdot .0125\ ft^3/s \cdot 25\ ft}{13.2\ ft\ (2 \cdot 25\ ft - 13.2\ ft)} = .0016\ ft^2/s = 135\ ft^2/d$

$K = \frac{135\ ft^2/d}{25\ ft} = 5.4\ ft/d$

#2: $T = \frac{2.43 \cdot .0149\ ft^3/s \cdot 24\ ft}{15.1\ ft\ (2.24\ ft - 15.1\ ft)} = .0017\ ft^2/s = 151\ ft^2/d$

$K = \frac{151\ ft^2/d}{24\ ft} = 6.3\ ft/d$

#3: $T = \frac{2.43 \cdot .011\ ft^3/s \cdot 20\ ft}{19.3\ ft\ (2 \cdot 20\ ft - 19.3\ ft)} = .0013\ ft^2/s = 117\ ft^2/d$

$K = \frac{117\ ft^2/d}{20\ ft} = 5.8\ ft/d$

B-1

Specific capacity analysis:

$S = 10.5\ ft$

$Q = .0133\ ft^3/s$

$M = 50.1\ ft$

$T = \frac{2.43 \cdot .0133\ ft^3/s \cdot 50.1\ ft}{10.5\ ft\ (2 \cdot 50.1\ ft - 10.5\ ft)} = .0172\ ft^2/s = 149\ ft^2/d$

$K = \frac{149\ ft^2/d}{50.1\ ft} = 2.97\ ft/d$

Thiem analysis:

$Q = .0133\ ft^3/s$

$S = 10.5\ ft$

$\frac{r_1}{r_2} = 27.6$

$T = \frac{Q}{2\pi S} \ln \frac{r_1}{r_2} = \frac{.0133\ ft^3/s}{2\pi(10.6\ ft)} \ln 27.6 = .00067\ ft^2/S = 57.8\ ft^2/d$

$K = \frac{57.8\ ft^2/d}{50.1\ ft} = 1.16\ ft/d$

Sawmill Canyon Well

Specific capacity analysis:

$S = 2.8\ ft$

$Q = .004\ ft^3/s$

$M = 28\ ft$

$T = \frac{2.43 \cdot .004\ ft^3/s \cdot 28\ ft}{2.8\ ft\ (2 \cdot 28\ ft - 2.8\ ft)} = .0019\ ft^2/S = 164\ ft^2/d$

$K = \frac{174\ ft^2/d}{28\ ft} = 5.86\ ft/d$

Santa Rita Well

Specific capacity analysis:

$S = 21\ ft$

$Q = .011$

$M = 150\ ft$

$T = \frac{2.43 \cdot .011\ ft^3/s \cdot 150\ ft}{21\ (2 \cdot 150\ ft - 21\ ft)} = .0007\ ft^2/s = 60\ ft^2/d$

$K = \frac{60\ ft^2/d}{150\ ft} = .4\ ft/d$

Table D.1. Data From Time-Drawdown Test at Well RR3

Time (min)	Hold (ft)	Cut (ft)	Measuring Point (ft)	Water Level (ft)	Drawdown (ft)
0	50	13.78	1.6	34.62	
.5	53	16.3	1.6	35.10	.48
1	50	12.95	1.6	35.45	.83
2	53	14.85	1.6	36.55	1.93
3.5	51	13.3	1.6	36.10	1.48
4.5	52	14.06	1.6	36.34	1.72
5	50	11.8	1.6	36.60	1.98
5.5	53	14.66	1.6	36.74	2.12
6.5	52	13.47	1.6	36.93	2.31
7.5	53	14.3	1.6	37.10	2.48
8.5	53	14.14	1.6	37.26	2.64
9.5	53	13.9	1.6	37.50	2.88
10.5	53	13.8	1.6	37.60	2.98
12	53	13.72	1.6	37.68	3.06
13	53	13.56	1.6	37.84	3.22
14	55	15.54	1.6	37.86	3.24
15	54	14.28	1.6	38.12	3.5
16	54	14.24	1.6	38.16	3.54
18	54	14.2	1.6	38.20	3.58
20	54	13.91	1.6	38.49	3.87
22	54	13.75	1.6	38.65	4.03
24	54	13.6	1.6	38.80	4.18
26	54	13.5	1.6	38.90	4.28
30	54	13.36	1.6	39.04	4.42
66	54	12.63	1.6	39.77	5.15

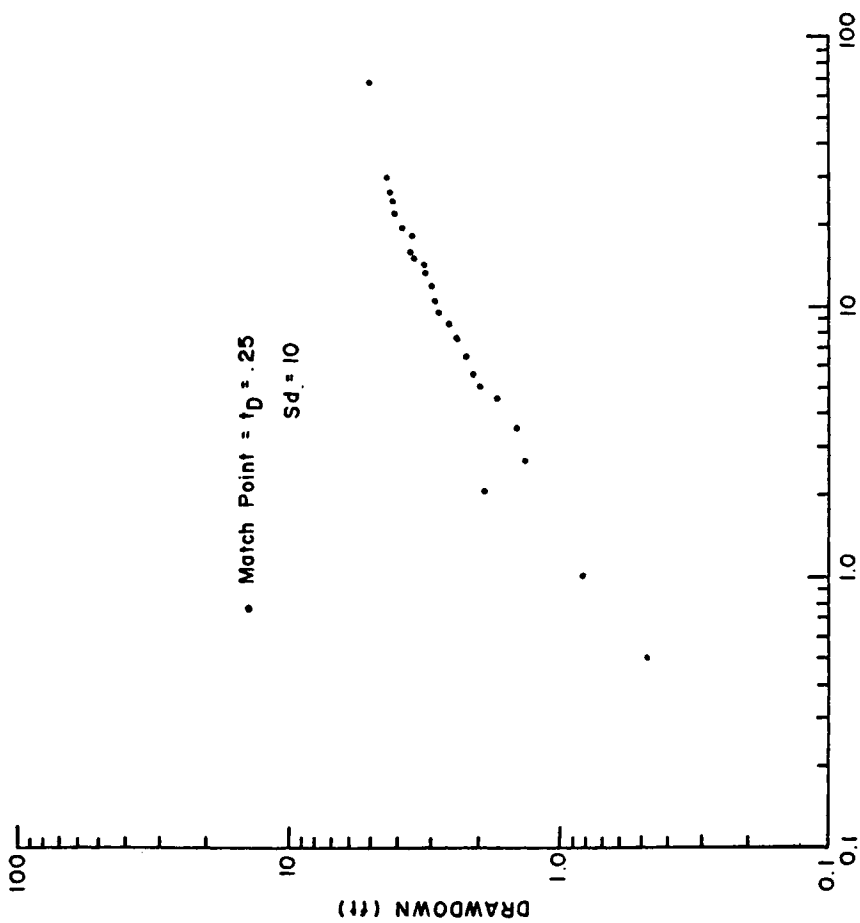

Figure D.1. Log-log plot of time-drawdown test at well RR3.

APPENDIX E

MONTHLY AND ANNUAL PRECIPITATION

Monthly and Annual Precipitation: Average (top) and for September 1982-August 1983 (bottom). Location numbers refer to Figure 3.1. Values in inches.

Station	Number	Elevation	Jan	Feb	Mar	Apr	May	Jun	Jul	Aug	Sep	Oct	Nov	Dec	Total
Desert	1	3880	1.11	.93	.87	.38	.119	.134	3.45	3.52	1.76	.95	.75	1.21	15.38
Grassland			2.39	.68	2.74	.63	.13	0.0	2.67	5.08	2.68	.01	.69	3.01	20.71
Forest	2	4160	1.21	1.15	1.03	.46	.12	.54	3.79	3.74	1.89	1.02	1.04	1.56	17.55
			2.47	.69	2.71	.32	.14	.05	2.46	5.37	2.13	.02	.80	3.64	21.30
Florida	3	4300	1.51	1.47	1.33	.47	.17	.69	4.51	4.17	2.20	1.12	1.22	1.82	20.78
			3.39	2.91	4.21	1.15	.35	0.0	3.25	7.47	3.33	--	--	5.35	--
McGibbon	4	4550	1.30	1.06	1.12	.40	.13	.63	4.22	3.65	1.91	1.21	.91	1.77	18.31
			2.75	2.02	3.47	1.02	.29	0.0	3.21	4.60	--	0.0	--	4.13	--
Parker	5	4320	1.19	1.10	1.03	.50	.12	.52	3.67	3.65	1.86	.95	1.01	1.44	17.04
			3.11	1.80	2.91	.90	.45	.01	2.18	3.86	2.82	0.0	.74	3.42	22.20
Road	6	3540	.93	.90	.81	.37	.11	.42	3.11	3.24	1.68	.87	.82	1.15	14.41
			2.49	1.24	1.91	.50	.24	0.0	2.76	5.95	2.34	.01	.84	2.65	20.93
White House	7	3880	1.08	1.01	.93	.39	.13	.39	3.61	3.78	1.86	.94	.91	1.33	16.36
			2.12	1.26	2.59	.34	.62	0.0	2.63	5.93	3.38	0.0	.88	2.43	22.18
Smithsonian*	8	8550	1.7	2.8	3.4	.433	.85	.10	5.6	3.9	2.95	2.49	1.00	1.80	27.02
			1.8	3.95	4.38	1.0	1.20	0.0	4.9	3.5	3.25	0.0	1.45	5.16	30.06

*Averages based on 3 years of data.

APPENDIX F

CALCULATION OF MOUNTAIN-FRONT RECHARGE

MADERA CANYON

Flow-net Analysis

$Q = Tw \frac{\Delta h}{\Delta L}$; parameters from Figure 5.1.

$T = 63, 103\ ft^2/day$.

Streamtube 1:

Section	w (ft)	Δh (ft)	ΔL (ft)	Q (ft^3/day) $T = 63\ ft^2/day$	Q (ft^3/day) $T = 130\ ft^2/day$	Q (ac-ft/yr/mi) $T = 63\ ft^2/day$	Q (ac-ft/yr/mi) $T = 130\ ft^2/day$
A	1531	100	1320	7198	15,000	208	435
B	1531	100	1214	7945	16,400	230	474
C	1584	100	1584	6300	13,400	176	363
					average	205	424

Streamtube 2:

Section	w (ft)	Δh (ft)	ΔL (ft)	Q (ft^3/day) $T = 63\ ft^2/day$	Q (ft^3/day) $T = 130\ ft^2/day$	Q (ac-ft/yr/mi) $T = 63\ ft^2/day$	Q (ac-ft/yr/mi) $T = 130\ ft^2/day$
A	1320	100	2112	3940	8,125	132	272
B	1373	100	1584	5461	1,127	176	373
					average	154	318

Water Budget

GR = P - ET - RO; parameters from Tables 3.3 and 3.4.

P = 12,132 ac-ft/yr
ET = 6,687 ac-ft/yr

$$RO = 4.2\ ft^3/s \cdot \frac{86{,}400\ s}{d} \cdot \frac{365\ d}{yr} \cdot \frac{1\ ac\text{-}ft}{43{,}560\ ft^3} = 3041\ ac\text{-}ft/yr$$

$$GR = 12132 \cdot 6687 - 3041 = 2404\ ac\text{-}ft/yr = \frac{2404}{4.6\ mi} = 523\ ac\text{-}ft/yr/mi$$

FLORIDA CANYON

Water Budget

GR = P - ET - RO, parameters from Tables 3.3 and 3.4.

P = 4070 ac-ft/yr
ET = 2232 ac-ft/yr

$$RO = 1.93 \text{ cfs} \cdot 365 \frac{d}{yr} \cdot \frac{86400 \text{ s}}{d} \cdot \frac{\text{ac-ft}}{43560 \text{ ft}^3} (.5 \text{ yr}) = 699 \text{ ac-ft/yr}$$

$$GR = 4070 - 2232 - 699 \text{ yr} = 1139 \text{ ac-ft/yr} = \frac{1139}{.9 \text{ mi}} = 1266 \text{ ac-ft/yr/mi}$$

REFERENCES

Anderson, T. W., 1972, Electric-analog analysis of the hydrologic systems, Tucson basin, southwestern Arizona. U.S. Geological Survey Water-Supply Paper 1939-c, 34 p.

Belan, R. A., 1972, Hydrogeology of a portion of the Santa Catalina Mountains. Unpublished M.S. thesis, University of Arizona, Tucson, 68 p.

Ben-Asher, J., Randall, J., and Resnick, S., 1976, Determining areal precipitation in the Basin and Range province of southern Arizona, Sonoita Creek Basin. Hydrology and Water Resources in Arizona and the Southwest, in Proceedings of the 1976 meeting of the Arizona Section of the American Water Resources Association, Tucson, Arizona, v. 6, p. 161-167.

Davidson, E. S., 1960, Geology of the eastern part of the Safford Valley, Graham County, Arizona. Arizona Geological Digest, v. 3, p. 123-136.

_____, 1961, Facies distribution and hydrology of intermontane basinfill, Safford Basin, Arizona. U.S. Geological Survey Professional Paper 242-C, p. C151-C153.

Davis, R. W., 1967, A geophysical investigation of hydrologic boundaries in the Tucson Basin, Pima County, Arizona. Unpublished M.S. thesis, University of Arizona, Tucson, 64 p.

Drever, J. I., 1982, The Geochemistry of Natural Waters. Englewood Cliffs, New Jersey, Prentice-Hall, Inc., 388 p.

Drewes, H., 1971a, Geologic Map of the Sahuarita Quadrangle, southeast of Tucson, Arizona. U.S. Geological Survey Misc. Inv. Ser. Map I-613.

_____, 1971b, Mesozoic stratigraphy of the Santa Rita Mountains, southeast of Tucson, Arizona. U.S. Geological Survey Prof. Paper 658-6, 81 p.

_____, 1971c, Geologic Map of Mount Wrightson Quadrangle, southeast of Tucson, Santa Cruz and Pima Counties, Arizona. U.S. Geological Survey Misc. Inv. Ser. Map I-614.

_____, 1972a, Structural geology of the Santa Rita Mountains, southeast of Tucson, Arizona. U.S. Geological Survey Prof. Paper 748, 35 p.

_____, 1972b, Cenozoic rocks of the Santa Rita Mountains, southeast of Tucson, Arizona. U.S. Geologic Survey Prof. Paper 746, 66 p.

_____, 1976, Plutonic rocks of the Santa Rita Mountains, southeast of Tucson, Arizona. U.S. Geological Survey Prof. Paper 915, 75 p.

Duckstein, L., Fogel, M. M., and Thames, J. L., 1973, Elevation effects on rainfall: A stochastic model. J. Hydrology, v. 18, p. 21-35.

Feth, J. B., 1964, Hidden recharge. Ground Water, v. 2, no. 4, p. 14-17.

Feth, J. H., Roberson, C. E., and Polzer, W. L., 1964, Sources of mineral constituents in water from granitic rocks, Sierra Nevada, California and Nevada. U.S. Geological Survey Water-Supply Paper 1535, 70 p.

Fontes, J. Ch., and Zuppi, G. M., 1976, Isotopes and water chemistry in sulphide bearing springs of central Italy, in Interpretation of Environmental Isotope and Hydrochemical Data in Groundwater Hydrology, IAEA, Vienna, p. 143-158.

Freeze, R. A., and Cherry, M. A., 1979, Groundwater. Englewood Cliffs, New Jersey, Prentice-Hall, Inc., 604 p.

Gallaher, B. M., 1979, Recharge properties of the Tucson Basin Aquifer as reflected by the distribution of a stable isotope. Unpublished M.S. thesis, University of Arizona, Tucson, 92 p.

Garrels, R. M., and Christ, C. L., 1965, Solutions, Minerals, and Equilibria. Freeman, Cooper, San Francisco, California, 450 p.

Green, L. R., and Martin, S. G., 1967, An evaluation of precipitation, vegetation, and related factors on the Santa Rita Experimental Range. Technical Reports on the Meteorology and Climatology of Arid Regions, No. 17, University of Arizona Institute of Atmospheric Physics, 82 p.

Hem, J. D., 1970, Study and interpretation of the chemical characteristics of natural water. U.S. Geological Survey Water-Supply Paper 1473, 363 p.

Kafri, V., and Ben-Asher, J., 1978, Computer estimates of natural recharge through soils in southern Arizona. J. Hydrology, v. 38, p. 125-138.

Logan, J., 1964, Estimating transmissivity from routine production test of water wells. Ground Water, v. 2, no. 2, p. 35-37.

Mifflin, M. D., 1968, Delineation of ground-water flow systems in Nevada. Technical report series H W, Hydrology and Water Resource Publication No. 4, University of Nevada.

Mohrbacher, C. J., 1983, Mountain-front recharge to the Tucson Basin from the Santa Catalina Mountains, Arizona. Unpublished M.S. thesis, University of Arizona, Tucson, 87 p.

Olsen, M. C., 1982, Mountain-front recharge to the Tucson Basin from Tanque Verde Canyon, Arizona. Unpublished M.S. thesis, University of Arizona, Tucson, 145 p.

Payne, B. R., and Yurtsever, Y., 1974, Environmental isotopes as a hydrogeological tool in Nicaragua. In Isotope Techniques in Groundwater Hydrology, 1., IAEA, Vienna, 193-202.

Rutledge, J., 1984, Personal communication, Department of Geosciences, University of Arizona, Tucson.

Simpson, E. S., Thourud, D., and Friedman, I., 1970, Distinguishing seasonal recharge to groundwater by deuterium analysis in southern Arizona, in World Water Balance, Proceedings of the Reading Symposium, July 1970. International Association of Scientific Hydrology, p. 112-121.

Smalley, R. C., 1984, An isotopic and geochemical investigation of the hydrogeologic and geothermal systems in the Safford Basin, Arizona. Unpublished M.S. thesis, University of Arizona, Tucson, 85 p.

Tardy, Y., 1971, Characterization of the principal weathering types by the geochemistry of waters from some European and African crystalline massives. Chemical Geology, v. 7, p. 253-271.

Thorne, D. P., 1982, A chemical and isotopic study of ground-water flow in the Tucson Mountains, Arizona. Unpublished M.S. thesis, University of Arizona, Tucson, 75 p.

Toran, L., 1983, Isotopes in ground-water investigations. Ground Water, v. 19, no. 6, p. 740-745.

Turner, J., 1983, Unpublished data, Department of Hydrology and Water Resources, University of Arizona, Tucson.

Wilson, L. G., DeCook, H. J., and Neuman, S. P., 1980, Final Report--Regional recharge research for southwest alluvial basins. Unpublished U.S. Geological Survey report by the Water Resources Research Center, University of Arizona, Tucson.

PLATE 1. Santa Rita Mountain Study Area Showing Physiography and Data Sites

Legend

- Study Area boundary; 3 dots indicate topographic divide
- Road
- Canyon
- PROCTOR RANCH — Cultural Site
- MT. HOPKINS 8585 — Topographic Peak with elevation in feet

Data Sites

- 13o Well, sampled
- o Well, unsampled
- 2δ Spring
- 44X Surface water
- 3□ Mine
- M2 ◇ Stream gaging site
- R1 • Stream gage

Sample numbers refer to Appendix II or relevant figures and tables. Underlined symbols indicate isotope data available

N

0 1 2 miles

R13E R14E R15E

T19S T18S T20S

SANTA RITA RANCH

EXP. RANGE HEADQUARTERS

PROCTOR RANCH

ELEPHANT HEAD 5648

MT. WRIGHTSON 9453

MT. HOPKINS 8585

7665

6897

8357

Sawmill Canyon

Florida Canyon

Madera Canyon

Chino Canyon

Agua Caliente Canyon

Faber Canyon

August Merz III, M.S.
Department of Hydrology
University of Arizona, 1985

PLATE 2. GEOLOGIC MAP OF SANTA RITA STUDY AREA.

LEGEND

- Geologic contact, all locations approximate
- U / D — Fault, U on upthrown side, D on downthrown side
- Tertiary dike

GEOLOGY (Lithologies in Appendix I)

Q	Quaternary & Tertiary Units	Kba	Apache Canyon Formation	Pcn	Concha Limestone
Ke	Elephant Head Quartz Diorite	Km	Madera Canyon Granodiorite	Ps	Scherrer Formation
Kj	Josephine Canyon Diorite	Tqd	Quartz Diorite	Dm	Martin Formation
Kf	Fort Crittenden Formation	Tp	Piper Gulch Monzonite	Ca	Abrigo Formation
Kbt	Turney Ranch Formation	Tw	Mt. Wrightson Formation	PCn	Continental Grandiorite

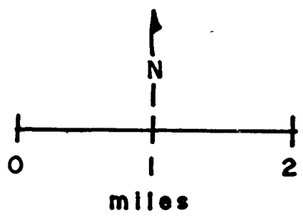

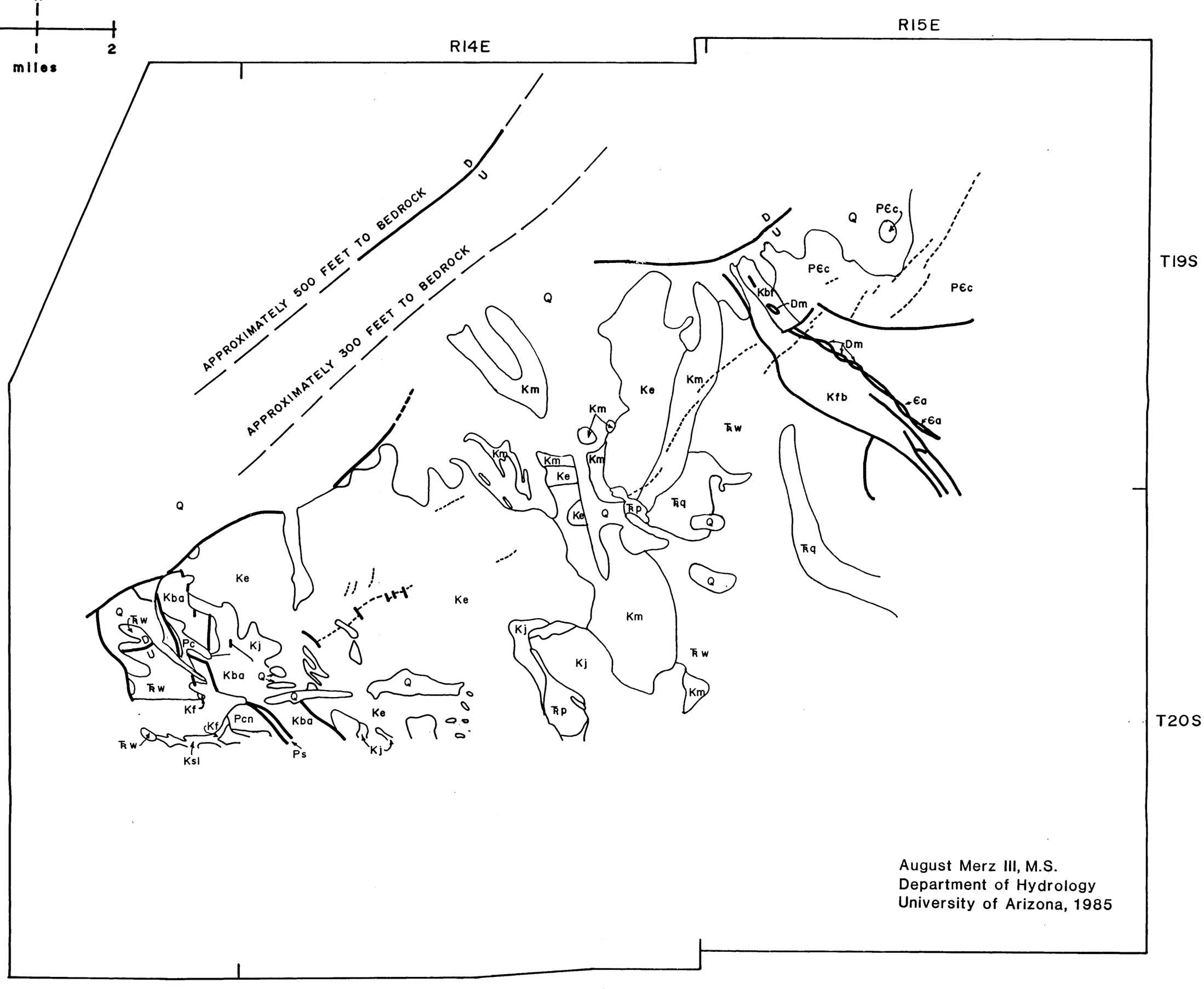

August Merz III, M.S.
Department of Hydrology
University of Arizona, 1985